C. P. No. 710

C. P. No. 710

MINISTRY OF AVIATION

AERONAUTICAL RESEARCH COUNCIL

CURRENT PAPERS

Low-Speed Wind-Tunnel Tests on a Delta-Wing Aircraft Model (S.R.177) with Blowing over the Trailing-Edge Flaps and Ailerons.

By

S. F. J. Butler and M. B. Guyett

LONDON: HER MAJESTY'S STATIONERY OFFICE

1966

PRICE 17s 0d NET

U.D.C. No. A.I.(42) Saunders-Roe P177 : 533.693.3 : 533.6.013.412 : 533.694.72 : 533.6.011.34

C.P. No. 710

August, 1962

LOW-SPEED WIND-TUNNEL TESTS ON A DELTA-WING AIRCRAFT MODEL (S.R.177), WITH BLOWING OVER THE TRAILING-EDGE FLAPS AND AILERONS

by

S. F. J. Butler
and
M. B. Guyett

SUMMARY

Low speed longitudinal stability measurements are described on a delta-wing aircraft model of aspect-ratio 2·9 and 40° leading-edge sweepback, with shroud blowing over trailing-edge flaps and ailerons.

With blowing over the flap alone at a flap angle of 60° (aileron undeflected), increases were obtained of 0·27 in trimmed C_L at constant incidence and of 0·18 in trimmed $C_{L_{max}}$, at the value of C_μ (0·031) envisaged for the projected aircraft. Corresponding reductions in landing and take-off speeds of about 10 knots could have been expected in practice. By distributing the same total jet momentum to flap and aileron, with 30° aileron mean droop, further lift increases were obtained corresponding to additional reductions of about 8 knots in aircraft speeds.

The beneficial effect of the L.E. flap was large, amounting to 5° increase of stalling angle and 0·3 increase in $C_{L_{max}}$ with blowing over trailing-edge flaps and ailerons.

The measured effects of blowing correlated well with results of other model tests involving similar wing-flap arrangements. In particular, part-span blown flaps were again found to produce large drag increments significantly affecting the aircraft minimum drag speed.

Replaces R.A.E. Report No. Aero 2671 - A.R.C. 24 502.

LIST OF CONTENTS

LIST OF CONTENTS (Contd)

LIST OF APPENDICES

LIST OF ILLUSTRATIONS

LIST OF ILLUSTRATIONS (Contd)

LIST OF ILLUSTRATIONS (Contd)

1 INTRODUCTION

A series of experimental investigations has been completed in the No.2 $11\frac{1}{2}$ ft × $8\frac{1}{2}$ ft Wind Tunnel on the application of boundary layer control by blowing for high lift to several specific aircraft configurations. These comprised T.E. flap blowing tests on the De Havilland Sea Venom[1], the Vickers-Supermarine Scimitar[2], the Saunders-Roe P.177, and subsequent tests on a sweptback wing with blowing at the wing nose as well[3].

The present paper discusses lift, drag, and pitching moment measurements made on a half-model of the Saunders-Roe P.177, which was a proposed development of the S.R.53 as a high-altitude interceptor with a mixed power plant (Gyron Junior/Sceptre). Some principal aerodynamic features were the 6% thick cropped delta wing, of aspect ratio 2·29 and 40° leading-edge sweepback, with leading-edge flaps and blowing over the trailing-edge flaps and ailerons, combined with a high position for the tailplane.

A comparison is included between the estimated and the measured effects of blowing.

2 MODEL DETAILS

A quarter-scale starboard-wing half model was mounted on the lower balance of the R.A.E. No.2 $11\frac{1}{2}$ ft × $8\frac{1}{2}$ ft Wind Tunnel (see Fig.1). The model, which was constructed by Saunders-Roe, was of composite construction. The blowing ducts and nozzles, and the mounting brackets were made of dural and mild steel; the flap and the aileron from hydrolignum; the remainder of the wing, also the fuselage, from mahogany.

The wing was fitted (see Fig.2) with a full-span tapered main duct supplying the high-pressure air to the nozzles (see Fig.3a) in the wing shrouds ahead of the flap and the aileron. The ejected air impinged tangentially on the upper surfaces of the flap and aileron in a typical shroud-blowing installation. It was possible to seal off parts of the nozzle span to obtain varying spanwise extents of blowing, or to simulate the effect of local blockages due to flap and aileron support gear (see Fig.3b). The nozzle depth was set by small 0·2 inch wide spacers at 1·5 inch intervals across the span. The blowing coefficient was normally varied by changing the pressure ratio, but sometimes by altering the test speed.

Principal details of the model geometry are given in Table 1. The wing, of full aspect ratio 2·29, had a cropped delta planform of taper ratio 2·87, with a 6% thick R.A.E. 102 section streamwise. A mid-wing position was chosen, with 3° wing-body angle and 5° anhedral. The flap and aileron angle ranges

tested were 0° to 80° and 0° to 50° respectively. The wing was equipped with alternative leading-edge flaps, simulating settings of 0° and 30° (normal to hinge-line), and were split at mid semi-span to permit a part-span case to be tested. Most of the tests were made with 30° full-span deflection. Comparative tests were also made with a small sharp leading-edge extension (see Fig.5).

Normally, a tip weapon was attached, since this was the proposed standard aircraft condition (see Fig.2). Tests were made to find the effects of removing this weapon, and of adding an underwing drop tank, an airbrake, and the main undercarriage assembly (see Fig.4).

A half-tailplane without elevator was supported by a flat-plate fin, the normal fin not being represented. A foreplane was also added to the model for a few tests. Internal engine flow was not represented, the intake and tail pipe being faired over.

Most of the tests were made at 200 ft/sec, corresponding to a wing Reynolds number of $4{\cdot}0 \times 10^6$ (based on aerodynamic mean chord).

3 TEST PROCEDURE

3.1 The effect of blowing air supply on balance zeros

The air supply feed to the model was similar to that adopted earlier for the tests on the D.H. Sea Venom[1]. As previously, the zeros for blow-on runs had to be taken with the correct static pressure conditions in the canvas sleeve connecting the "live" model to "earth". The zero scatter was only slightly greater than that which would have occurred normally with a conventional (non-blowing) model on this balance.

A full description of the air supply arrangement can be found in Ref.4.

3.2 Definition and measurement of blowing momentum coefficient, and range of values covered

The sectional momentum coefficient C'_μ [$\equiv mv_j/\frac{1}{2}\rho U_o^2 S'g$] is defined in terms of the mass flow rate m and the theoretical jet velocity v_j assuming isentropic expansion to free-stream static pressure. It may be calculated from the pressure ratio P_D/P_o and the cross-sectional area S" of the nozzle:-

$$C'_\mu = \frac{3{\cdot}840 \times 10^3}{\frac{1}{2}\rho_o U_o^2} \frac{S''}{S'} \frac{P_D}{P_o} \left\{ 1 - \left(\frac{P_o}{P_D} \right)^{2/7} \right\}^{\frac{1}{2}} \qquad \left(\frac{P_D}{P_o} > 1{\cdot}893 \right)$$

and

$$C'_\mu = \frac{1{\cdot}483 \times 10^4}{\frac{1}{2}\rho_o U_o^2} \frac{S''}{S'} \left\{ \left(\frac{P_D}{P_o} \right)^{2/7} - 1 \right\} \qquad \left(\frac{P_D}{P_o} < 1{\cdot}893 \right)$$

or, alternatively, from the pressure ratio and the measured mass flow rate m (lb/sec)

$$C'_\mu = \frac{4{\cdot}572\ m\ T_D^{\frac{1}{2}}}{\frac{1}{2}\rho_o U_o^2 S'} \left\{1 - \left(\frac{P_o}{P_D}\right)^{2/7}\right\}^{\frac{1}{2}} .$$

The symbols and units are defined in the list of symbols at the end of the text. The momentum coefficient, C_μ, based on gross wing area can be derived from C'_μ by writing

$$C_\mu = C'_\mu \frac{S'}{S} .$$

To measure the momentum coefficient on the tunnel model, it was therefore necessary either to know the pressure ratio and the throat area of the nozzle (assuming full flow in nozzle), or else the pressure ratio and the mass flow rate. Both methods were used. The spanwise distribution of total head at the nozzle was measured for a prescribed static pressure at the orifice plate, the latter being used during test runs to set the required mean pressure ratio at the nozzle. The throat area at the nozzle was calculated from the net span of the nozzle and the average depth, the latter being checked by feeler traverses. The mass flow rate was measured by standard orifice plates in the supply lines. The alternative methods agreed within 5%; values derived from actual mass flow measurements, which were the smaller as expected, have been used throughout.

Typical spanwise variations in nozzle depth and total head, P_D, are shown in Fig.6 for this model. The small variations found would not be expected to have had any large adverse effects on the results.

The formulae given above show how the sectional momentum coefficient, C'_μ, could be varied by altering one of three test variables, namely nozzle depth, pressure ratio, or wind speed. It has been established elsewhere[4] that the momentum coefficient is the primary parameter determining the effects of blowing. Usually, the momentum coefficient was varied by altering the pressure ratio. However, to obtain the higher values of the momentum coefficient, a few tests were made with the test speed reduced from 200 ft/sec to 140 ft/sec.

The principal range of conditions tested is summarised by the following table, page 9.

On the aircraft, it was envisaged that $C_\mu = 0{\cdot}031$ would be available. This would be equivalent to $C'_{\mu_F} = 0{\cdot}072$, $C'_{\mu_A} = 0$ (blowing over flap only) or $C'_{\mu_F} = C'_{\mu_A} = 0{\cdot}044$ (blowing over both flap and aileron), at which two conditions most of the present tests were therefore made. These are average values; the local sectional momentum coefficient varied inversely with the local wing chord because the nozzle depth was constant across the span of each control (see Section 4.2).

Spanwise extent of blowing	Test speed	C'_{μ_F}	C'_{μ_A}	C_μ	Pressure ratios	Flap angle β	Aileron angle ξ
Blowing over the flap only	200 ft/sec	0 0·020 0·035 0·051 0·072	0 0 0 0 0	0 0·009 0·015 0·022 0·031	Up to 3:1	Usually 45° or 60° (Also 65° and 75° at C'_{μ_F} = 0·072)	Usually 0° (Also 0° to 60° with β = 60°, C'_{μ_F} = 0·072)
	140 ft/sec	0·101 0·143	0 0	0·044 0·062	Up to 3:1		
Blowing over both the flap and the aileron	200 ft/sec	0 0·018 0·029 0·044	0 0·018 0·029 0·044	0·013 0·021 0·031	Up to 3:1	60°	Usually 30° or 45° (Also 0°, 15°, 60°, with $C'_{\mu_F} = C'_{\mu_A}$ = 0·044)

3.3 Corrections

Blockage corrections to $\frac{1}{2}\rho_o U_o^2$ have been calculated by Maskell's treatment[5], which allows for increased wake blockage when separations are present. It was found to be no longer satisfactory to apply a constant blockage correction, so a graduated allowance has been made as illustrated by the following table of typical values.

Flap and aileron	% correction to $\frac{1}{2}\rho_o U_o^2$		
	Low incidences	At stall	Above stall
Up	2%	5%	Up to 10%
Down	2-4%		

The following conventional tunnel constraint corrections were subsequently added:-

$$\Delta\alpha = 0{\cdot}879\, C_{L_{\text{no tailplane}}}$$

$$\Delta C_D = 0{\cdot}0153\, C_{L^2_{\text{no tailplane}}}$$

(Tailplane-on runs) $\Delta C_m = -0{\cdot}50 \left(\frac{d\,C_m}{d\,\eta_T}\right) C_{L_{\text{no tailplane}}}$ (η_T in degrees).

4 TEST RESULTS

4.1 Scope

The main results, described in para 4.2, were designed to establish the effects on the longitudinal static stability characteristics of varying both the amounts and the spanwise extent of blowing, for various combinations of flap and aileron angles, including the effect of local nozzle blockage to represent typical flap and aileron support gear. For these tests, a standard model configuration corresponding to take-off condition was adopted, with a full-span leading-edge deflection of 30° and a simulated weapon attached to the wing tip.

The remaining sections deal with the effects of various modifications to the standard configuration, a particular aim being to establish any interactions between such modifications and the effectiveness of blowing. Firstly, the effect of varying the leading-edge flap deflection is considered in para 4.3. The effect of a small sharp extension to the wing leading edge is examined in para 4.4. The effects of the tip weapon, a drop tank, an undercarriage assembly and an airbrake are discussed in para 4.5. Lastly, the effect of a foreplane in addition to the usual tailplane is considered in para 4.6.

4.2 The effect of blowing over the flap and the aileron

Three spanwise extents of blowing were investigated (see Fig.3b):

(i) blowing over the flap only (nozzle configuration A);

(ii) blowing over both the flap and the aileron (C);

(iii) blowing over the aileron only (J).

The majority of the tests were done with A or C.

It will be seen from Fig.3b that the nozzle depth was maintained constant over each control span, as was proposed for the aircraft. Thus, the sectional momentum coefficient varied inversely with the local wing chord across the flap and the aileron, increasing continuously from the inboard to the outboard end of each control in the same sense as the local control chord/wing chord ratio. The sectional momentum coefficient values quoted represent mean values equal to the true sectional values at mid-span of each control.

Most of these tests on the standard model configuration (see para 4.1) were done without tailplane; ranges of tailplane settings sufficient to establish the mean downwash at the tail and to permit estimation of the tailplane settings to trim were tested in a few principal cases.

4.2.1 Lift and stalling behaviour

Figs.7(a) and (b) show the effect of blowing over the flap only at flap angles of 45° and 60°, with the aileron undeflected. Figs.7(c),(d), and (e) show the effect of blowing over the flap alone and over both the flap and the aileron, with a flap angle of 60° and aileron angles of 15°, 30°, and 45° respectively.

The application of blowing substantially increased the lift coefficient at constant incidence, the most rapid rate of increase occurring at the lower values of the momentum coefficient, as might be expected. The lift-incidence curve slope was practically unaffected by blowing, but the stalling incidence was reduced by two or three degrees. Tuft observations showed the wing stall to originate from flow separations at the knee of the deflected leading-edge flap, which were aggravated by the increased loading when blowing was applied to the trailing-edge controls. The stalling behaviour could presumably have been improved by applying B.L.C. to the knee of the L.E. flap.

In order to examine the effects on lift in more detail, it is convenient to consider the changes in the lift coefficient at a constant incidence of +5°. The variation of $\Delta C_{L_{F+B}}$ with the flap angle β is shown in Fig.8, where $\Delta C_{L_{F+B}}$ is the increment produced by the flap and blowing, referred to the plain-wing lift coefficient at the same incidence. $\Delta C_{L_{F+B}}$ increased with β, attaining a flat-topped maximum at 60° for $C_\mu = 0{\cdot}031$, where the lift increment due to blowing was about 0·35. There was evidently no advantage to be gained in this instance from larger flap angles as far as lift was concerned, moreover the flap drag rose appreciably above $\beta = 60°$ (see para 4.2.2).

The variation of the lift increment with momentum coefficient is shown in Fig.9. Once attached flow was attained, further increases in momentum coefficient produced less rapid increases in the lift increment (Fig.9a). The value of the momentum coefficient needed for flow attachment increased noticeably as the flap angle was increased above 45°, with the nozzle located in the wing shroud. Some reduction in the momentum coefficient required for attachment at the larger flap angles could probably have been achieved by locating the nozzle on the nose of the flap.

At the same total momentum coefficient ($C_\mu = 0{\cdot}031$) expected to be available on the projected aircraft, the lift increment could be increased appreciably by drooping the aileron, especially when blowing was applied to both flap and aileron (Fig.9b). This can be seen more clearly in Fig.10, which shows the variations with aileron angle of both the flap + aileron lift increment and the aileron lift increment. With blowing over the flap only, a mean aileron droop of 15° would be feasible whilst retaining adequate aileron power over a differential range of ±15°. By applying the same total rate to both flap and aileron, an increase in mean aileron droop to 30° would be feasible, although with some reduction in the contribution of the down aileron.

The variation of $C_{L_{max}}$ with momentum coefficient (Fig.11) is similar to that of $\Delta C_{L_{F+A+B}}$. However, the beneficial effect of blowing on $C_{L_{max}}$ was smaller, since the stalling incidence (Fig.12) was reduced with T.E. blowing. As has been suggested already, this could have been precluded by suitable B.L.C. at the wing L.E.

Feasible combinations of flap and aileron angles, and blowing spans, are compared in Fig.13 at the total momentum coefficient ($C_\mu = 0{\cdot}031$) expected to be available in an aircraft application. The flap angle has been limited to 60° and the mean aileron droop to 15° (no aileron blowing) and 30° (with aileron blowing). Both no tailplane and trimmed lift curves are shown (using a typical aircraft C.G. position at $0{\cdot}30\bar{c}$); the trimmed curve for a flap angle of 60° (aileron undeflected) without blowing is included for comparison.

The application of blowing at the rate expected to be available ($C_\mu = 0{\cdot}031$) over the flap only with aileron undeflected increased the trimmed C_L at 5° incidence from 0·54 to 0·81 and the trimmed $C_{L_{max}}$ from 1·21 to 1·39. By drooping the aileron 30° with the same total jet momentum applied to both flap and aileron, further increases were obtained to 1·04 and 1·56 respectively.

To attain the projected aerodynamic performance at take-off, it was found essential to prescribe the best available configuration. Therefore, most of the remaining tests (para 4.3 - para 4.6) were made at $\beta = 60°$, $\xi = 30°$, $C'_{\mu_F} = C'_{\mu_A} = 0{\cdot}044$ ($C_\mu = 0{\cdot}031$), although a few measurements were also made for comparative purposes at $\beta = 60°$, $\xi = 0°$, $C'_{\mu_F} = 0{\cdot}072$, $C'_{\mu_A} = 0$ ($C_\mu = 0{\cdot}031$).

Comparison between measured and estimated flap lift increments are made in para 5.1. Predictions of the effect of blowing on stalling, take-off and approach speeds are given in Appendix 1.

4.2.2 Drag

Figs.14(a)-(e) show the effect of blowing on the C_D v. C_L curves for various combinations of flap and aileron angles. The quoted drag coefficients include any jet thrust which might have been recovered. Even so, at large flap angles the drag coefficient at constant C_L (below the stall) increased appreciably with C_μ unless the aileron was deflected. Large increases in lift-dependent drag due to flap have been noted previously with part-span blown flaps. The detailed effects of flap and aileron settings at constant C_μ are shown in Figs.15 and 16. By partial deflection of the aileron, so that the spanwise loading became more uniform and the discontinuity between the flap and aileron was reduced, these drag penalties could be reduced or even eliminated altogether.

The drag curves for the projected aircraft blowing rate are shown in Fig.17 (corresponding to the lift curves of Fig.13). Two trimmed curves are shown; at a given incidence, the changes of drag on trimming were appreciable. The combination which was suggested from lift considerations as that likely to be most suitable on the aircraft at take-off ($\beta = 60°$, $\xi = 30°$, $C'_{\mu_F} = C'_{\mu_A} = 0{\cdot}044$) also tended to minimise the drag. Since this particular combination would lead to a higher minimum drag speed (see Appendix 2), a larger flap angle might be preferred for landing.

The measured effects of blowing on drag are compared with estimates in para 5.2. The predicted effects on minimum drag and minimum drag speeds are discussed in Appendix 2.

4.2.3 Pitching moments

The effect of blowing on pitching moments is illustrated by Figs.18 to 20. Figs.18(a) to (e) show the effect of blowing on the C_m v. C_L curves, referred to the test C.G. position ($0{\cdot}367\bar{c}$) for various arrangements of trailing-edge flap and aileron angles. As would be expected, the application of blowing increased the nose-down pitching moment (as well as the lift) at constant incidence, the variation with C_μ being particularly rapid at the lower values of the momentum coefficient, when attached flow was being attained over the flap. There was a small destabilising tendency resulting from blowing at high incidences below the stall. Blowing increased the severity of the pitch-up at

the stall, as the pitching-moment values above the stall tended to revert to the values for the unblown condition. At a given tail-setting, the tail-on curves with and without blowing were less displaced than the corresponding no-tail curves, as a result of the increased downwash at the tail. At low incidences with flap blowing, the tailplane partially stalled at the more negative tail-settings (see, for example, Fig.18(d)).

For the projected aircraft configuration, Fig.19 shows the effect of flap angle, aileron angle, and spanwise extent of blowing, on the pitching-moment curves at $C_\mu = 0{\cdot}031$. Note, in particular, the large nose-down pitching-moment coefficients which have to be trimmed out, and which result in considerable trimming lift losses (see Fig.13).

Fig.20 shows the variation of downwash at tail, and tail-setting to trim, with α_w. The downwash curves for flap angles of 45° and 60° with no blow are coincident within experimental accuracy; this is reasonable, since the lift increments produced by the unblown flap at these angles were virtually the same. When blowing was applied to the flap, with the aileron undeflected, the downwash at constant α_w was increased and the value of $\frac{d\varepsilon}{d\alpha}$ also was increased, so that the longitudinal stability was decreased. With blowing over both deflected flap and aileron, there was a further small increase in downwash at the tail, but no further loss of stability.

The tail-setting angles to trim in Fig.20 have been evaluated at a typical aircraft C.G. position of $0{\cdot}30\bar{c}$, for the symmetrical tail without tailplane flap. For the blow-on curves at low wing incidences, the tail-settings to trim have been estimated by extrapolation assuming a linear tail lift slope, as the tailplane had stalled in the model tests. However, on the full-scale aircraft, with the tailplane flap deflected, it would probably be just possible to trim in the worst case, that is, at low to moderate wing incidences with blowing over deflected flap and aileron.

The ratios of measured pitching moment and lift increments at constant incidence due to the trailing-edge controls are compared with estimates in para 5.3.

4.2.4 The effect of local nozzle blockage to represent flap and aileron support gear

Normally, all tests were done with configurations A,C, or J (see Fig.3(b)), the nozzle depth being set by a series of 0·2 inch wide spacers at 1·47 inch pitch spanwise, occupying in all about 13% of the control span. To determine the effect of local nozzle blockage produced by the support gear arrangement likely to be used on the aircraft, some of these spacers were replaced by wider spacers (0·5" to 1·2") for repeat tests at the same total momentum coefficient, the pressure ratio being adjusted to compensate for changes in nozzle cross-sectional area. Also, in one case (configuration G) all the small spacers were removed and the gap set by the 6 BA retaining screws alone, to ensure that the usual spacers were not having any appreciable adverse effect.

The effect of nozzle blockage on lift is shown in Figs.21(a)-(c) for various flap and aileron combinations. Fig.21(c) shows that the performance of the usual configuration, C, could be slightly improved by removing the 0·2 inch wide spacers (G). However, after due allowance has been made for the difference in momentum coefficient, the improvement in C_L was only about 0·01, with a somewhat larger increase in $C_{L_{max}}$. Thus, the usual test configurations A,C, and J represented a good nozzle installation.

The lift losses which resulted from introducing the wider spacers (0·5 - 1·2 inches model-scale) were, however, appreciable and demonstrate the desirability of avoiding such blockages. Tuft studies on the flap aft of a 1·2 inch spacer showed that a wedge of separation emanated from the unblown portion of the span and spread outboards and inboards towards the trailing-edge of the flap. On the other hand, no such wedge was detected behind the usual 0·2 inch wide spacer.

Configurations E,F,H, each having 2 inch span of wide spacers, behaved much the same (Fig.21(c)). So also did configurations, D,I, which each had 2·7 inch span of wide spacers. The lift losses, 0·12 and 0·16 respectively, were in the same ratio. This suggests that the span of wide blockage may be a useful parameter in determining the order of the lift loss which will occur. In two cases, H and I, the nozzle depth was increased locally next to the wide spacers to compensate for the local reduction in blowing rate but this clearly had negligible remedial effect.

As seems reasonable, the lift loss resulting from a given blockage was larger at lower values of the momentum coefficient and increased with flap angle (Fig.22(a)). The lift loss can easily be 20% to 30% of the increment due to blowing with moderate blockages quite likely to be encountered in practice without careful design.

4.3 The effect of the leading-edge flap

The leading-edge flap was usually deflected 30° (normal to hinge line) whenever the trailing-edge controls were deflected. However, some tests were done with a range of leading-edge flap settings, both for the plain-wing case and also with blowing over deflected trailing-edge flap and aileron.

The beneficial influence of deflecting the leading-edge flap on maximum lift and stalling incidence (Fig.23(a)) is seen to have been very large*, particularly when the trailing-edge controls were deflected; at low incidences, the loss of lift at constant incidence which resulted from deflecting the leading-edge flap was scarcely noticeable. The stalling behaviour of the wing with the leading-edge flap deflected could presumably have been improved still further by applying slot blowing or distributed suction at the knee of the leading-edge flap, as tuft studies showed that the initial separations occurred at the knee of the flap.

---

*The leading-edge separations which occurred with the leading-edge flap undeflected could have been reduced, with consequent improvements in $C_{L_{max}}$ and stalling incidence, by applying some nose camber.

Fig.23(b) shows the effect of the leading-edge flap on drag. At the higher incidences, the drag at constant C_L was larger with the flap undeflected, as a result of the more extensive separations. Even with the leading-edge flap deflected, the C_D v. C_L^2 curve remained linear only over a small incidence range, because the tip stall started to spread inboard at comparatively low incidences.

Finally, Fig.23(c) shows the effect of the leading-edge flap on pitching moments; both tailplane-off and tailplane-on curves are given for the plain-wing case, but only the tailplane-off condition was tested with trailing-edge controls deflected. The tailplane-on curves show that the pitch-up for the plain-wing case was more severe when the leading-edge flap was deflected, but occurred at a higher lift coefficient. With the trailing-edge controls deflected, there was a pitch-up in all the no-tailplane curves; the pitch-up occurred at higher lift coefficients, and was somewhat more severe, when the leading-edge flap was deflected.

4.4 The effect of the sharp wing leading-edge extension

The effect of adding a symmetrical sharp 1·019% chord extension to the basic wing section (RAE 102, 6% t/c along stream) is considered here. The effect on lift is shown in Fig.24(a). With the leading-edge flap undeflected, the sharp extension had negligible effect at moderate incidences, although reducing $C_{L_{max}}$ by 0·06 and the stalling incidence by about 2 degrees. With the leading-edge flap deflected 30°, the losses were even smaller, being about 0·02 and 1 degree respectively. This is reasonable, since the stall was then determined more by conditions at the knee of the leading-edge flap, rather than by the section shape at the wing leading edge.

Fig.24(b) shows the effect of the sharp extension on drag. With both leading-edge and trailing-edge controls undeflected, there was a drag penalty which increased with C_L, being zero at zero C_L. With the leading-edge flap deflected, there was then a drag penalty at low incidences, particularly with the trailing-edge controls undeflected (due to increased lower surface separations from the sharpened leading edge). The penalty over the working C_L range was, however, quite small. In particular, once blowing was applied to the deflected trailing-edge controls, the drag changes due to the sharp extension were negligible over the working range of C_L.

Fig.24(c) shows that the pitching-moment effects of sharpening the leading edge were not large.

4.5 The effects of the tip weapon, drop tank, main undercarriage assembly, and airbrake

Usually, tests were made with the tip weapon attached, and with the drop tank, main undercarriage assembly, and airbrake off. This was proposed as the standard aircraft configuration just after take-off, which was expected to be most critical.

4.5.1 Tip weapon

When the tip weapon was removed, the lift incidence curve slope (Fig.25(a)) was reduced by between 7% and 11%, whilst the lift increment due to the controls was reduced by about 4%. The stalling incidence was increased, however, and $C_{L_{max}}$ was virtually unaffected. An unexplained kink was introduced into the lift curve for one case ($\beta = 60°$, $\xi = 30°$; $C'_{\mu_F} = C'_{\mu_A} = 0{\cdot}044$).

The corresponding no-tailplane variations of C_D with C_L^2 are shown in Fig.25(b). The removal of the weapon did not affect the drag at zero lift, but did tend to increase the rate of growth with C_L^2. With blowing over deflected controls, the drag coefficient at constant C_L was increased considerably. The observed variation in effective induced drag factor would correspond to a 12% reduction of effective aspect ratio and a 5% reduction in lift-curve slope, which agrees better with the observed reduction in flap lift increment than the observed effect on lift-curve slopes.

Removal of the tip weapon did not produce very large changes in longitudinal stability (Fig.25(c)), although there were noticeable kinks in both the tailplane-on and tailplane-off curves corresponding to the kink in the lift curve already noted.

4.5.2 Main undercarriage assembly and airbrake

Adding the main undercarriage assembly* caused small reductions in C_L at constant incidence and in $C_{L_{max}}$ (see Fig.26(a)) of the order 0·01 to 0·03; addition of the airbrake resulted in further small reductions of the same order. The corresponding drag increments at constant C_L were about 0·015 for the undercarriage and 0·05 for the airbrake (see Fig.26(b)). Some changes in nose up trim occurred, particularly on addition of the airbrake, but the stability was unaltered (Fig.26(c)).

4.5.3 Drop tank

The effect of adding the drop tank was measured. It was also tested in one condition in conjunction with the main undercarriage assembly, in case there was any interference between the two, but no interference was found.

Addition of the drop tank resulted in a reduction of C_L at constant incidence of about 0·04 both with and without blowing (see Fig.27(a)). The reduction in $C_{L_{max}}$ was somewhat larger, up to 0·07. The drop tank was normally set parallel to fuselage datum; increase of drop tank incidence by 3° to be parallel to the wing did not reduce the lift penalty of the drop tank.

---

*Consisting of the main undercarriage and the front undercarriage door (see Fig.4).

Despite the noticeable effect on C_L at constant incidence, the drag curves with and without the drop tank were virtually coincident below the stall (see Fig.27(b)). Addition of the drop tank caused small trim changes and tended to reduce the longitudinal stability at high lift coefficients.

4.6 The effect of a foreplane

Brief tests were made with a foreplane added (see Fig.4), both with and without the tailplane, to try to reduce the considerable trimming losses (para 4.2.3). However, the practical results produced by the foreplane were disappointing. Since the wing was not in the usual canard position at the rear end of the fuselage, the foreplane arm was small and the downwash produced by the foreplane on the inboard wing was comparatively large. Moreover, with a tapered wing the overall effect tended to be accentuated.

The foreplane therefore failed to produce appreciable gains in lift on trimming (Figs.28(a) and 29(a)), although the pitching-moment curves (Figs.28(c) and 29(c)) show that the required positive pitching-moment increments were produced. In order to understand these results, it is necessary to separate the lift increment of the foreplane (C_{L_F}) and the interference wing lift ($C_{L_{WF}}$) due to the change of downwash created by the foreplane (both C_{L_F} and $C_{L_{WF}}$ being referred to the gross wing area S). The lift and pitching moment increments produced by the foreplane can be written approximately as:-

$$\Delta C_L = C_{L_F} + C_{L_{WF}}$$

$$\Delta C_m = \left(\frac{dC_m}{dC_L}\right)_{\text{Foreplane only}} \times C_{L_F} + \left(\frac{dC_m}{dC_L}\right)_{\text{wing only}} \times C_{L_{WF}}$$

where experimental values of $\left(\frac{dC_m}{dC_L}\right)_{\text{wing only}}$ have been used and the value of $\left(\frac{dC_m}{dC_L}\right)_{\text{Foreplane only}}$ has been taken as 1·29 (the distance in terms of $\bar{c}$ of the mean quarter-chord point of the foreplane ahead of the test C.G. position). The results of the analysis are shown in Fig.30. The foreplane lift is a function of $(\alpha_w + \eta_F)$, the foreplane incidence relative to wind, and is almost zero at $\alpha_w + \eta_F = 0$. However, the interference lift is of the same magnitude as C_{L_F}, and is negative at usable foreplane incidences, with a negative overall lift increment.

A corresponding analysis of the results of other tests where the foreplane arm was $1{\cdot}97\bar{c}$, yielded similar results, but with reduced values of $C_{L_{WF}}$, so that

positive trimming lift increments could be obtained. Although the use of a variable-incidence foreplane was not profitable in the present case, a successful application might well be possible with such an arrangement.

5 COMPARISON BETWEEN THE ESTIMATED AND THE MEASURED EFFECTS OF BLOWING

5.1 Comparison of values of $\Delta C_{L_{F+A+B}}$ at $\alpha_w = 5^\circ$

Direct theoretical estimates have been prepared, (based on Refs. 6-11), as for the Venom[1], of the lift increments due to the blown flap (or aileron), using a modified Jet Flap method at values of C'_μ above that necessary for attaching the flow, and a conventional empirical method to estimate the unblown lift; the portion of the curve for low values of C'_μ being sketched in accordance with the nearest experimental results available. Fig.31 shows the comparison which results for blowing over the flap only, with aileron undeflected, at flap angles of 45°, 60° and 75°. The agreement at 45° is reasonable, but the estimated additional lift increments produced by further increases of flap angle to 60° and 75° were not realised in practice. A similar, but less pronounced, effect occurred on the Venom[1]; on the Supermarine Scimitar[2], the comparison resembled that in the present case. Thus, although a reasonable estimate could be made of the order of lift increment to be expected from a blown flap at moderate flap angles, sufficiently accurate for choosing a control configuration for a particular project, the detailed effect of flap angle changes, and the actual magnitude of the lift increment produced by the blown flap could not be predicted reliably by this method.

Fig.32 shows a comparison between the estimated and the measured aileron lift increments, $\Delta C_{L_{A+B}}$, both no blow and with blow. The agreement is better here, since the angles involved are smaller, although the behaviour above $\xi = 45^\circ$ with $\beta = 60^\circ$ was not predicted.

An alternative scaling method is illustrated by Fig.33. Here, the lift increments measured in other experiments with blown flaps, preferably on wings of similar planform, aspect ratio, and flap geometry, have been scaled by the appropriate factor and the resulting curves used as estimates for the new arrangement. To derive the appropriate factors, we may put, following Ref.11,

$$\text{Estimated } \Delta C_{L_{\text{Flap+Blow}}} = \frac{a_1}{2\pi} \times \lambda_3 \times f(\beta) \times \left(\frac{dC_L}{d\beta}\right)_{\frac{c_f}{c}} \times \beta \qquad (1)$$

For small values of C'_μ,

$$\left(\frac{dC_L}{d\beta}\right)_{\frac{c_f}{c}} \simeq \frac{\lambda_1\left(\frac{c_f}{c}\right)}{\lambda_1\left(\frac{c_f}{c} = 0{\cdot}2\right)} \left(\frac{dC_L}{d\beta}\right)_{\frac{c_f}{c} = 0{\cdot}2} \qquad (2)$$

therefore at a given flap angle and value of C'_μ,

$$\Delta C_{L_{F+B}} \propto \frac{a_1}{2\pi} \times \lambda_3\left(\frac{b_f}{b}\right) \times \frac{\lambda_1\left(\frac{c_f}{c}\right)}{\lambda_1\left(\frac{c_f}{c} = 0{\cdot}2\right)} \quad . \tag{3}$$

This formula applies equally well for an unblown flap. In either case, we can use the ratio of this product as a conversion factor at a prescribed angle.

Fig.33 shows the result of applying such a factor, to the increments measured in tests of the D.H. Sea Venom[1] and the Supermarine Scimitar[2], to provide estimates for the present configuration. These test results have been used to make estimates for the case of blowing over the flap only at angles of 45°, 60°, and 75°, with the aileron undeflected (Fig.33). The estimates are in reasonable agreement with the experimental results, and the effect of flap angle is more accurately predicted than by thin aerofoil theory.

In the full-span case, Fig.33(b), this scaling method was found to be equally successful for comparing subsequent tests of a sweptback wing[3] and the present tests. The conversion factor used was the ratio of the terms

$$\frac{a_1}{2\pi}\left\{\left[\lambda_3\left(\frac{b_f}{b}\right) \times \frac{\lambda_1\left(\frac{c_f}{c}\right)}{\lambda_1(0{\cdot}2)} \times f(\beta)\beta\right]_{\text{Flap}} + \left[\lambda_3\left(\frac{b_f}{b}\right) \times \frac{\lambda_1\left(\frac{c_f}{c}\right)}{\lambda_1(0{\cdot}2)} \times f(\beta)\beta\right]_{\text{Aileron}}\right\}$$

for the two configurations.

5.2 Comparison of values of zero-lift drag

Estimates have been made of zero-lift drag by conventional methods and also incorporating an additional empirical correction for blown flaps[12]. These estimates are compared in Figs.34,35 with experimental values of the nominal zero-lift drag obtained by extrapolating the C_D v. C_L^2 curves to zero C_L.

Although the conventional method gives reasonable agreement for the unblown flap (Fig.34(a)), the drag of the blown flap exceeds the estimate (Fig.34(b)). Such a discrepancy has been found in other tests with part-span blown flaps, and an empirical method is given in Ref.12 which allows revised estimates for the blown flap, which are in better agreement with experiment.

Fig.35 shows the variation of zero-lift drag with aileron angle, at a flap angle of 60° with blowing over both controls. The unblown flap estimates are again in good agreement with experiment. The conventional blown flap estimates are low, particularly at $\xi = 0°$ and 60°, and better agreement can be obtained by including the additional empirical correction. For intermediary aileron angles, where the discontinuity between the flap and the aileron is

smaller, there is less discrepancy between the conventional method and the experimental results.

5.3 Comparison of no-tail values of $\left(\frac{\Delta C_m}{\Delta C_L}\right)_{F+A+B}$ at $\alpha_w = 5°$

Values of $\left(\frac{\Delta C_m}{\Delta C_L}\right)_{F+A+B}$ referred to the mean quarter-chord position are given in the following table:-

β	ξ	C'_{μ_F}	C'_{μ_A}	Mean quarter chord values of $\left(\frac{\Delta C_m}{\Delta C_L}\right)_{F+A+B}$
45°	0°	0 to 0·143	0	-0·40
60°	0°	0 0·020 0·035 to 0·143	0	-0·36 -0·38 -0·39
60°	30°	0 0·018 0·029 0·044	0 0·018 0·029 0·044	-0·38 -0·38 -0·39 -0·39
60°	45°	0 0·018 0·029 0·044	0 0·018 0·029 0·044	-0·39 -0·39 -0·40 -0·40

As in the case of the Sea Venom[1], the values tend to become more negative as the momentum coefficient is increased. Estimates have been prepared, making allowance for wing sweep, taper, and the spanwise extent of the flaps, and also for the variation of $\Delta C_{L_{F+A+B}}$ with a_1. For the unblown flap, using Ref.11, the resulting estimate was about -0·44. The estimate for the blown flap, using Ref.8, was -0·46.

The following table shows for comparison other experimental results[1,2,13] on blown flaps.

	$\frac{a_1}{2\pi}$	Mean hinge line distance aft of mean quarter chord position	Blow	Values of $\left(\frac{\Delta C_m}{\Delta C_L}\right)_{F+A+B}$
D.H. Sea Venom	0·725	$0·52\bar{c}$	Off	-0·20
			On	-0·25
S.R.177	0·54	$0·53\bar{c}$	Off	-0·38
			On	-0·40
Supermarine Scimitar	0·47	$0·55\bar{c}$	Off	-0·36
			On	-0·39
N.P.L. Delta	0·37	$0·60\bar{c}$	Off	-0·42
			On	-0·45

As expected, the value of $\left(\frac{\Delta C_m}{\Delta C_L}\right)$ increases substantially in magnitude as a_1 decreases since ΔC_L (but not ΔC_m) depends on a_1. The effect of rearward movement of hinge-line position is also important. The usual effect of blowing is to make $\left(\frac{\Delta C_m}{\Delta C_L}\right)$ more negative by about -0·03. Thus, when unblown plain flap values of $\left(\frac{\Delta C_m}{\Delta C_L}\right)$ are available, the corresponding values with a blown flap can be predicted with reasonable accuracy.

6 CONCLUSIONS

Low speed longitudinal stability measurements have been made on a delta-wing aircraft model of aspect-ratio 2·9 and 40° leading-edge sweepback (S.R.177), with shroud blowing over trailing-edge flaps and ailerons.

With blowing over the flap alone at a flap angle of 60° (with aileron undeflected), increases were obtained of 0·27 in trimmed C_L at constant incidence and of 0·18 in trimmed $C_{L_{max}}$, at the value of C_μ (0·031) envisaged for the projected aircraft. Corresponding reductions in take-off and landing speeds of about 10 knots could be expected in a typical practical configuration.

By distributing the same total jet momentum to flap and aileron, with 30° aileron mean droop, further increases of 0·23 in trimmed C_L and 0·17 in trimmed $C_{L_{max}}$ were obtained, corresponding to additional reductions of about 8 knots in aircraft speeds.

Large trim changes resulted from blowing, and the associated trimming lift losses were appreciable. A trimming foreplane was tested to try to reduce these losses, but was unsuccessful because of the strong downwash produced at

the wing with a conventional wing position and the short foreplane arm feasible in the present case.

The beneficial effect of the leading-edge flap was large, amounting to 5° increase of stalling angle and 0·30 increase in $C_{L_{max}}$ with blowing over trailing-edge flaps and ailerons. With the L.E. flap deflected, the wing stalled as a result of the inboard spread of separations from the flap knee, and sharpening of the nose was only found to have minor adverse effects. Additional B.L.C. could have been applied at the knee of the deflected L.E. flap to further improve the stalling incidence and maximum lift.

The measured effects of blowing correlated well with the results of other model tests involving similar wing-flap arrangements. In particular, part-span blown flaps were again found to produce large drag increments significantly affecting the aircraft minimum drag speed.

For completeness, predictions have been included of the effect of blowing on stalling, take-off, and landing speeds, as well as on minimum drag speeds and minimum drag, for the projected aircraft configuration.

7 ACKNOWLEDGEMENTS

Saunders-Roe constructed the model and provided some staff to assist with testing and analysis of results.

LIST OF REFERENCES

No.	Author(s)	Title, etc
1	Butler, S.F.J., Guyett, M.B.	Low-speed wind-tunnel tests on the De Havilland Sea Venom with blowing over the flaps. A.R.C. R. & M. 3129. February, 1957.
2	Anscombe, A., Butler, S.F.J.	Low-speed wind-tunnel tests on the Vickers-Supermarine N.113 (Scimitar) with blowing over the flaps. Unpublished I.o.A. Report.
3	Butler, S.F.J.	Low-speed wind-tunnel tests on a sweptback wing model with blowing at the wing leading edge and blowing over the flaps and ailerons. Unpublished I.o.A. Report.

LIST OF REFERENCES (Contd)

No.	Author(s)	Title, etc
4	Anscombe, A., Williams, J.	Some comments on high-lift testing in wind tunnels with particular reference to jet-blowing models. A.G.A.R.D. Report No.63. Journ. Roy. Ae. Soc. 61 (560) 529-40. August, 1957.
5	Butler, S.F.J., Williams, J.	Further comments on high-lift testing in wind tunnels with particular reference to jet-blowing models. Aero. Quart. 11. August, 1960.
6	Williams, J. Butler, S.F.J.	Aerodynamic aspects of boundary layer control for high lift at low speeds. Journ. Roy. Ae. Soc. 67 (628). April, 1963.
7	-	Royal Aeronautical Society Aerodynamic Data Sheets.
8	Spence, D.A.	The lift on a thin aerofoil with a blown flap. Aero. Quart 9 part 3, August, 1958, 287-299.
9	Keune, F.	Auftrieb einer geknickten eberen platte. Luftfahrtforschung Vol.13, 1936. (Translated in N.A.C.A. T.M. 1340).
10	Hay, J.A., Eggington, W.J.	An exact theory of a thin aerofoil with large flap deflection. Aerodynamics Department Report Vickers-Armstrong (Aircraft) Limited. April, 1956.
11	Young, A.D.	The aerodynamic characteristics of flaps. A.R.C. R. & M. 2622. February, 1947.
12	Butler, S.F.J.	The drag increments associated with part-span blown flaps. Unpublished M.o.A. Report.

LIST OF REFERENCES (Contd)

No.	Author(s)	Title, etc
13	Williams, J., Alexander, A.J.	Some exploratory jet-flap tests on a 60° Delta Wing. A.R.C. R. & M. 3138. March, 1957.
14	-	S.R.177 Low speed aerodynamic characteristics with flap and aileron blowing. Saunders-Roe Publication No. T.P.251. June, 1957.

NOTATION

A	aspect ratio of wing
a_1	lift slope
c_f	local flap chord
c	local wing chord
$\bar{c}$	standard mean chord
$\bar{\bar{c}}$	aerodynamic mean chord
C_D	drag coefficient (including any jet thrust recovered)
C_L	lift coefficient
$C_{L_{max}}$	maximum lift coefficient
C_m	pitching-moment coefficient based on $\bar{\bar{c}}$, at test C.G. $(0{\cdot}37\bar{\bar{c}})$
C_{L_F}	lift coefficient generated on the foreplane, based on S
$C_{L_{WF}}$	interference lift coefficient generated on wing, due to presence of the foreplane, based on S
ΔC_{L_B}	lift increment at constant incidence due to blowing, referred to unblown-flap C_L
$\Delta C_{L_{A+B}}$	lift increment at constant incidence due to aileron + blow, referred to C_L with unblown and undeflected aileron, and constant flap angle and blowing condition
$\Delta C_{L_{F+B}}$	lift increment at constant incidence due to flap + blow, referred to plain-wing C_L
$\Delta C_{L_{F+A+B}}$	lift increment at constant incidence due to flap + aileron + blow, referred to plain-wing C_L
$\left(\frac{\Delta C_m}{\Delta C_L}\right)_{F+A+B}$	ratio of no-tail increments in C_m and C_L at constant incidence, referred to plain-wing C_L (C_m referred to mean-quarter-chord position on wing)
$C_\mu = \frac{\dot{m} v_j}{\frac{1}{2}\rho_o U_o^2 S_g} = C'_\mu \frac{S'}{S}$	momentum coefficient based on gross wing area

NOTATION (Contd)

$C'_{\mu_F} = \dfrac{m_F v_j}{\frac{1}{2} \rho_o U_o^2 S'_F g}$ mean sectional momentum coefficient for flap

$C'_{\mu_A} = \dfrac{m_A v_j}{\frac{1}{2} \rho_o U_o^2 S'_A g}$ mean sectional momentum coefficient for aileron

$\left(\dfrac{dC_L}{d\beta}\right)_{\frac{c_f}{c}}$ theoretical flap effectiveness factor[9]

D predicted drag in lb during normal approach at A.U.W. of 17,000 lb

D_{min} minimum value of D

$f(\beta)$ theoretical reduction in flap effectiveness at large flap angles[10,11]

m mass flow rate (lb/sec)

m_F mass flow rate to flap nozzle

m_A mass flow rate to aileron nozzle

p_D total head at nozzle (absolute)

p_o tunnel static pressure (absolute)

S wing area (projected)

S' blown wing area

S'_F blown wing area spanned by flap

S'_A blown wing area spanned by aileron

S'' blowing nozzle cross-sectional area

T_D supply temperature, degrees absolute

U_o tunnel speed (ft/sec)

v_j jet velocity after expansion to free stream static pressure

NOTATION (Contd)

$V_{D_{min}}$	minimum drag speed (knots)
V_s	stalling speed (knots)
α_s	wing stalling incidence
α_w	wing incidence (degrees)
β	flap angle
δC_D	drag discrepancy
ε	downwash angle (degrees)
η_F	foreplane setting relative to wing (degrees)
η_T	tail setting relative to wing (degrees)
$\lambda_1\left(\frac{c_f}{c}\right)$	control-chord ratio factor[12]
$\lambda_2(\beta)$	flap angle factor for unblown plain flap[12]
$\lambda_3\left(\frac{b_f}{b}\right)$	part-span lift conversion factor[12]
ξ	aileron angle (degrees)
ρ_o	mainstream density
$\frac{1}{2}\rho_o U_o^2$	tunnel dynamic head, expressed in lb/sq ft in the momentum formula

APPENDIX 1

THE PREDICTED EFFECT OF BLOWING OVER THE FLAP AND THE AILERON ON STALLING, TAKE-OFF, AND LANDING SPEEDS OF THE SAUNDERS-ROE P.177

Stalling speeds have been predicted for the projected aircraft from the trimmed values (C.G. at $0{\cdot}30\bar{c}$) of the maximum lift coefficient measured on the tunnel model, without any allowance for possible increases in $C_{L_{max}}$ at full-scale Reynolds number. The standard model configuration (L.E. flap deflected 30°, tip weapon on, drop tank, undercarriage assembly, and airbrake off) has been used. Take-off and landing weights of 28,300 and 17,000 lb respectively have been assumed[14]. Take-off and approach speeds based on $1{\cdot}10\ V_s$ (rocket-assisted take-off) and $1{\cdot}25\ V_s$ respectively are given in the following tables:-

Take-off (A.U.W. 28,300 lb)

β	ξ	C'_{μ_F}	C'_{μ_A}	C_μ	Trimmed $C_{L_{max}}$	Stalling speeds in knots	Take-off speed in knots
60°	0°	0	0	0	1·21	145	160
60°	0°	0·072	0	0·031	1·39	135	149
60°	30°	0·044	0·044	0·031	1·56	128	141

Approach (A.U.W. 17,000 lb)

β	ξ	C'_{μ_F}	C'_{μ_A}	C_μ	Trimmed $C_{L_{max}}$	Stalling speeds in knots	Approach speed in knots
60°	0°	0	0	0	1·21	113	141
60°	0°	0·072	0	0·031	1·39	105	131
60°	30°	0·044	0·044	0·031	1·56	99	124

The incorporation of blowing over the trailing-edge flap alone, without deflecting the aileron, ought to reduce the take-off and approach speeds by about 10 knots (relative to the unblown flap deflected 60°). With the same total blowing quantity applied over the flap and drooped aileron, further reductions of about 8 knots should be possible.

APPENDIX 2

THE PREDICTED EFFECT OF BLOWING ON MINIMUM DRAG AND MINIMUM DRAG SPEED

Figs.36 and 37 show the variation of absolute drag (in lb) with approach speed, as predicted from the tunnel tests, at an A.U.W. of 17,000 lb, trimmed for a C.G. at $0{\cdot}30\bar{c}$.

Fig.36 shows the effects of the weapon, the main undercarriage assembly, and the airbrake, with blowing over deflected flap and aileron. Removal of the weapon increased the drag coefficient at constant lift coefficient, increasing minimum drag from 4710 to 5200 lb. The corresponding effects on $V_{D_{min}}$ and $\frac{V_{D_{min}}}{V_s}$ were small, removal of the weapon increasing $V_{D_{min}}$ from 125 knots to 128 knots, and correspondingly increasing the ratio $\frac{V_{D_{min}}}{V_s}$ from 1·26 to 1·28. Addition of the main undercarriage assembly reduced $V_{D_{min}}$ from 125 to 123 knots, and reduced $\frac{V_{D_{min}}}{V_s}$ from 1·26 to 1·23, whilst at the same time increasing D_{min} from 4710 to 5000 lb. On adding the airbrake as well as the undercarriage $V_{D_{min}}$ and $\frac{V_{D_{min}}}{V_s}$ were further reduced to 119 knots and 1·18 respectively, whilst D_{min} was increased to 5860 lb.

Fig.37 shows the effects of blowing and aileron angle on the drag variation with speed, with both the main undercarriage assembly and the airbrake on. At $\beta = 60°$, with the aileron undeflected, blowing over the flap reduced $V_{D_{min}}$ from 133 to 110 knots and reduced $\frac{V_{D_{min}}}{V_s}$ from 1·16 to 1·03, as a result of the additional drag term (see para 5.2), whilst the minimum drag was increased by nearly 1000 lb from 5440 lb to 6360 lb. When the aileron was deflected, with blowing over both flap and aileron, the additional drag was reduced, and the behaviour was more like that of the unblown flap, with $V_{D_{min}}$ = 119 knots, $\frac{V_{D_{min}}}{V_s}$ = 1·18, and a minimum drag of 5860 lb.

On the aircraft, the approach speed would be expected to lie between $1{\cdot}25\ V_s$ and $1{\cdot}33\ V_s$; thus, there would be no necessity to approach below the minimum drag speed unless both the undercarriage and airbrake were retracted.

TABLE 1

Model data

All dimensions model scale ($\frac{1}{2}$th scale half-model, starboard wing only).

Wing (one wing only)

Area (projected) S	10·19 sq ft
Semi-span (excluding weapon) b/2	3·42 ft
Standard mean chord $\bar{c}$	2·97 ft
Aerodynamic mean chord $\bar{\bar{c}}$	3·21 ft
$\bar{c}/\bar{\bar{c}}$	0·925
Aspect ratio (full span) A	2·29
Section	RAE 102
Position of maximum thickness	0·356c
Thickness-chord ratio	0·06
Centre-line projected chord	4·42 ft
Tip chord	1·54 ft
Sweepback of quarter-chord line	32·3°
Sweepback of leading edge	40·2
Sweepback of trailing edge	0°
Taper ratio (centre-line chord/tip chord)	2·87
Anhedral	5°
Wing-fuselage angle	3°
Distance of mean quarter-chord point aft of L.E. apex	2·01 ft

Leading edge flap

Inboard limit (fraction semi-span)	0·19
Outboard limit (fraction semi-span)	0·95
Control chord ratio (constant ratio across the span)	0·13

Trailing edge flap

Inboard limit (fraction semi-span)	0·21
Outboard limit (fraction semi-span)	0·61
Mean control chord ratio	0·17
Chord (constant across span)	0·57 ft
Area of wing spanned by flap S'_F	4·45 sq ft = 0·437S

Trailing edge aileron

Inboard limit (fraction semi-span)	0·61
Outboard limit (fraction semi-span)	1·00
Mean control chord ratio	0·21
Chord (constant across span)	0·45 ft
Area of wing spanned by aileron S'_A	2·81 sq ft = 0·276S

TABLE 1 (Contd)

Tailplane (half-tailplane only)

Area S_t	2·05 sq ft
Semi-span $b_t/2$	1·62 ft
Standard mean chord $\bar{c}_t$	1·28 ft
Aerodynamic mean chord $\bar{\bar{c}}_t$	1·40 ft
Aspect ratio (full span) A_t	2·51
Section	RAE 102 (modified)
Position of maximum thickness	0·343c
Thickness - chord ratio	0·06
Centre-line chord	1·95 ft
Tip chord	0·58 ft
Sweepback of quarter-chord line	32·3°
Sweepback of leading edge	40·1°
Sweepback of trailing edge	0°
Taper ratio	3·25
Anhedral	0°
Distance of mean quarter-chord point aft of L.E. apex	0·92 ft
Distance of hinge point aft of L.E. apex	1·00 ft
Distance of hinge point above wing chord plane	2·28 ft
Distance of hinge point above fuselage datum	2·08 ft

General

Overall length	12·625 ft
Fuselage nose to wing L.E. apex	4·25 ft
Wing L.E. apex to tailplane L.E. apex	6·45 ft

Test C.G. Position

Below centre-line wing chord	0·04 ft
Above fuselage datum	0·02 ft
Aft of projected wing apex	2·39 ft
Aft of leading edge of S.M.C.	0·376$\bar{c}$
Aft of leading edge of A.M.C.	0·367$\bar{c}$

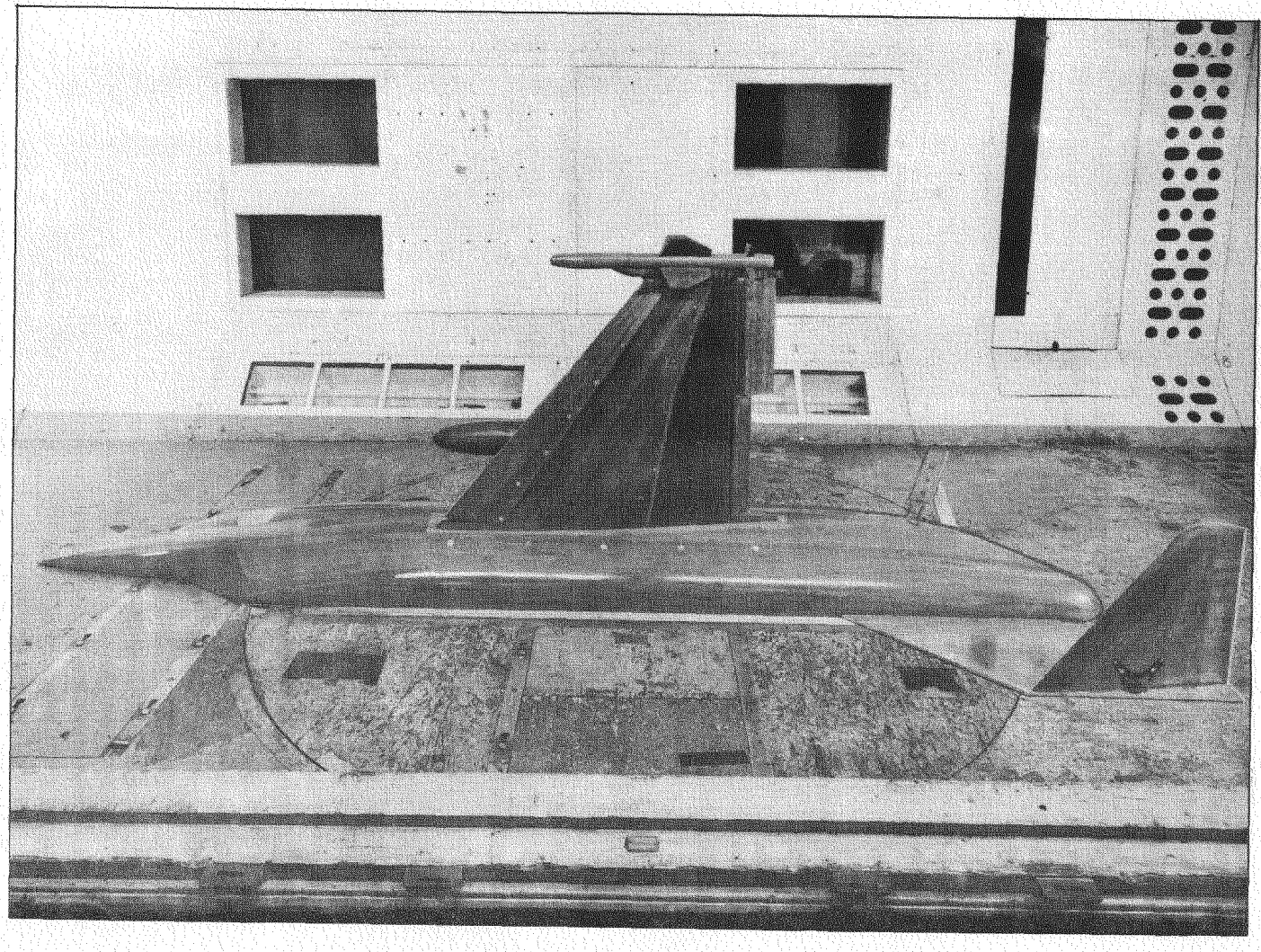

FIG.1. S.R. 177 HALF MODEL IN R.A.E. No 2
11½ ft. x 8½ ft. WIND TUNNEL

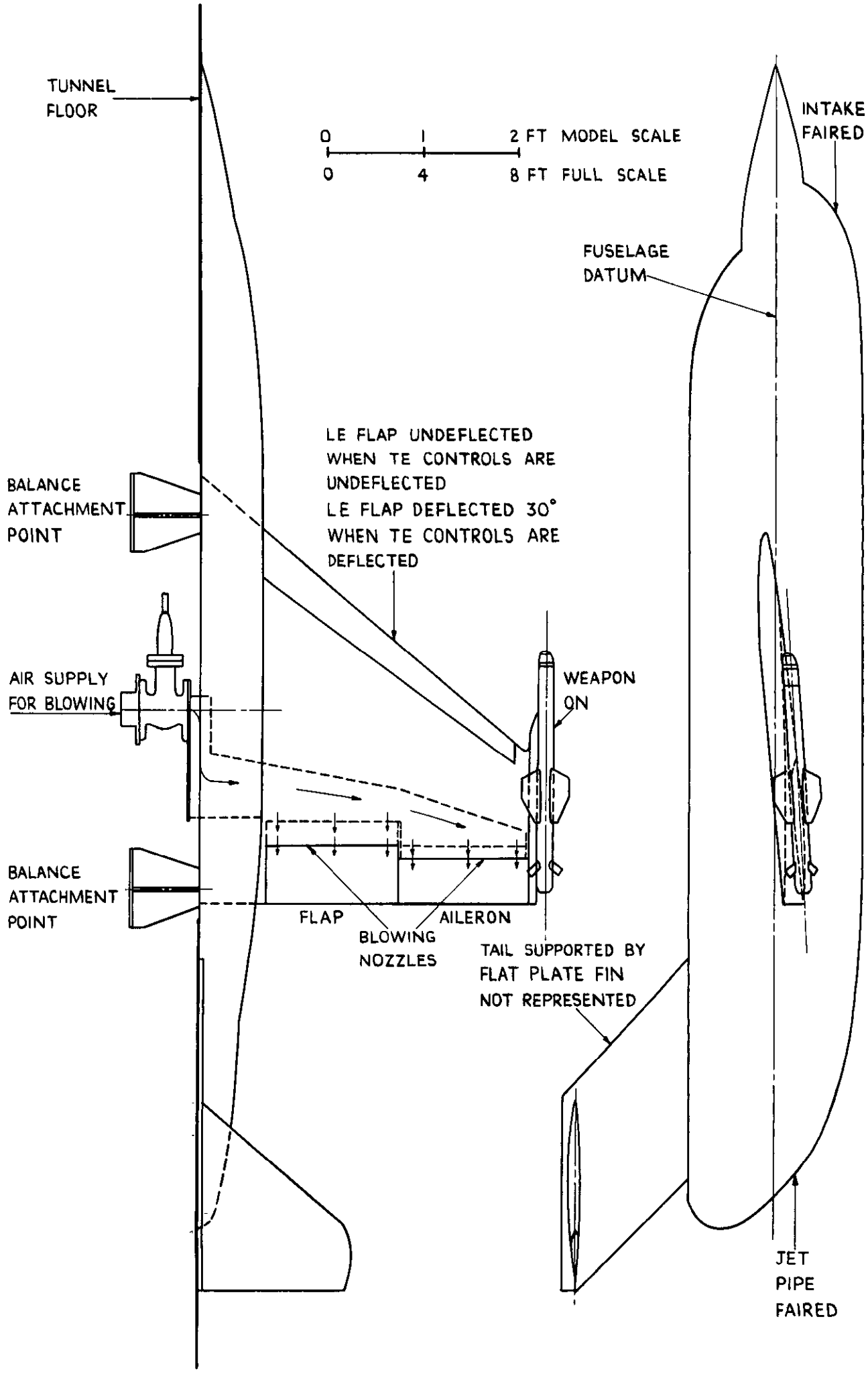

FIG. 2. G.A. OF MODEL IN STANDARD TEST CONDITION.

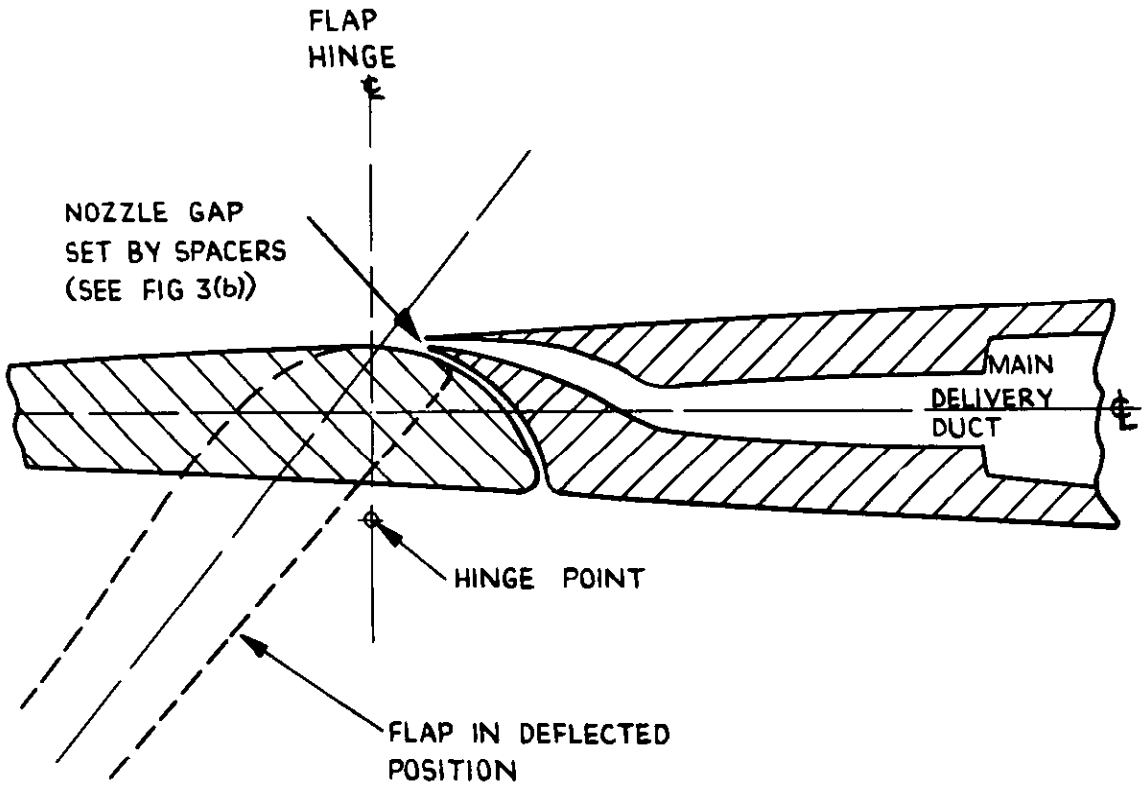

FIG. 3 (a). SECTION SHOWING DETAILS OF FLAP BLOWING NOZZLE (ALONGSTREAM).

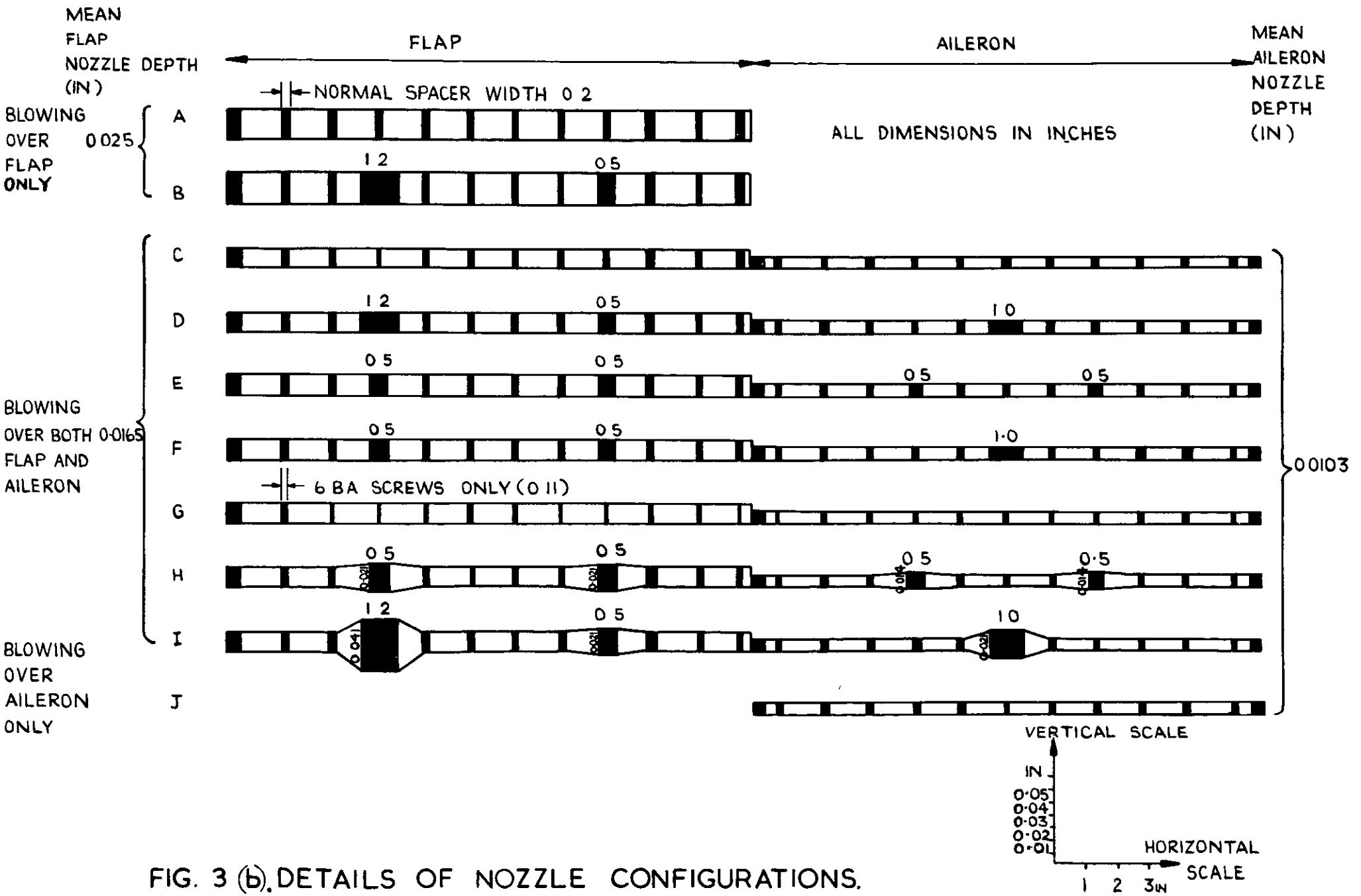

FIG. 3 (b). DETAILS OF NOZZLE CONFIGURATIONS.

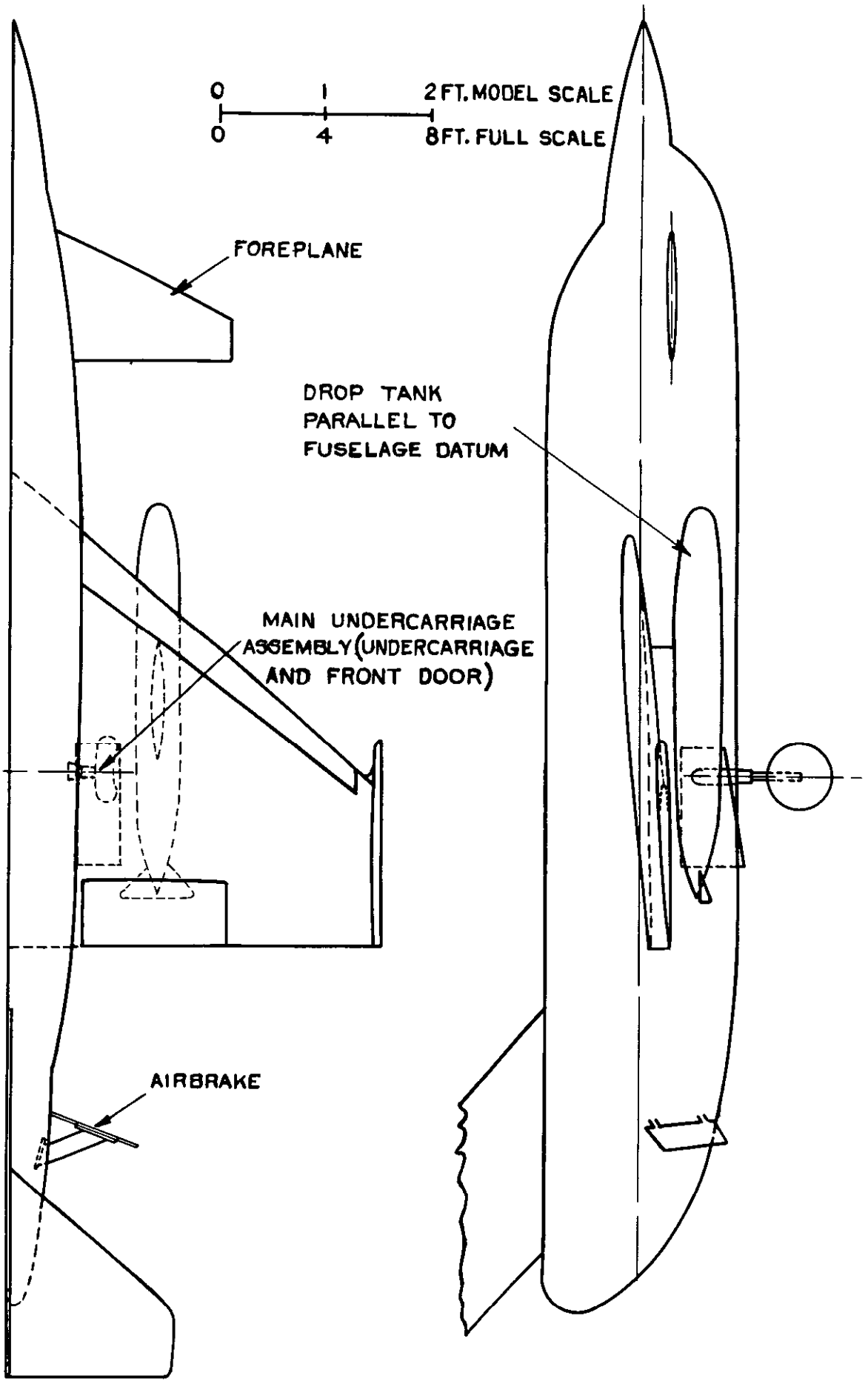

FIG.4. G.A. OF MODEL WITH DROP TANK, MAIN UNDERCARRIAGE ASSEMBLY, AIRBRAKE, AND FOREPLANE.

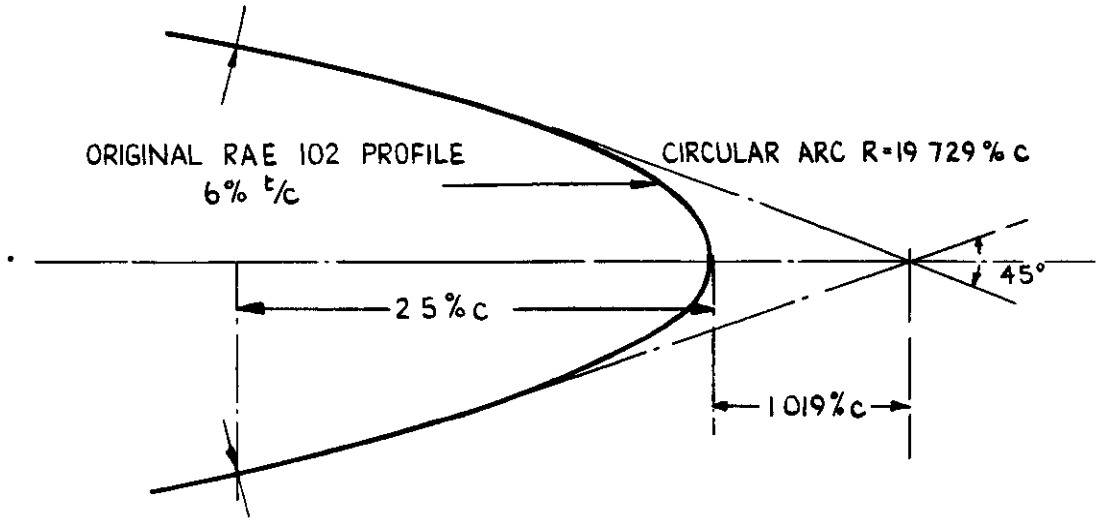

FIG 5. SECTION OF SHARP WING LEADING-EDGE EXTENSION (ALONGSTREAM).

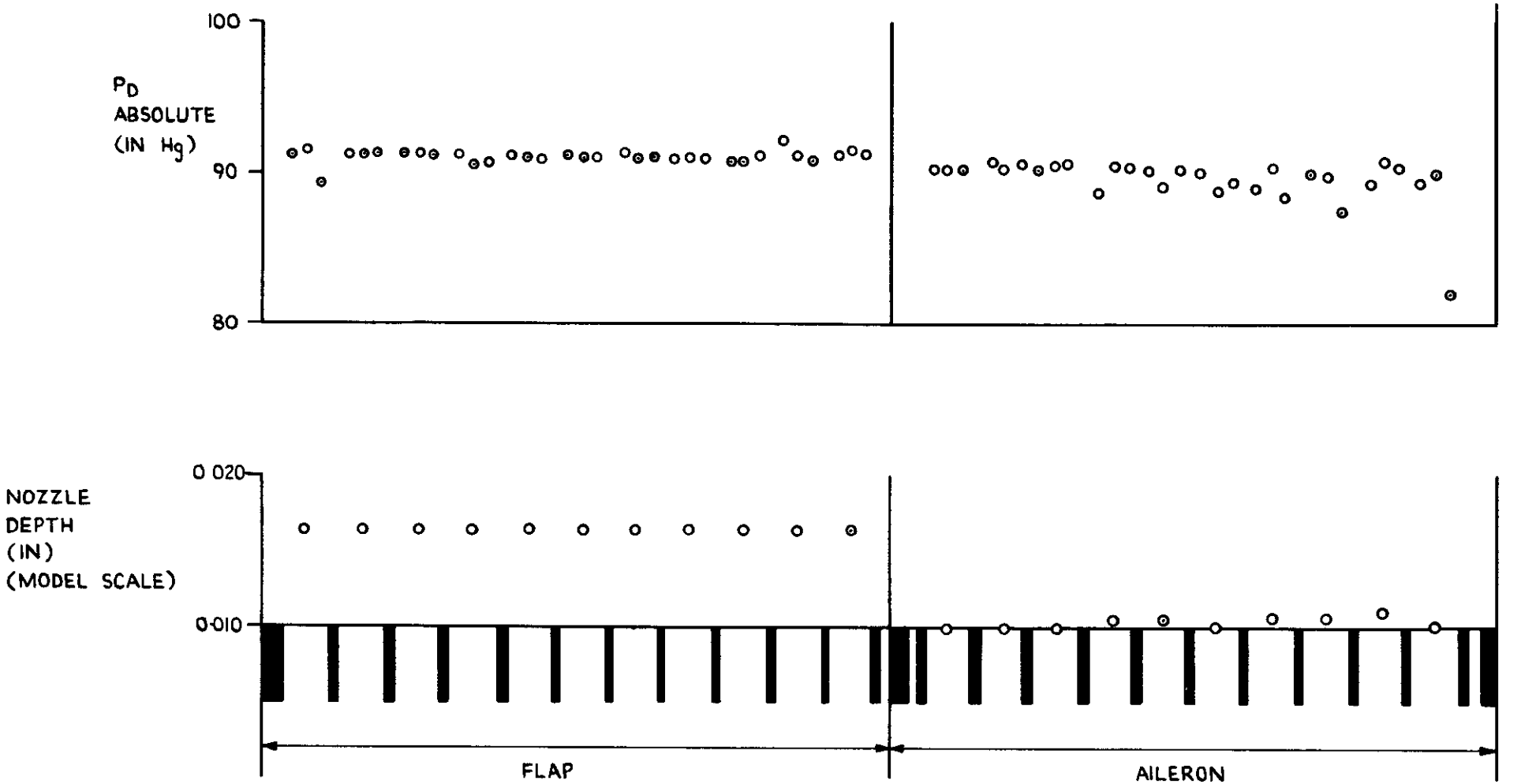

FIG. 6. TYPICAL SPANWISE DISTRIBUTIONS OF TOTAL HEAD AND NOZZLE DEPTH ON THE MODEL.

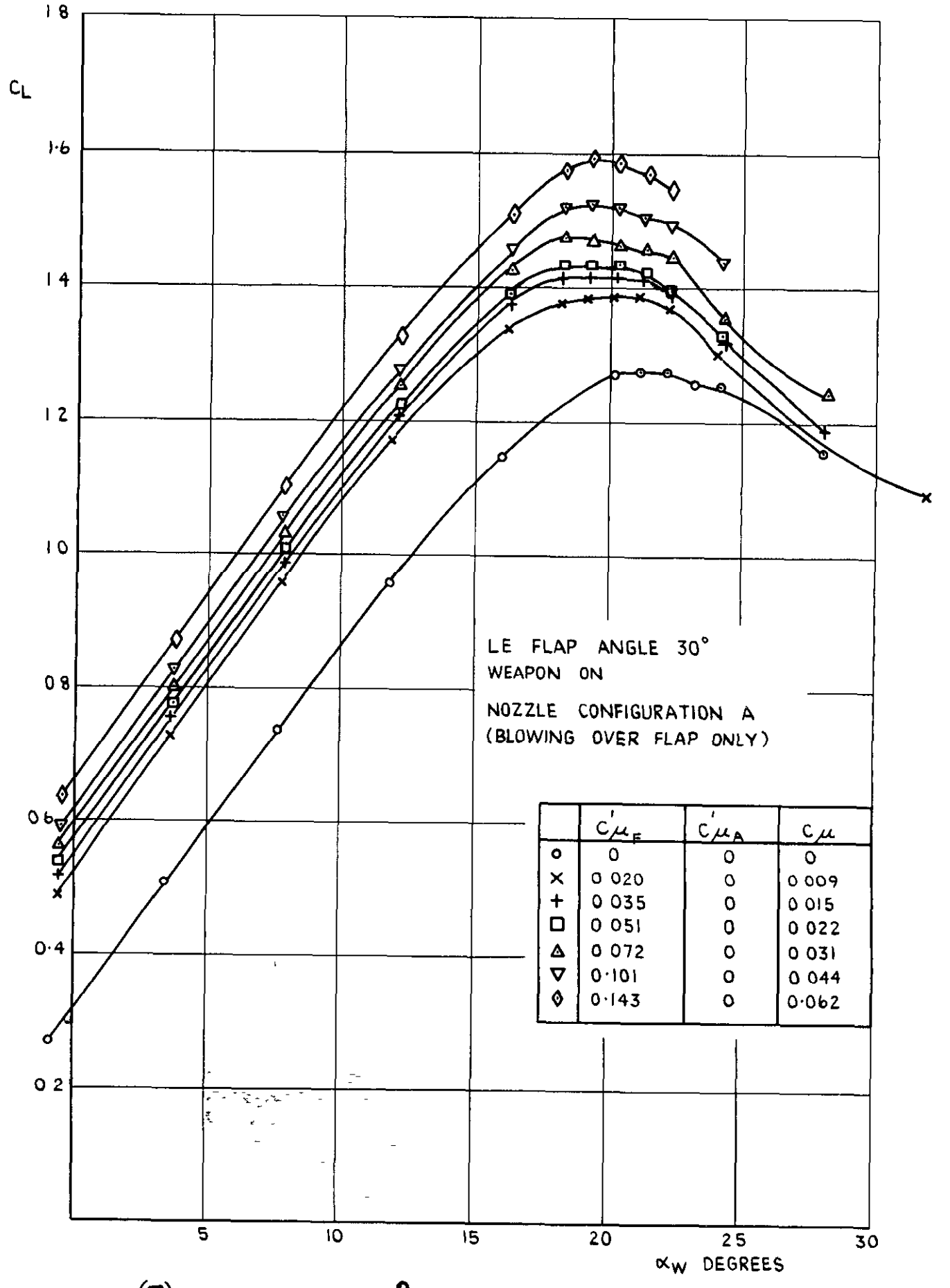

(a). FLAP ANGLE = 45°; AILERON UNDEFLECTED.

FIG. 7. THE EFFECT OF BLOWING ON C_L (NO TAILPLANE) V α_W.

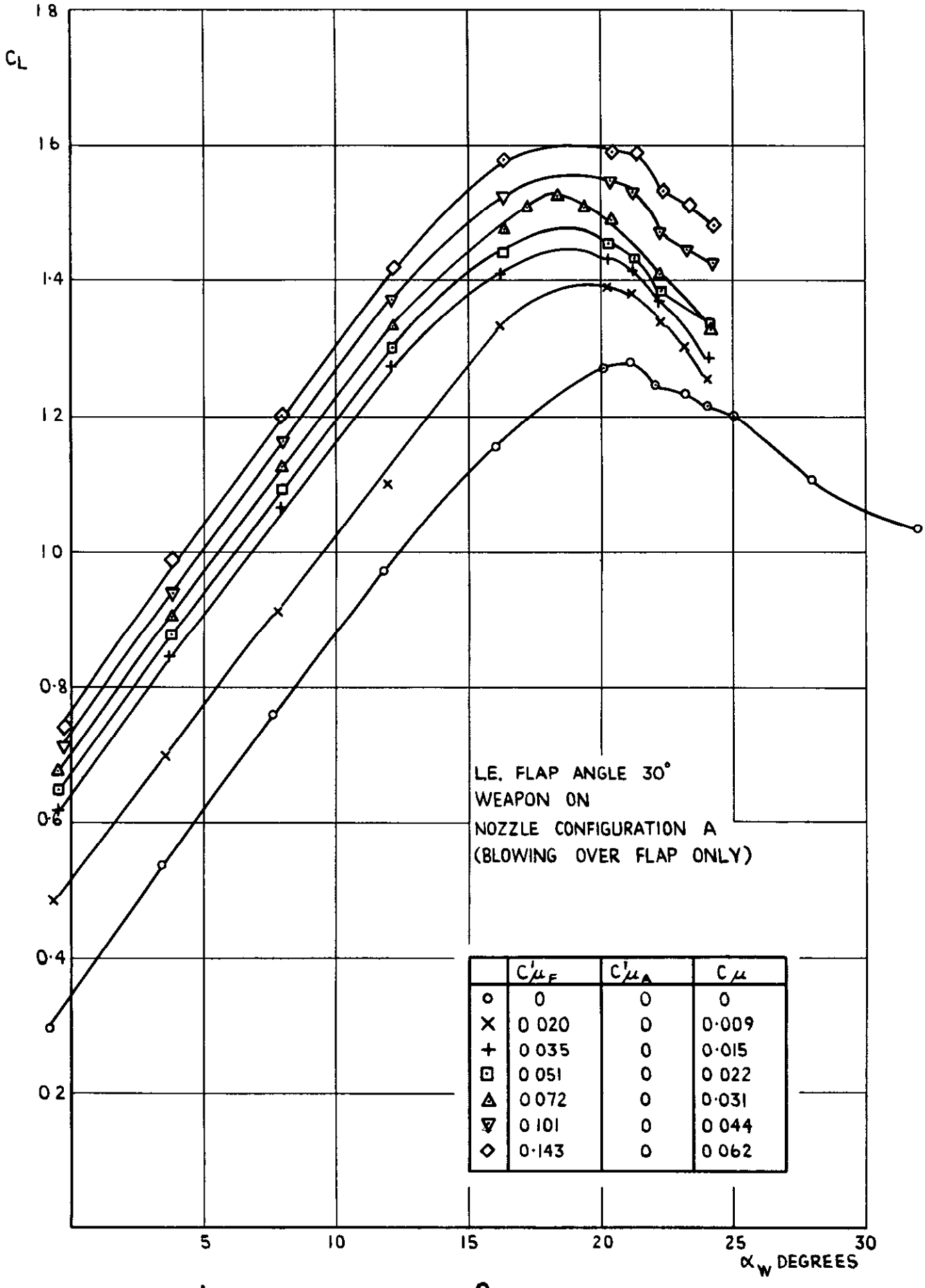

(b). FLAP ANGLE = 60°; AILERON UNDEFLECTED.

FIG. 7 (CONTD).

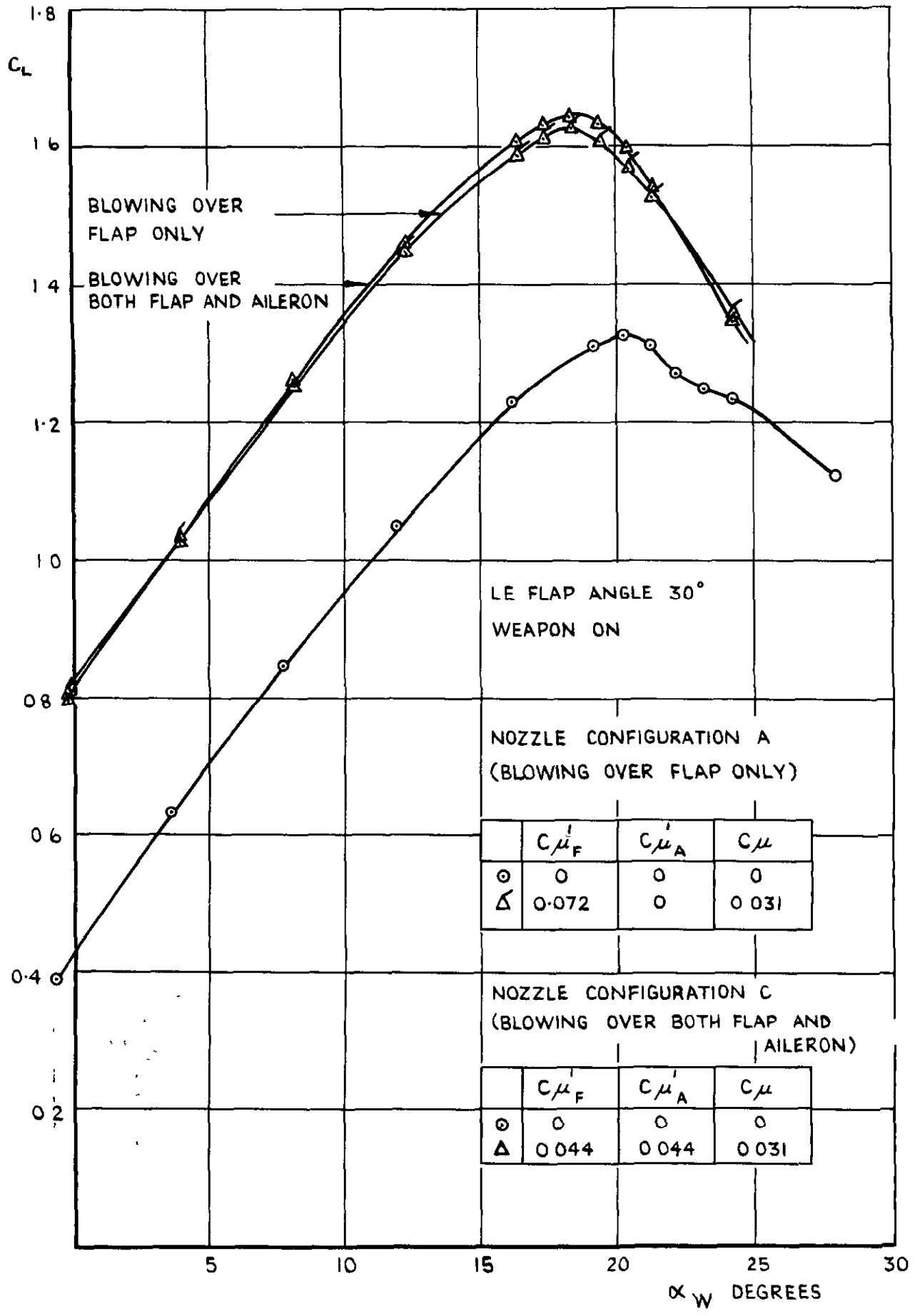

(C). FLAP ANGLE = 60°; AILERON ANGLE = 15°.
FIG. 7 (CONT'D).

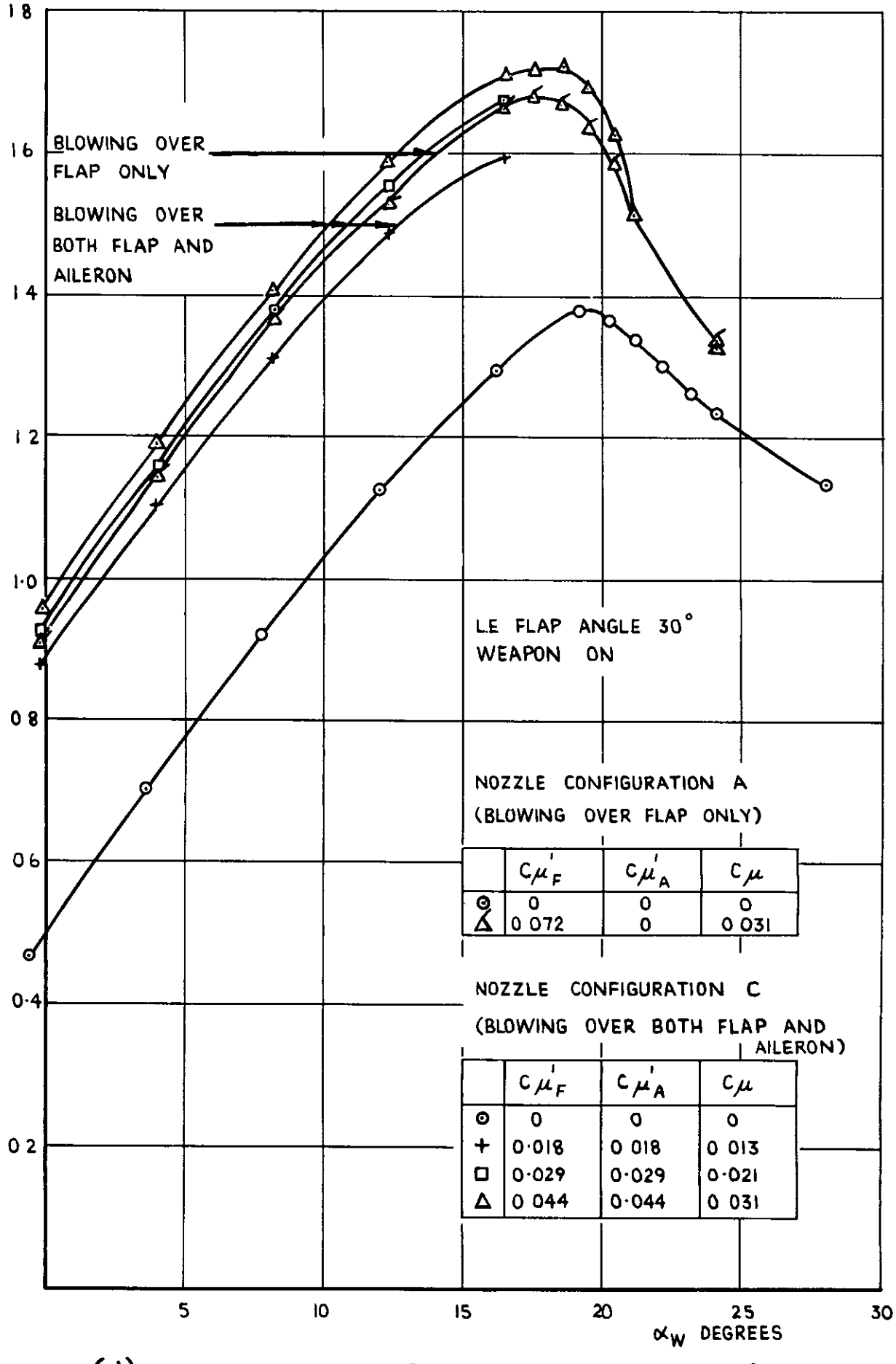

(d). FLAP ANGLE = 60°; AILERON ANGLE = 30°.

FIG. 7 (CONT'D).

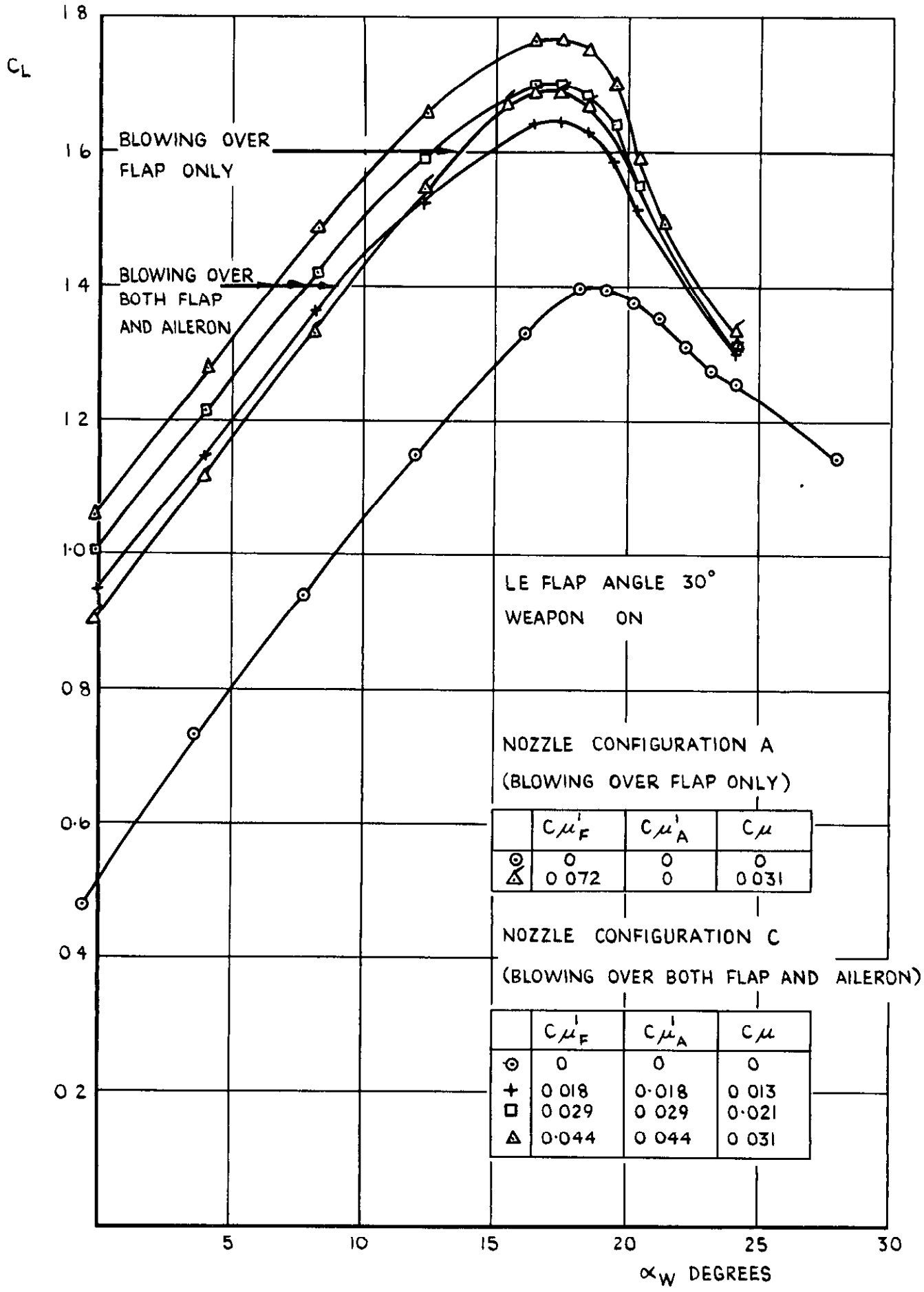

(e). FLAP ANGLE = 60°; AILERON ANGLE = 45°.

FIG. 7 (CONCL'D).

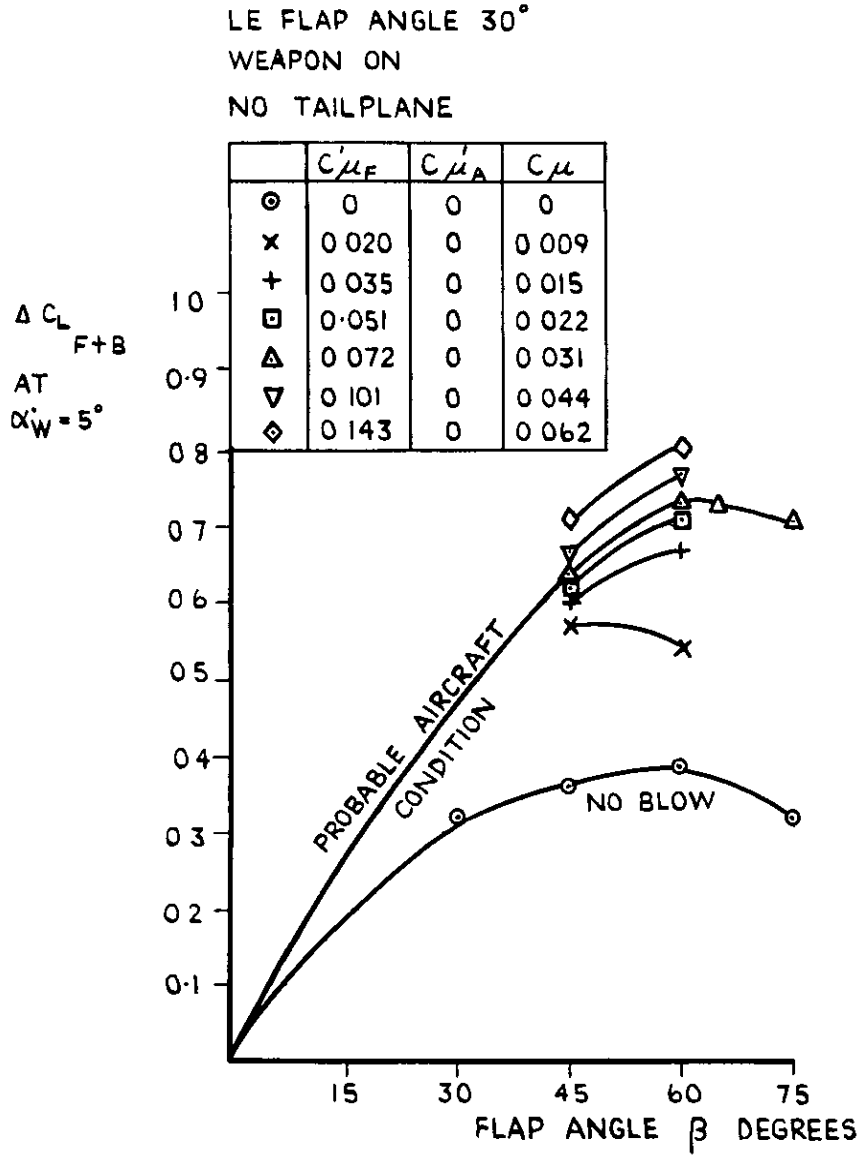

FIG.8. THE VARIATION OF $\Delta C_{L_{F+B}}$ WITH FLAP ANGLE FOR DIFFERENT VALUES OF MOMENTUM COEFFICIENT (BLOWING OVER FLAP ONLY WITH AILERON UNDEFLECTED).

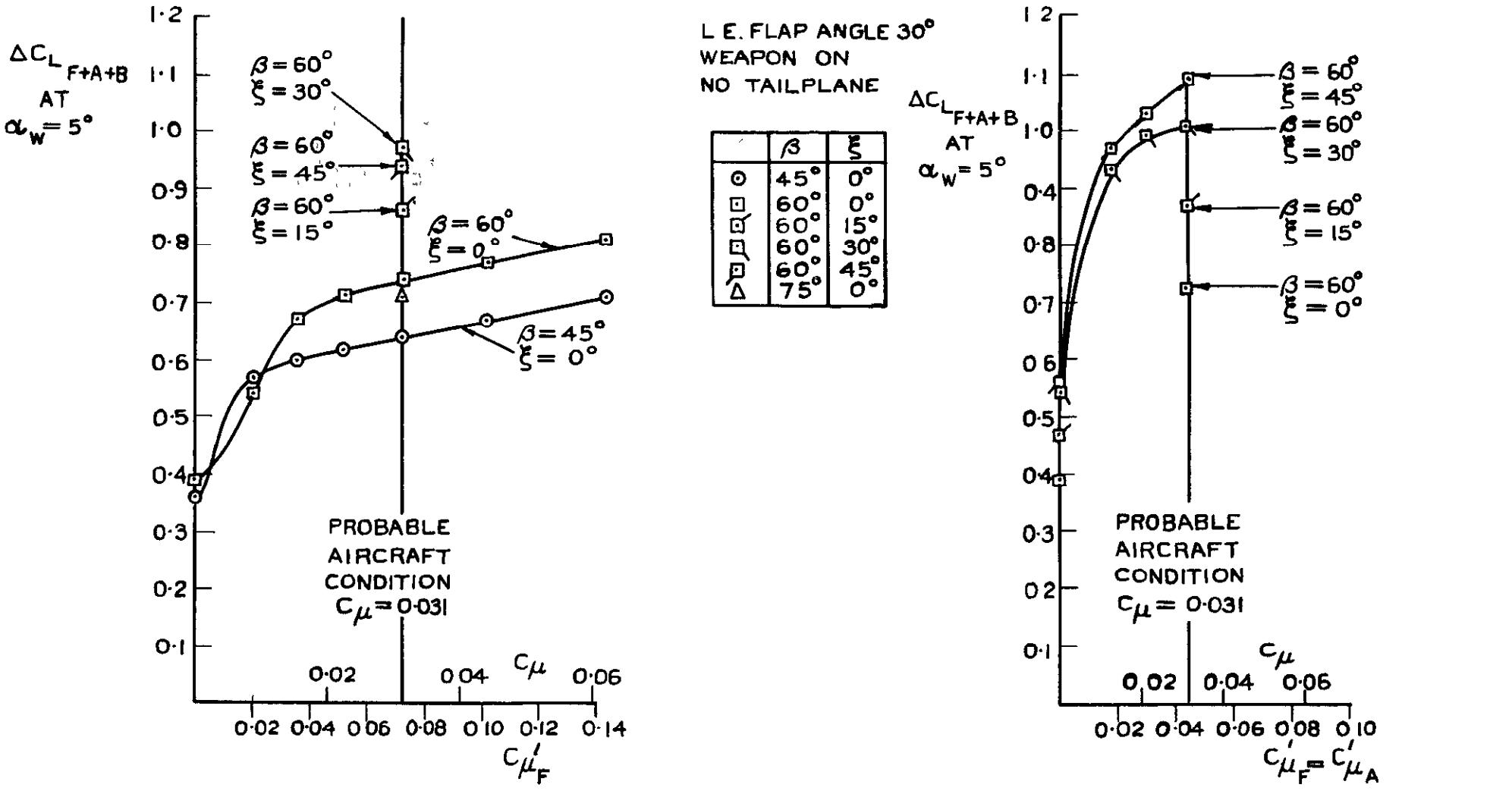

(a). NOZZLE CONFIGURATION A
(BLOWING OVER FLAP ONLY, $C'_{\mu_A} = 0$).

(b). NOZZLE CONFIGURATION C
(BLOWING OVER BOTH FLAP AND AILERON).

FIG. 9. THE VARIATION OF $\Delta C_{L_{F+A+B}}$ WITH MOMENTUM COEFFICIENT.

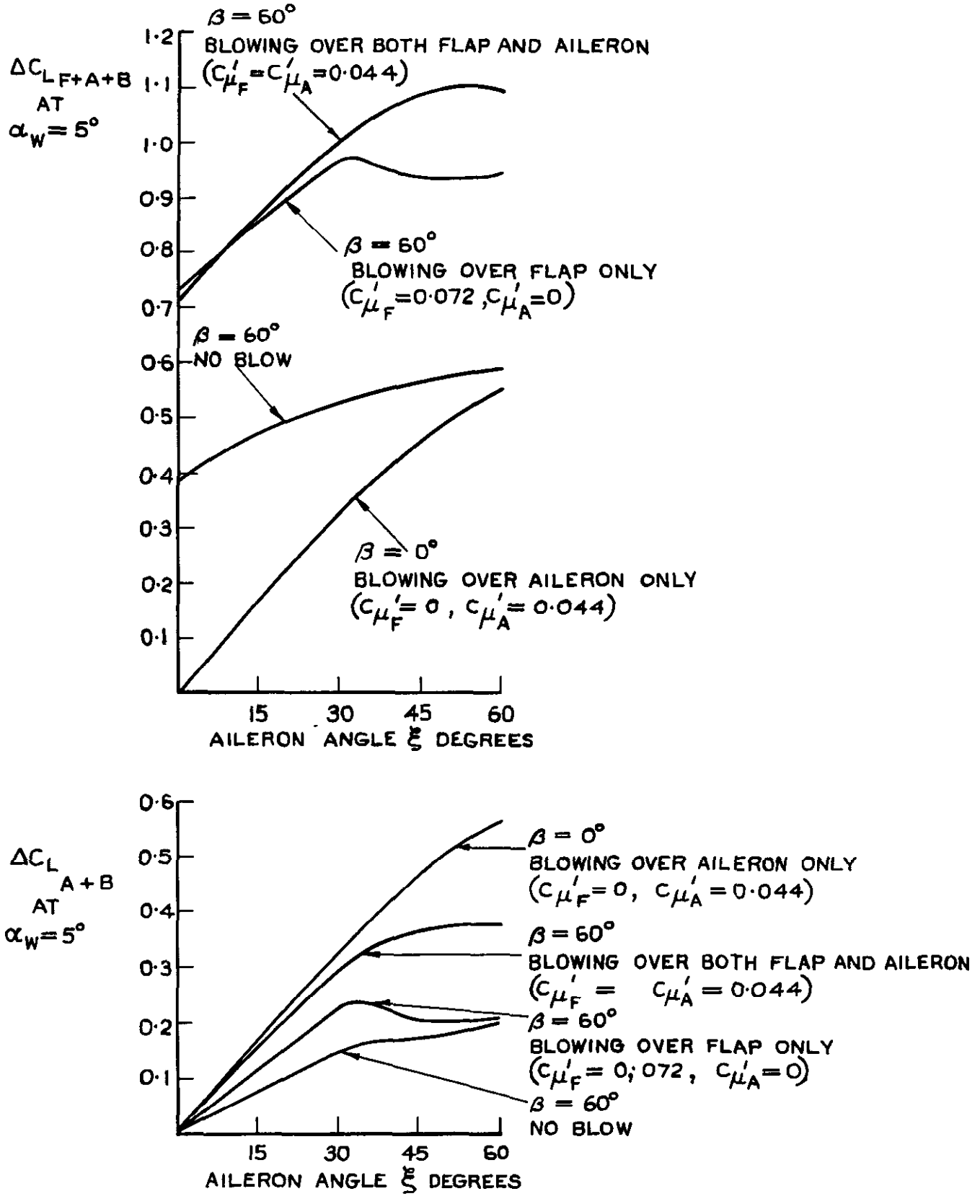

FIG. 10. THE VARIATION OF $\Delta C_{L\ F+A+B}$ AND $\Delta C_{L\ A+B}$ WITH AILERON ANGLE.

L.E. FLAP ANGLE 30°
WEAPON ON
NO TAILPLANE

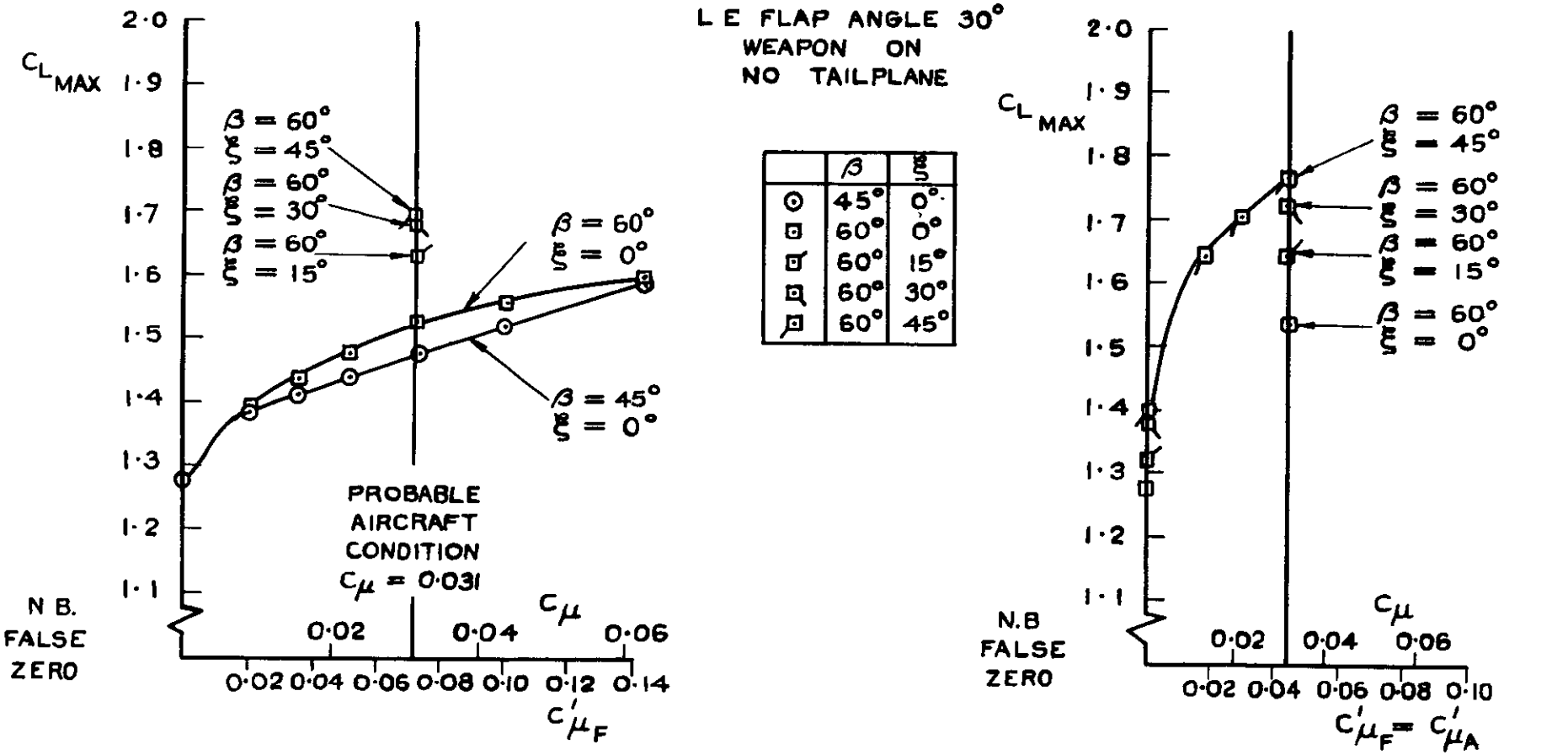

(a). NOZZLE CONFIGURATION A
(BLOWING OVER FLAP ONLY, $C'_{\mu_A} = 0$).

(b). NOZZLE CONFIGURATION C
(BLOWING OVER BOTH FLAP AND AILERON).

FIG. 11. THE VARIATION OF $C_{L\,MAX}$ WITH MOMENTUM COEFFICIENT.

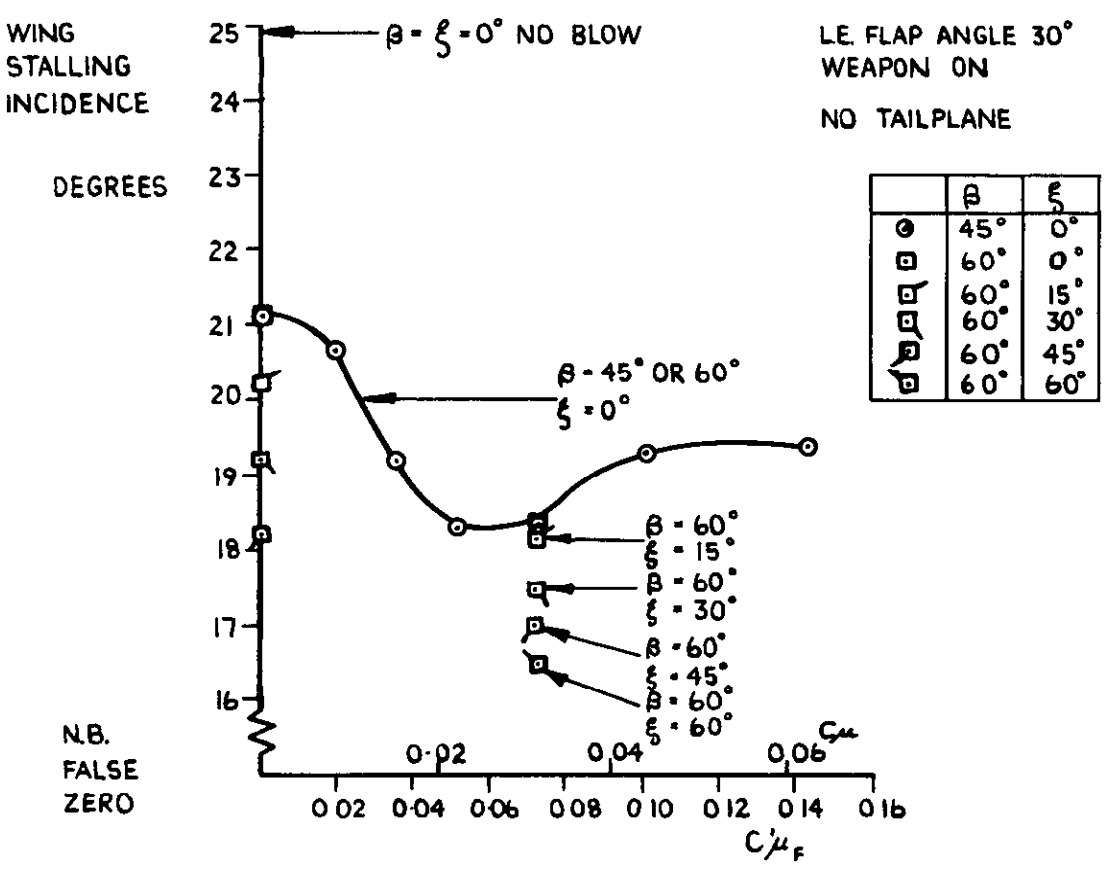

(a). NOZZLE CONFIGURATION A
(BLOWING OVER FLAPS ONLY, $C\mu'_A = 0$).

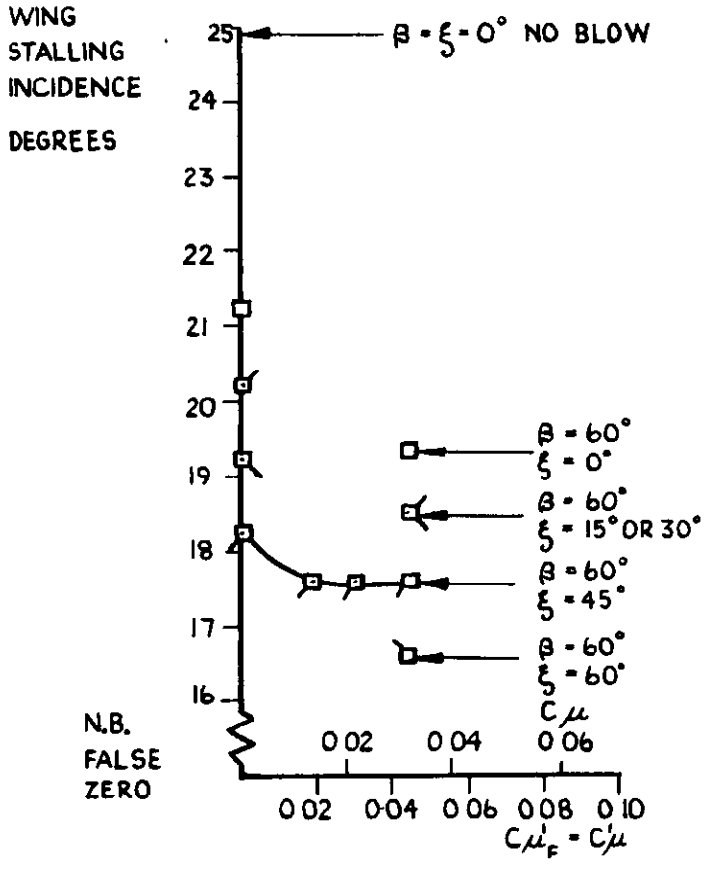

(b). NOZZLE CONFIGURATION C
(BLOWING OVER BOTH FLAP AND AILERON).

FIG.12. THE VARIATION OF WING STALLING INCIDENCE WITH MOMENTUM COEFFICIENT.

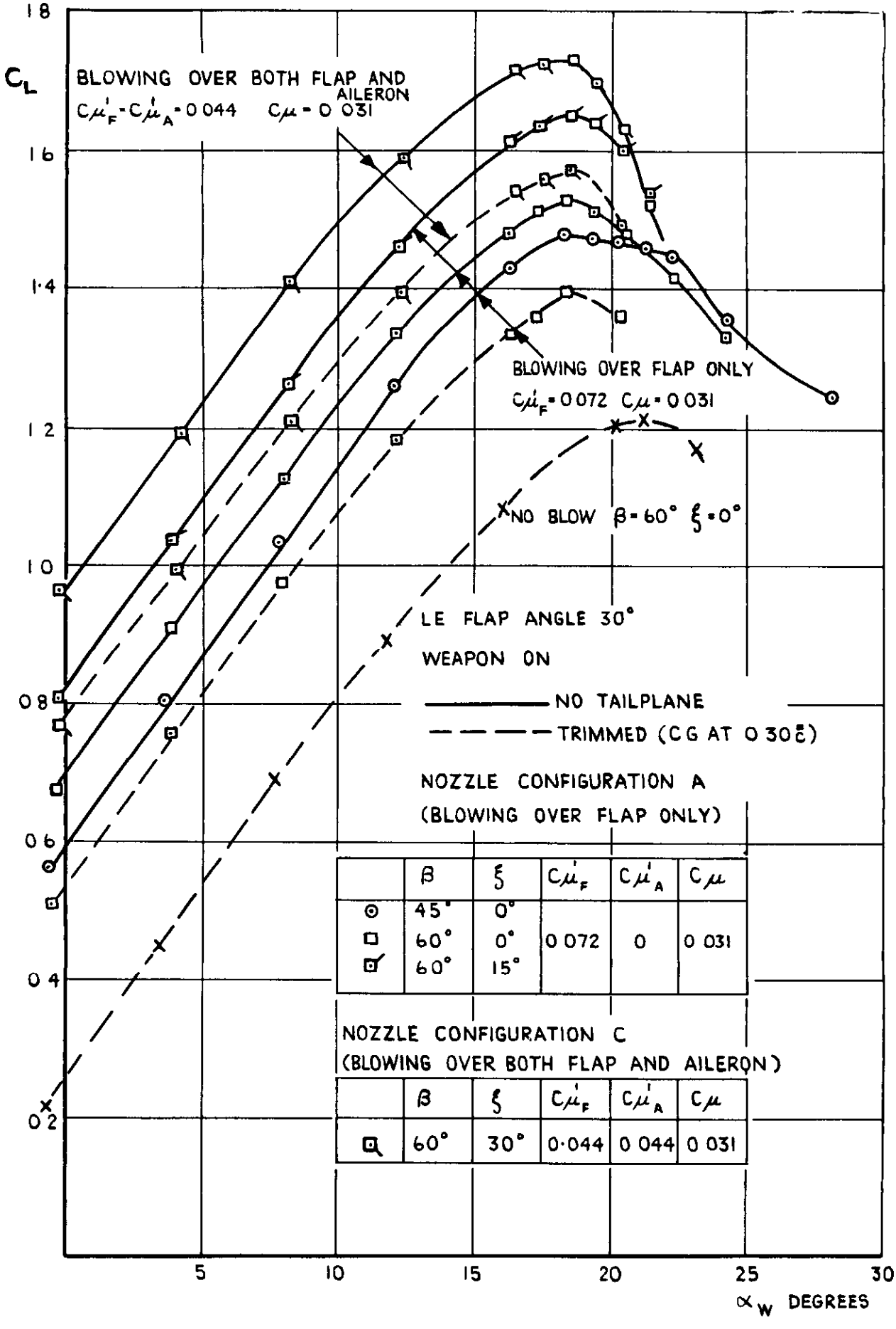

	β	ξ	$C\mu'_F$	$C\mu'_A$	$C\mu$
⊙	45°	0°	0.072	0	0.031
□	60°	0°			
⊡	60°	15°			

	β	ξ	$C\mu'_F$	$C\mu'_A$	$C\mu$
⊡	60°	30°	0.044	0.044	0.031

FIG. 13. THE EFFECTS OF FLAP ANGLE, AILERON ANGLE, AND SPANWISE EXTENT OF BLOWING ON C_L V α_W AT $C\mu = 0.031$.

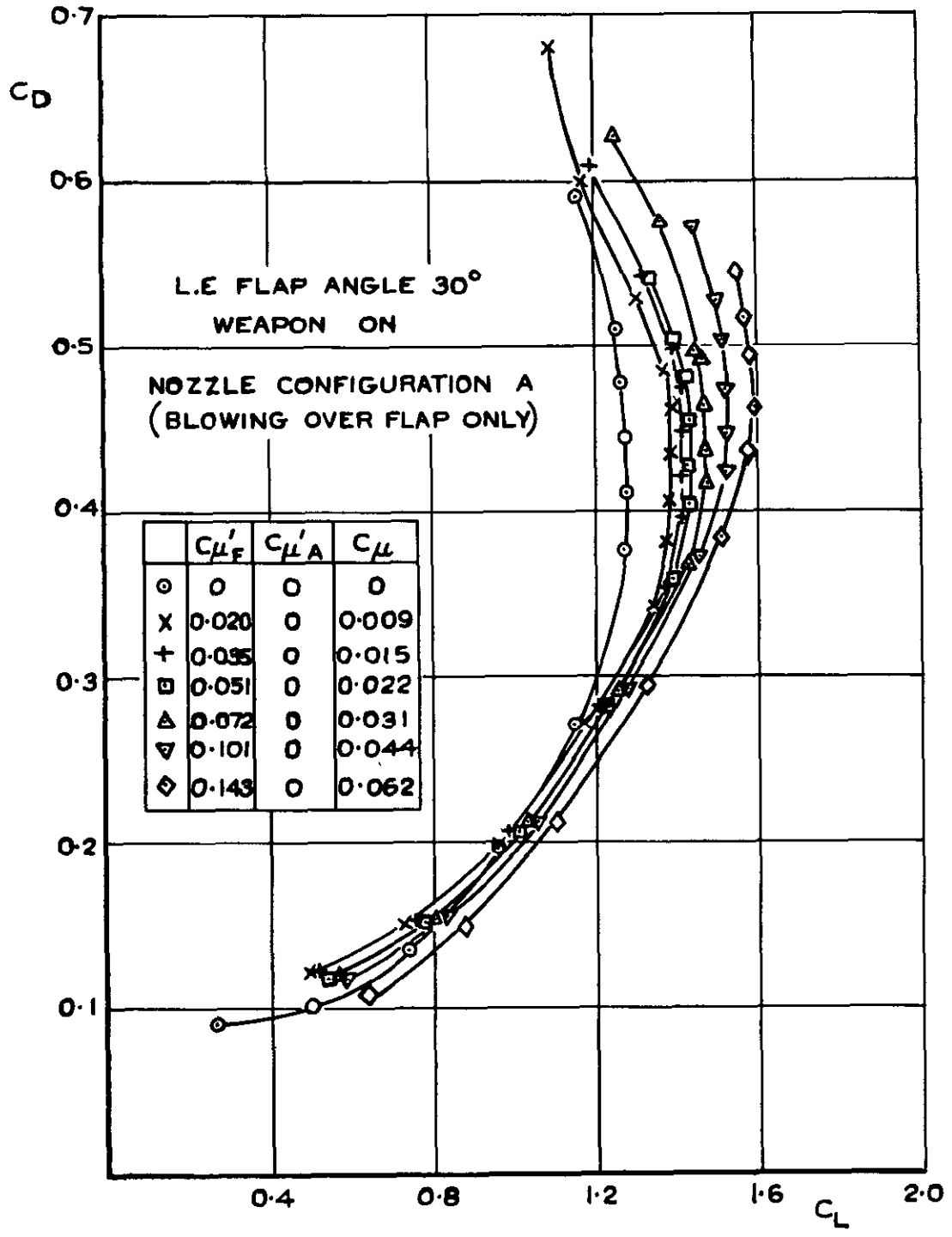

(a). FLAP ANGLE = 45°; AILERON UNDEFLECTED.

FIG.14. THE EFFECT OF BLOWING ON C_D V C_L (NO TAILPLANE).

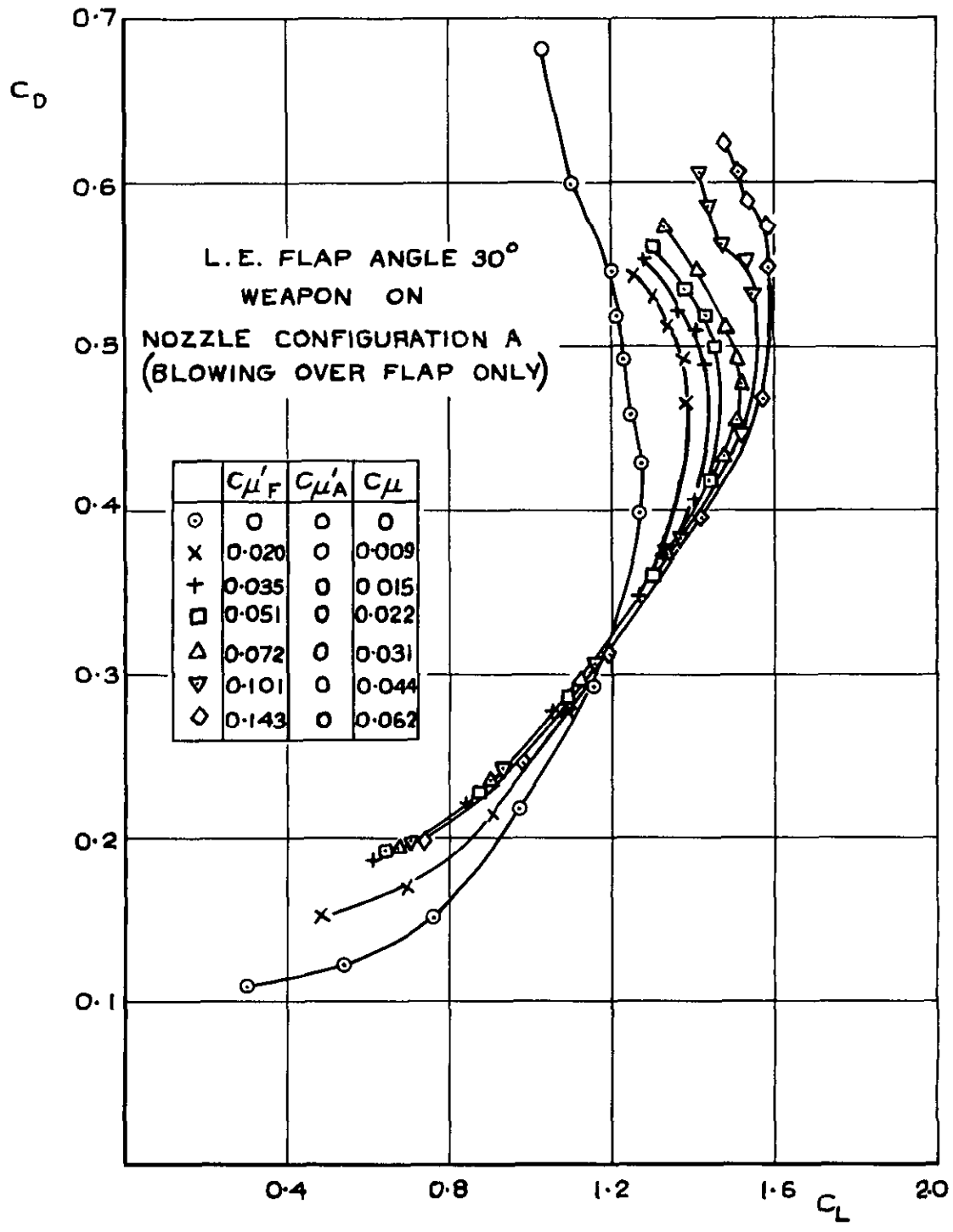

(b). FLAP ANGLE = 60°; AILERON UNDEFLECTED.

FIG. 14 (CONT'D).

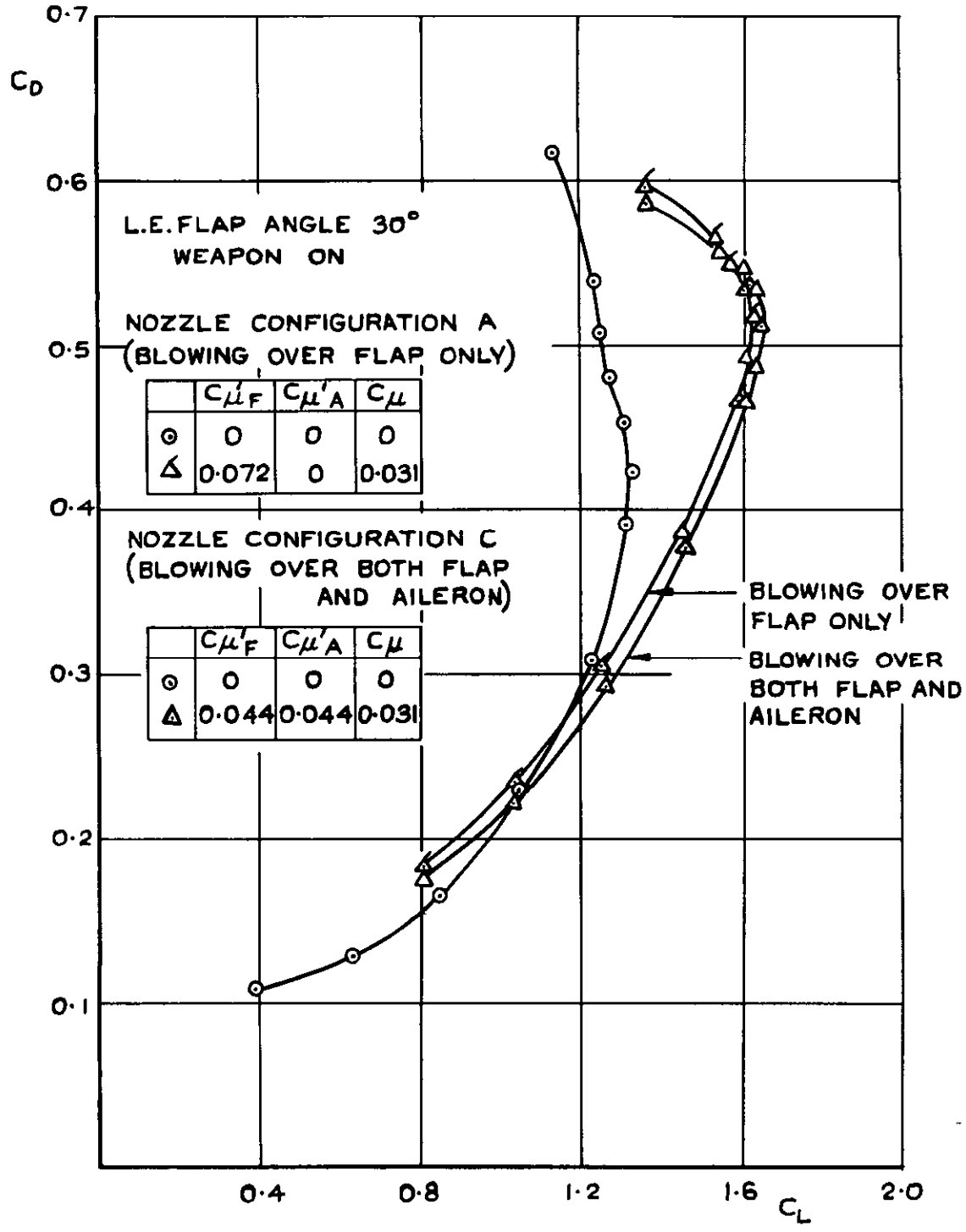

(C). FLAP ANGLE = 60°; AILERON ANGLE = 15°.

FIG. 14. (CONT'D.).

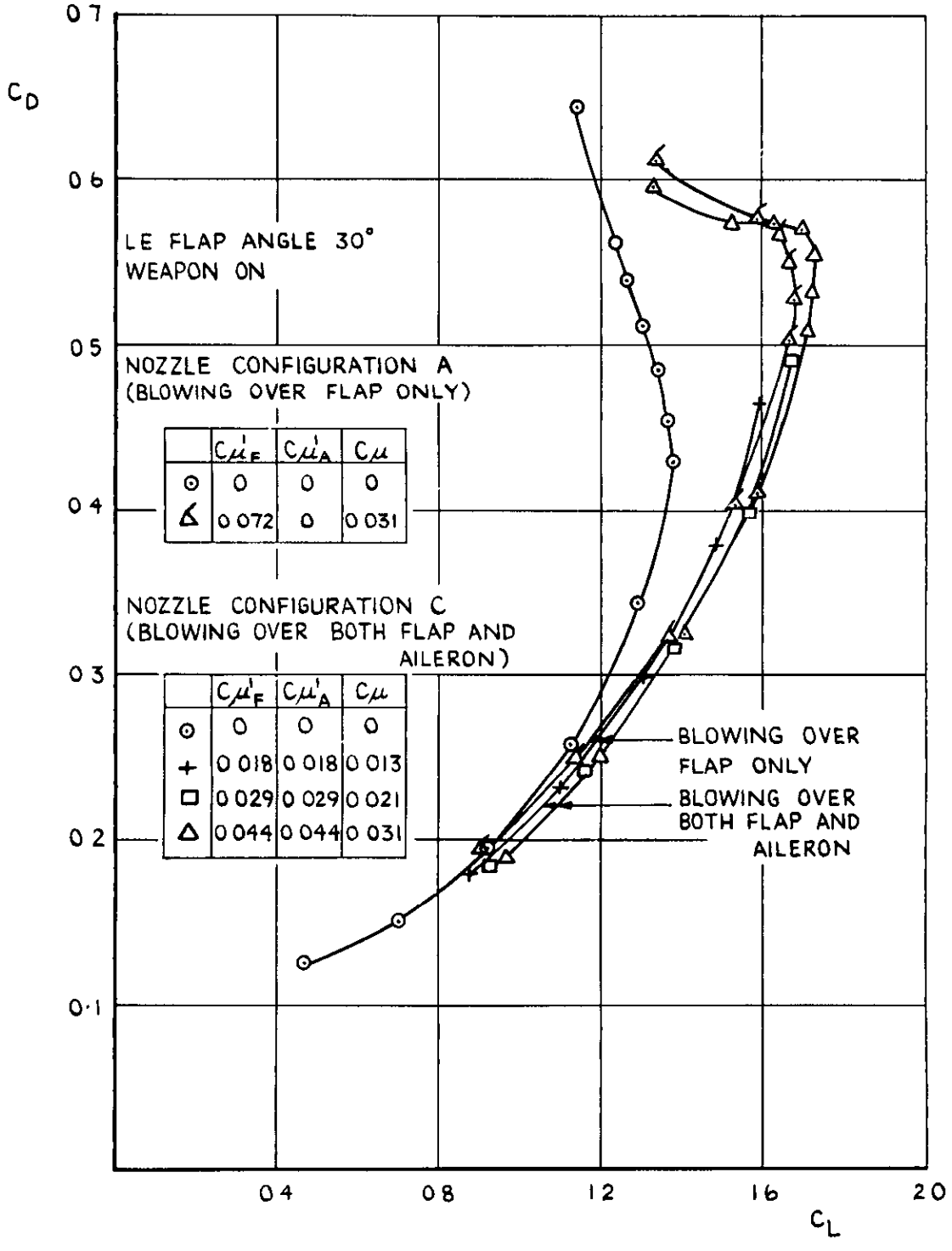

(d). FLAP ANGLE=60°; AILERON ANGLE=30°.
FIG. 14 (CONT'D.).

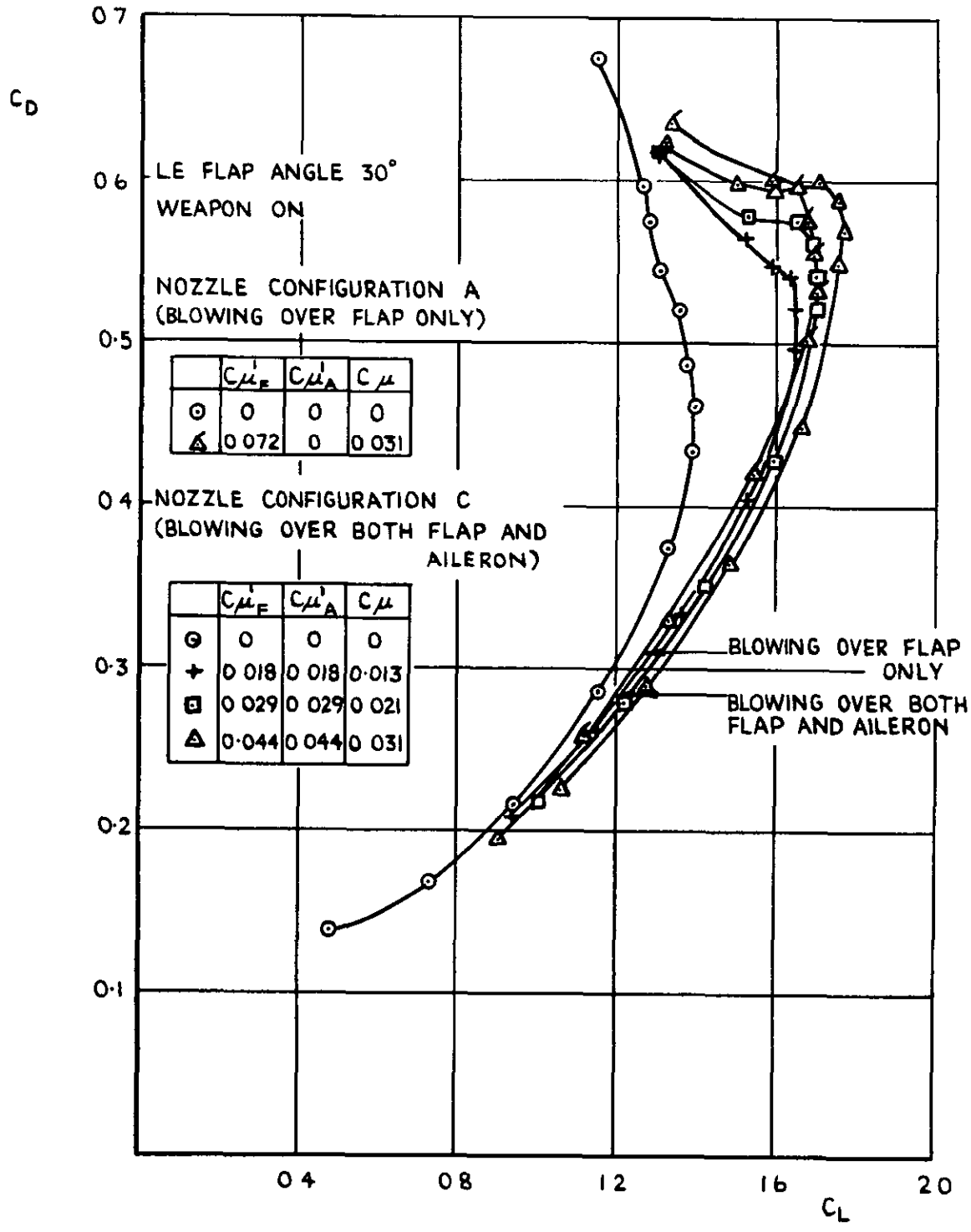

(e). FLAP ANGLE = 60°; AILERON ANGLE = 45°.

FIG. 14 (CONCL'D).

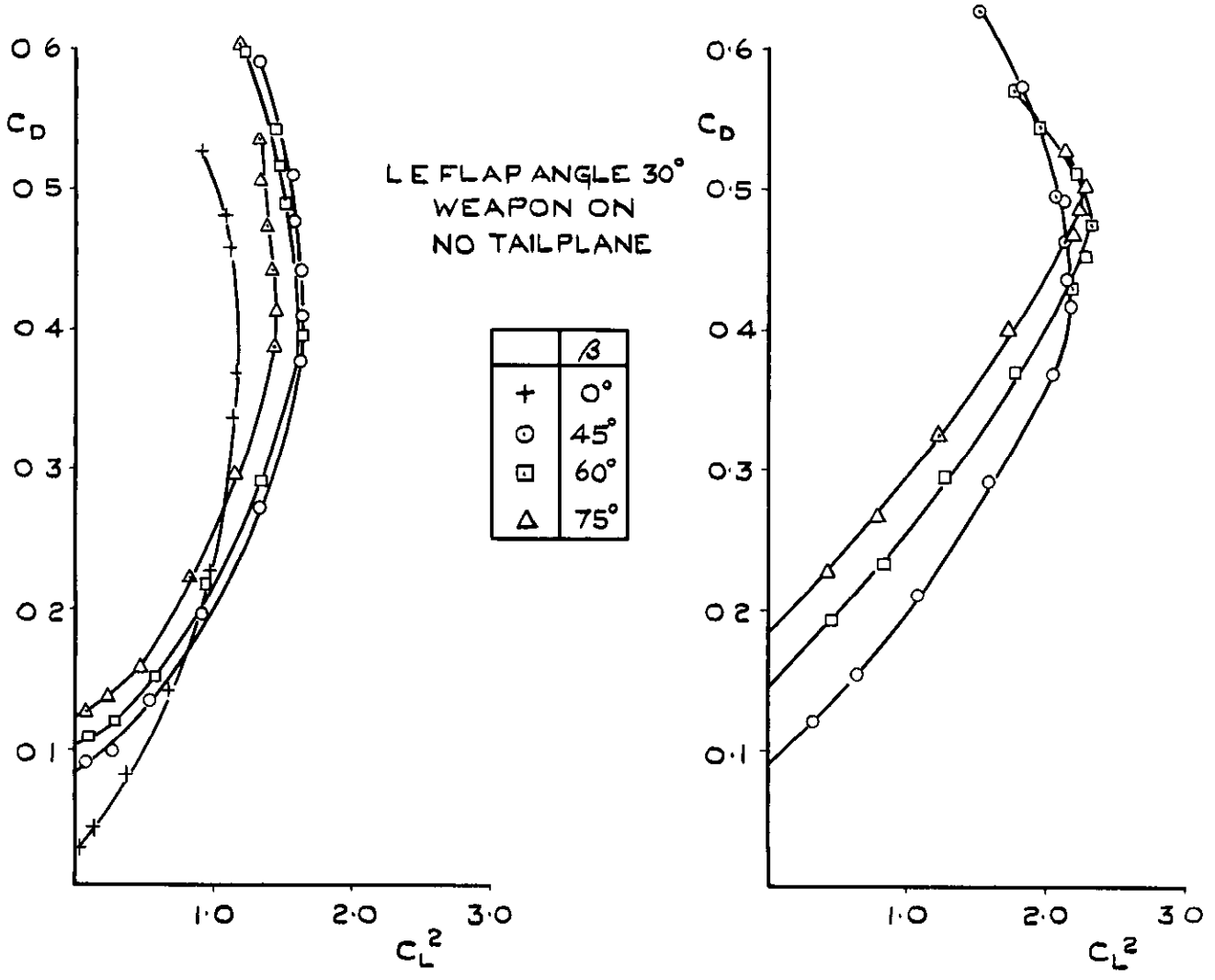

FIG. 15. THE EFFECT OF FLAP ANGLE ON C_D v C_L^2 (AILERON UNDEFLECTED).

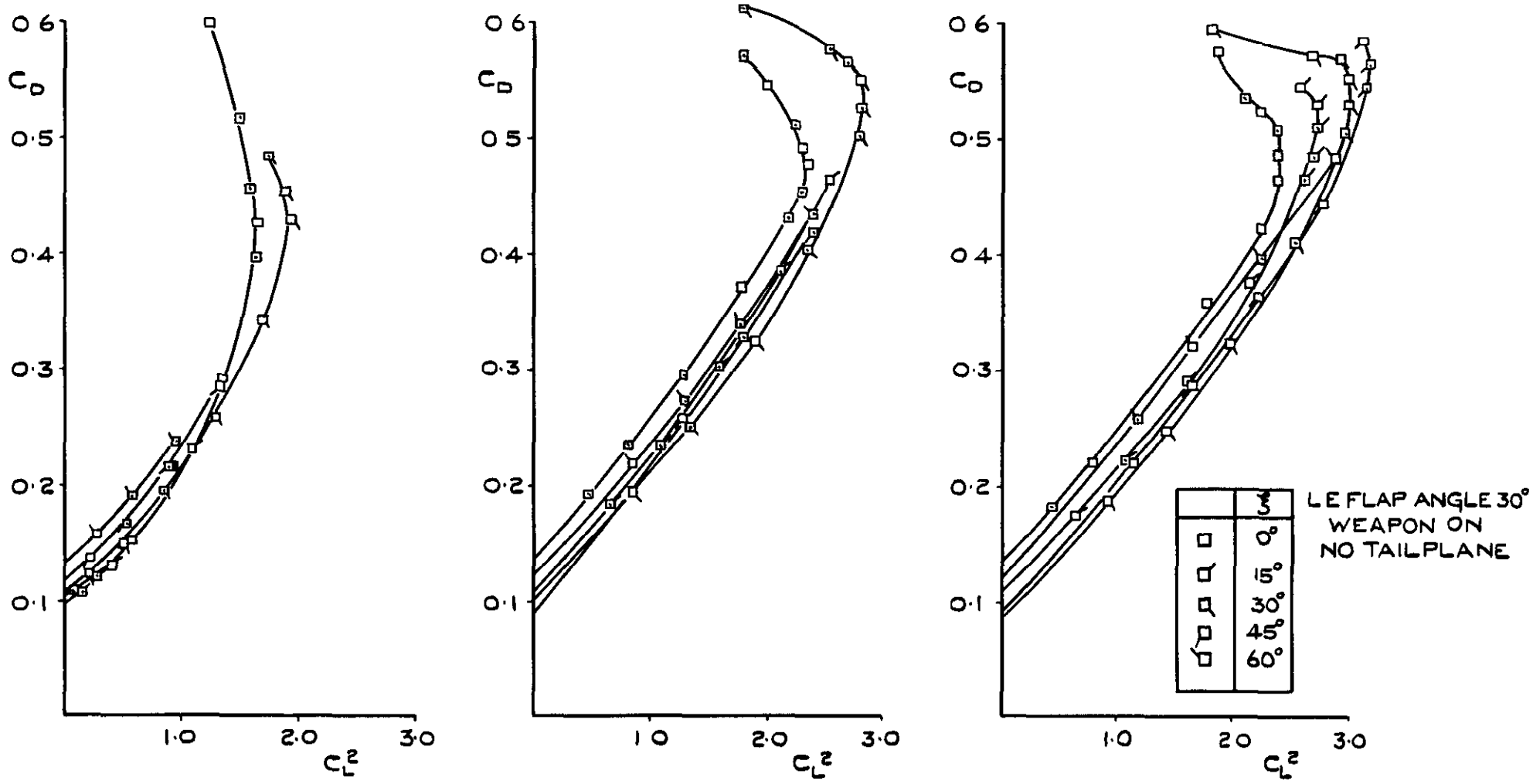

(a). NO BLOW.

(b). BLOWING OVER FLAP ONLY. $C_{\mu'_F} = 0{\cdot}072$; $C_{\mu'_A} = 0$; $C_\mu = 0{\cdot}031$.

(c). BLOWING OVER BOTH FLAP AND AILERON. $C_{\mu'_F} = C_{\mu'_A} = 0{\cdot}044$; $C_\mu = 0{\cdot}031$.

FIG. 16. THE EFFECT OF AILERON ANGLE ON C_D v C_L^2 (FLAP ANGLE = 60°).

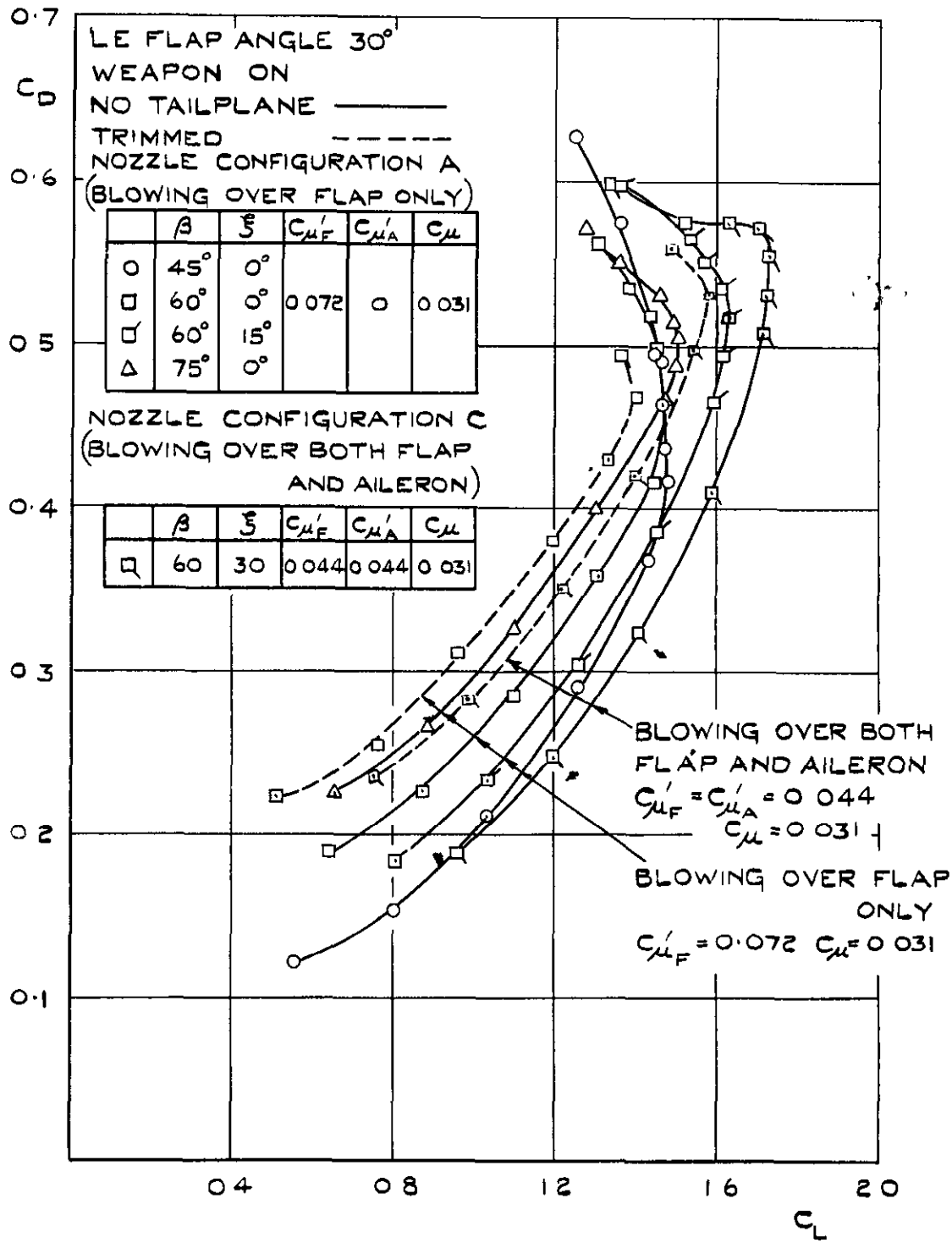

	β	ξ	C'_{μ_F}	C'_{μ_A}	C_μ
○	45°	0°			
□	60°	0°	0·072	0	0·031
□	60°	15°			
△	75°	0°			

	β	ξ	C'_{μ_F}	C'_{μ_A}	C_μ
□	60	30	0·044	0·044	0·031

FIG.17. THE EFFECTS OF FLAP ANGLE, AILERON ANGLE, AND SPANWISE EXTENT OF BLOWING ON C_D v C_L AT $C_\mu = 0.031$.

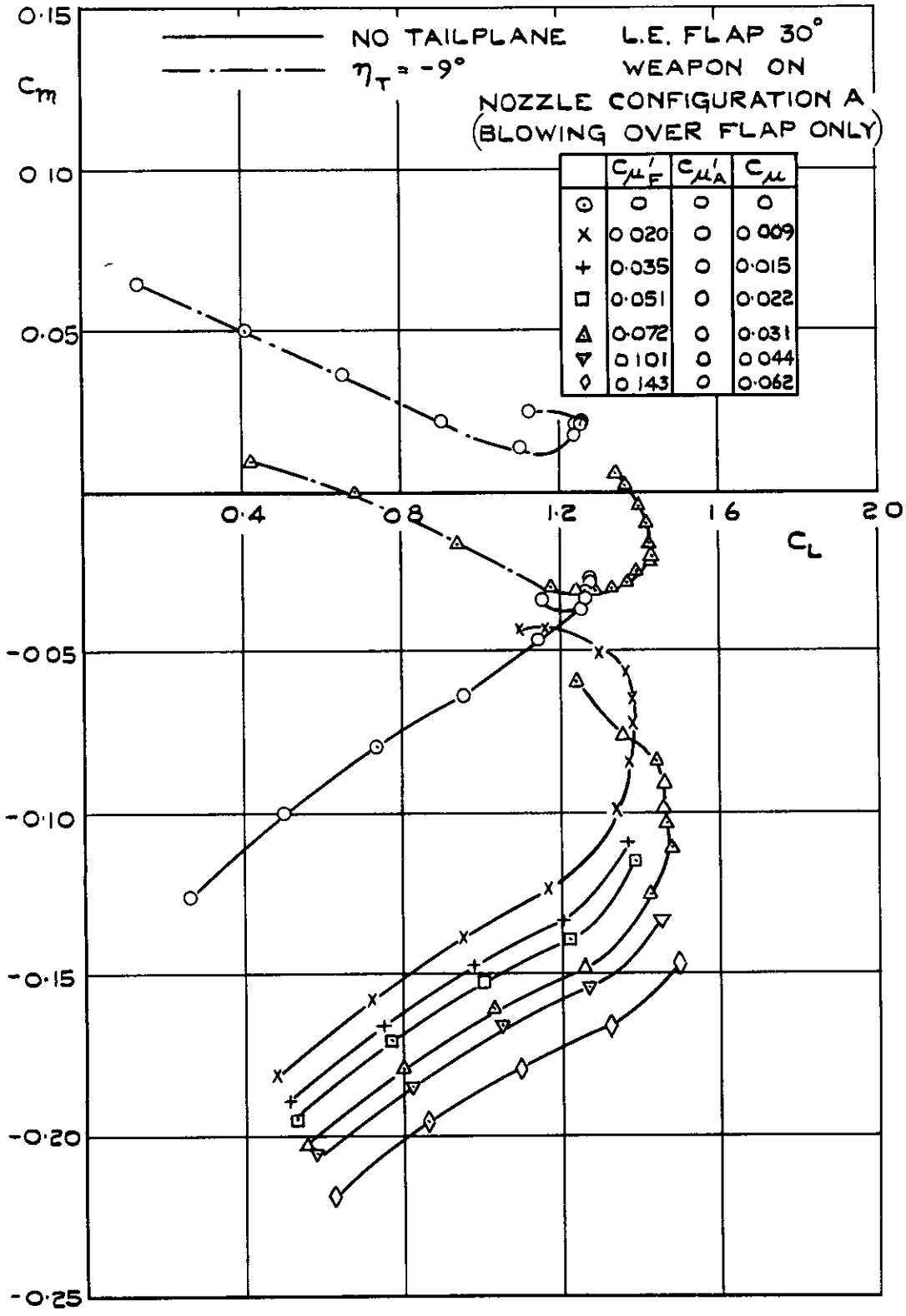

(a) FLAP ANGLE = 45°; AILERON UNDEFLECTED.

FIG. 18 THE EFFECT OF BLOWING ON C_m & C_L.

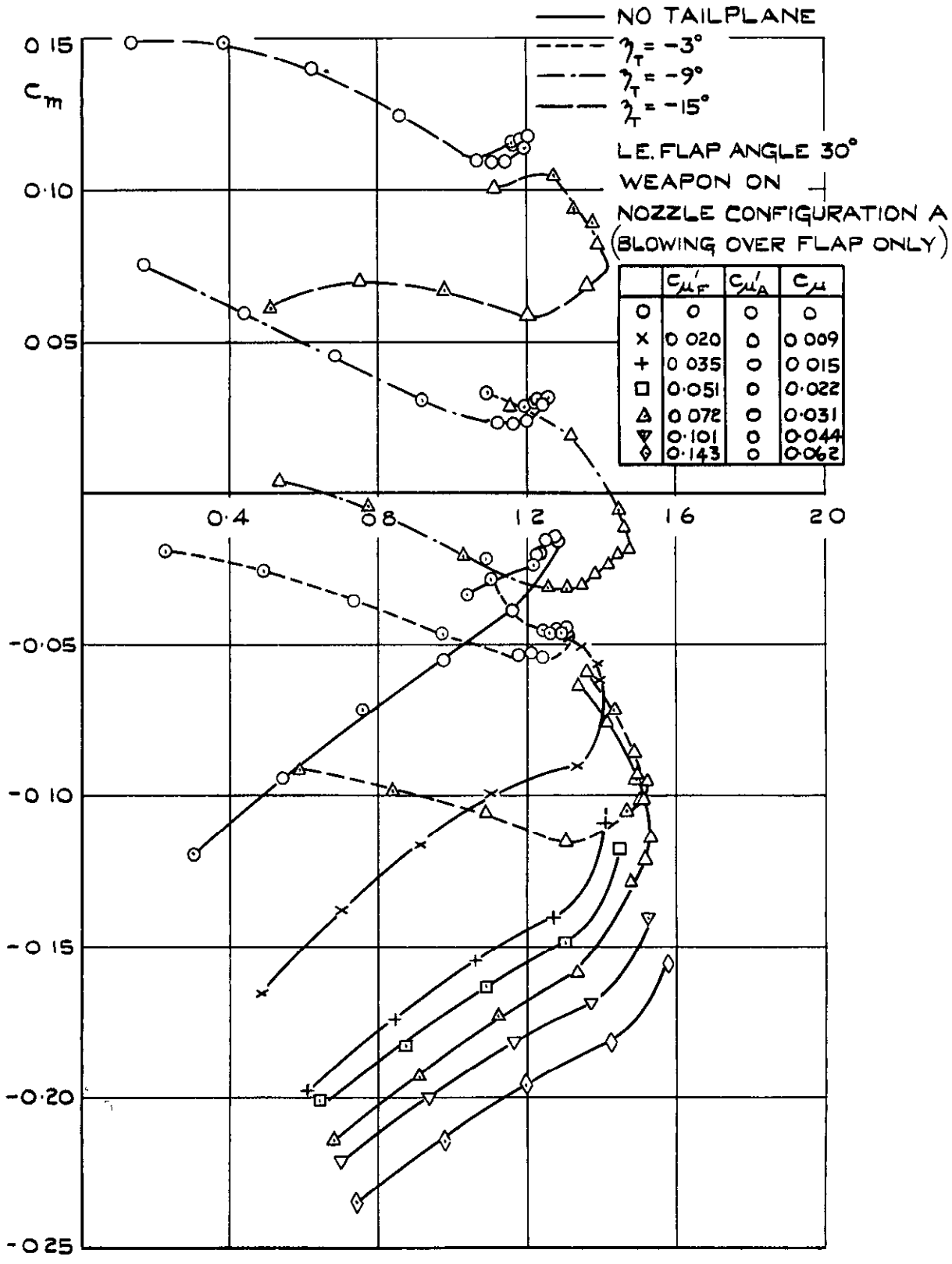

(b). FLAP ANGLE = 60°; AILERON UNDEFLECTED

FIG. 18 (CONT'D).

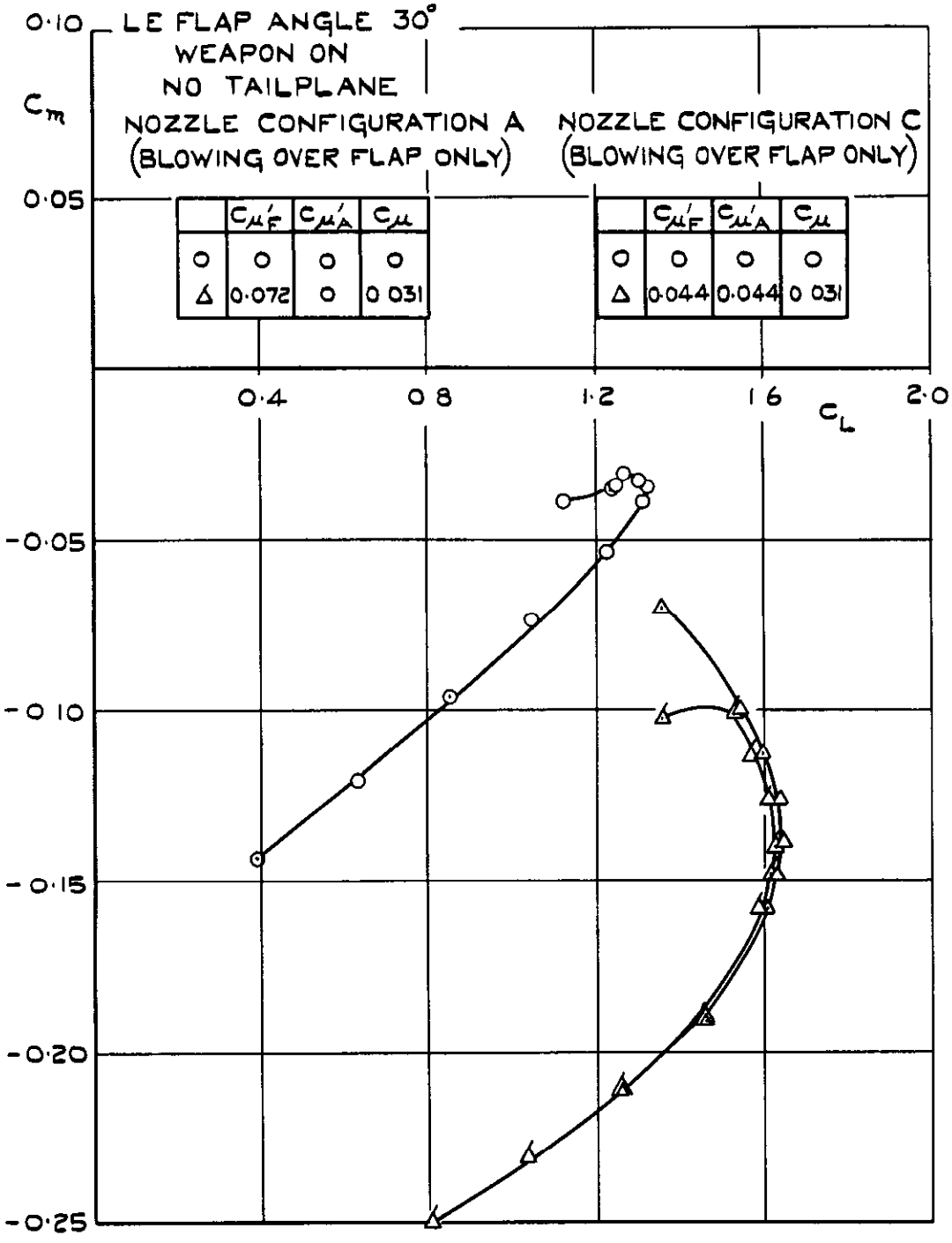

(C). FLAP ANGLE = 60°, AILERON ANGLE = 15°

FIG. 18. (CONT'D.).

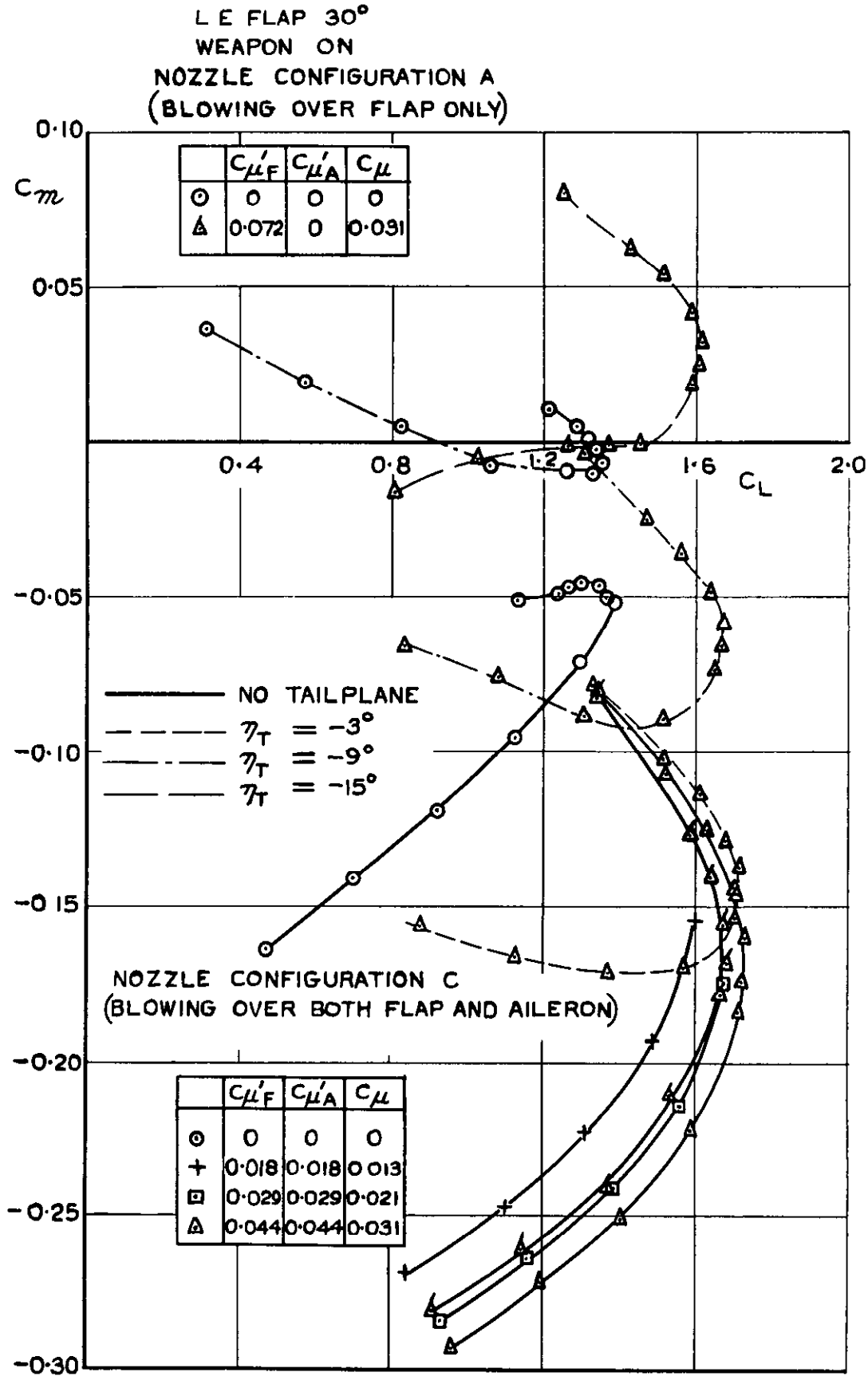

(d). FLAP ANGLE = 60°; AILERON ANGLE = 30°.

FIG. 18. (CONT'D.).

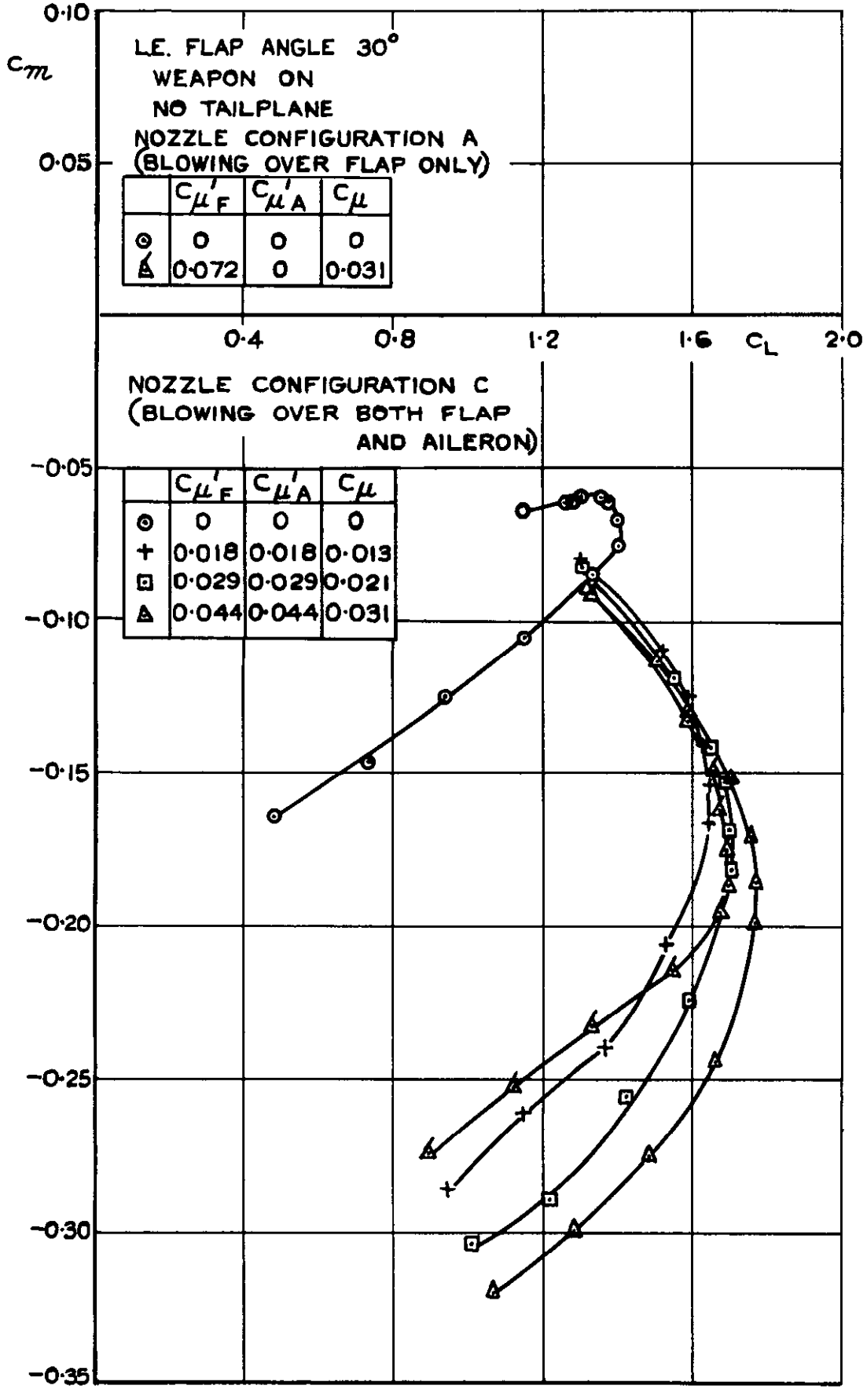

(e). FLAP ANGLE = 60°; AILERON ANGLE = 45°.

FIG. 18. (CONCL'D.).

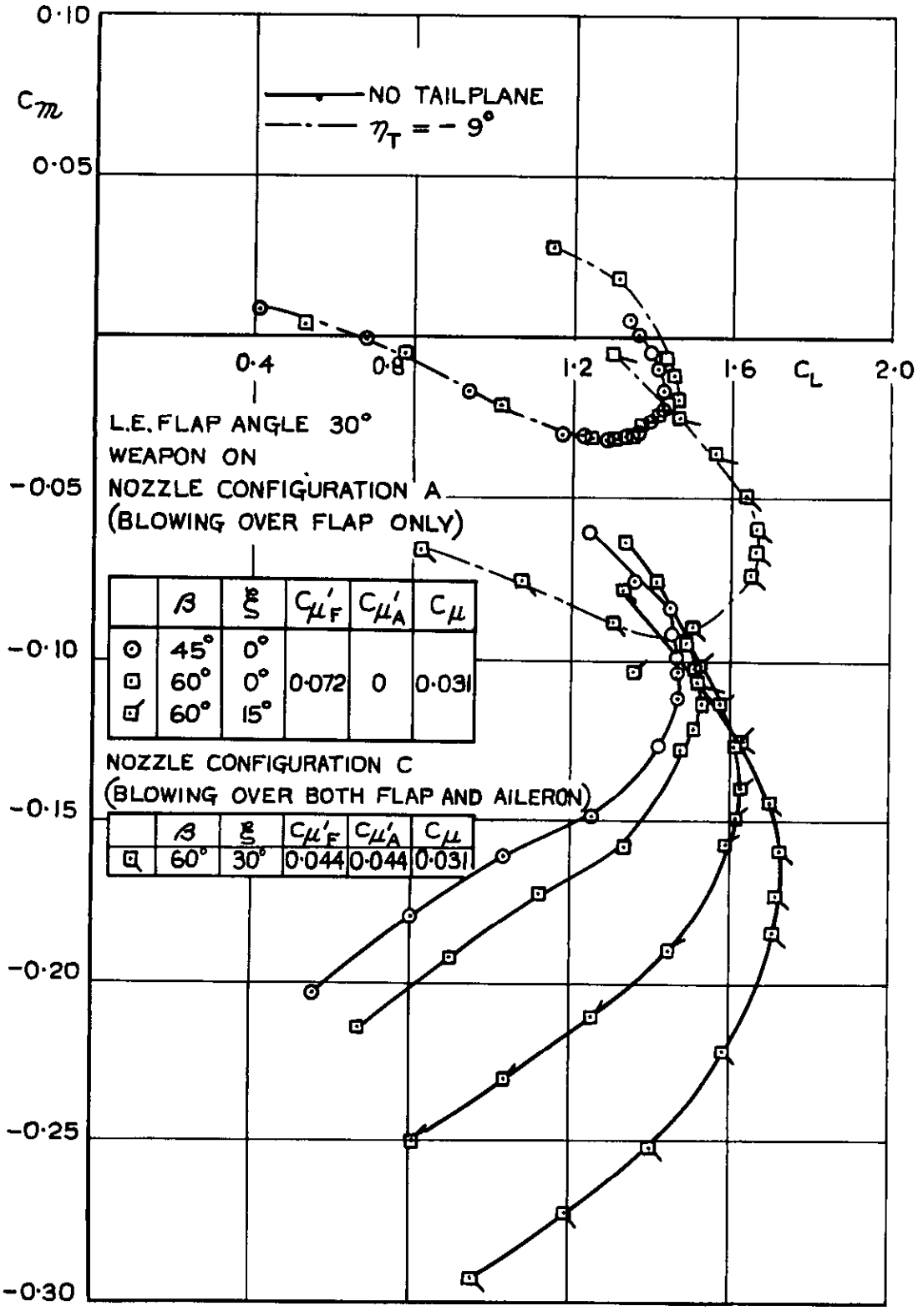

	β	ξ	$C_{\mu'_F}$	$C_{\mu'_A}$	C_μ
⊙	45°	0°			
⊡	60°	0°	0·072	0	0·031
⊡	60°	15°			

	β	ξ	$C_{\mu'_F}$	$C_{\mu'_A}$	C_μ
⊡	60°	30°	0·044	0·044	0·031

FIG. 19. THE EFFECTS OF FLAP ANGLE, AILERON ANGLE, AND SPANWISE EXTENT OF BLOWING ON C_m v C_L AT $C_\mu = 0·031$.

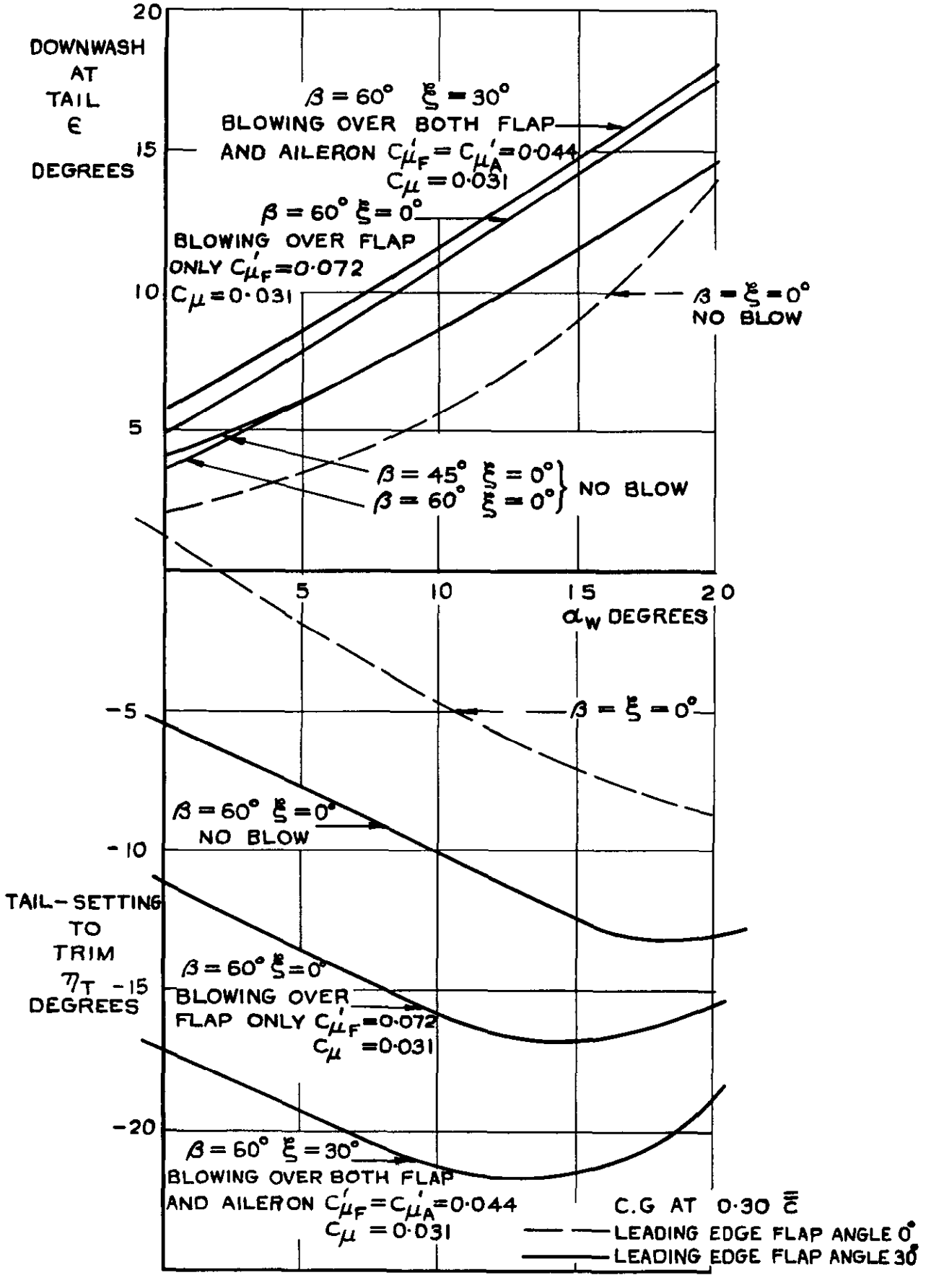

FIG. 20. DOWNWASH AT TAIL AND TAIL-SETTING TO TRIM v α_W.

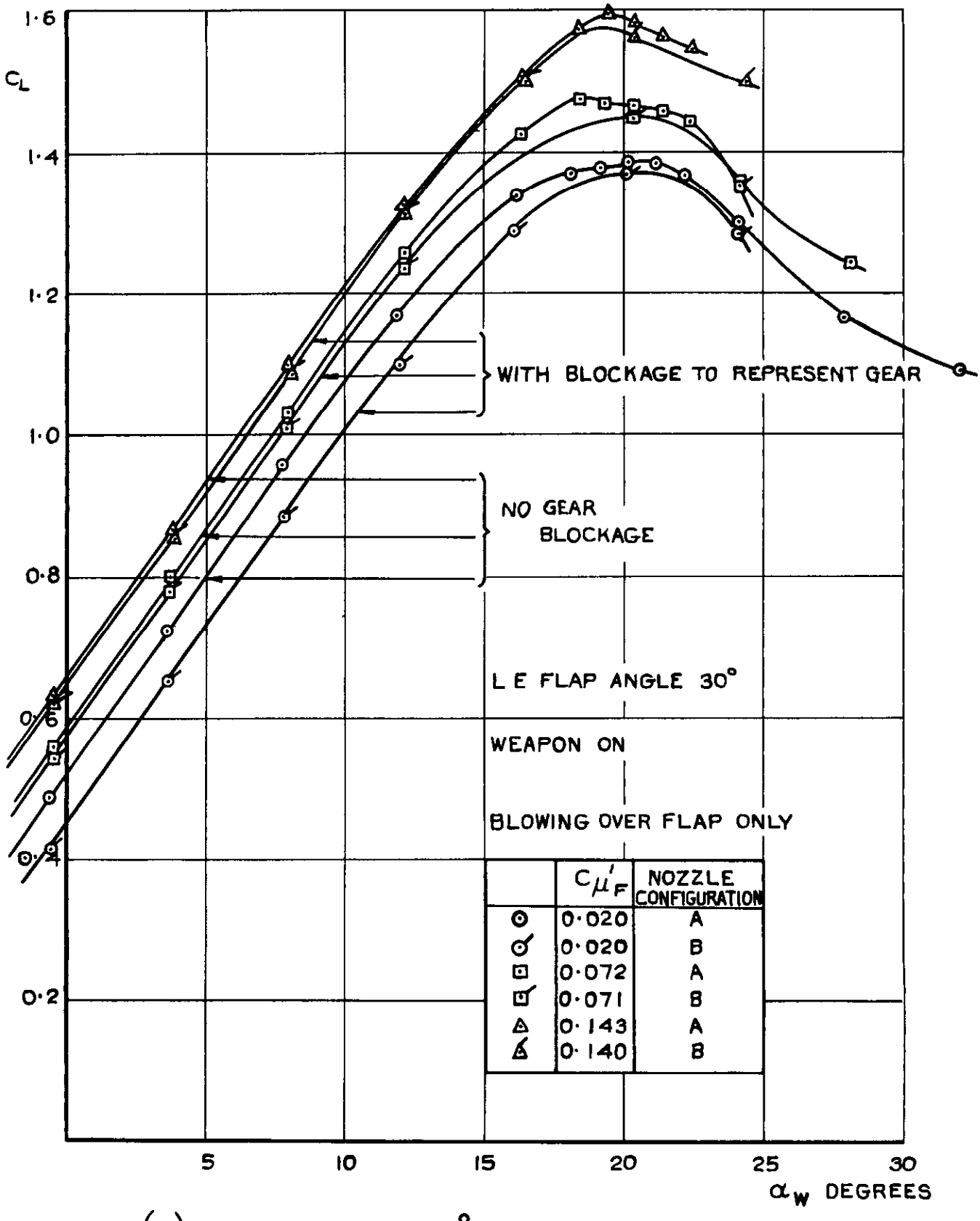

(a). FLAP ANGLE = 45°; AILERON UNDEFLECTED.

FIG.21. THE EFFECT OF LOCAL NOZZLE BLOCKAGE TO REPRESENT FLAP AND AILERON SUPPORT GEAR ON C_L (NO TAILPLANE) v α_w.

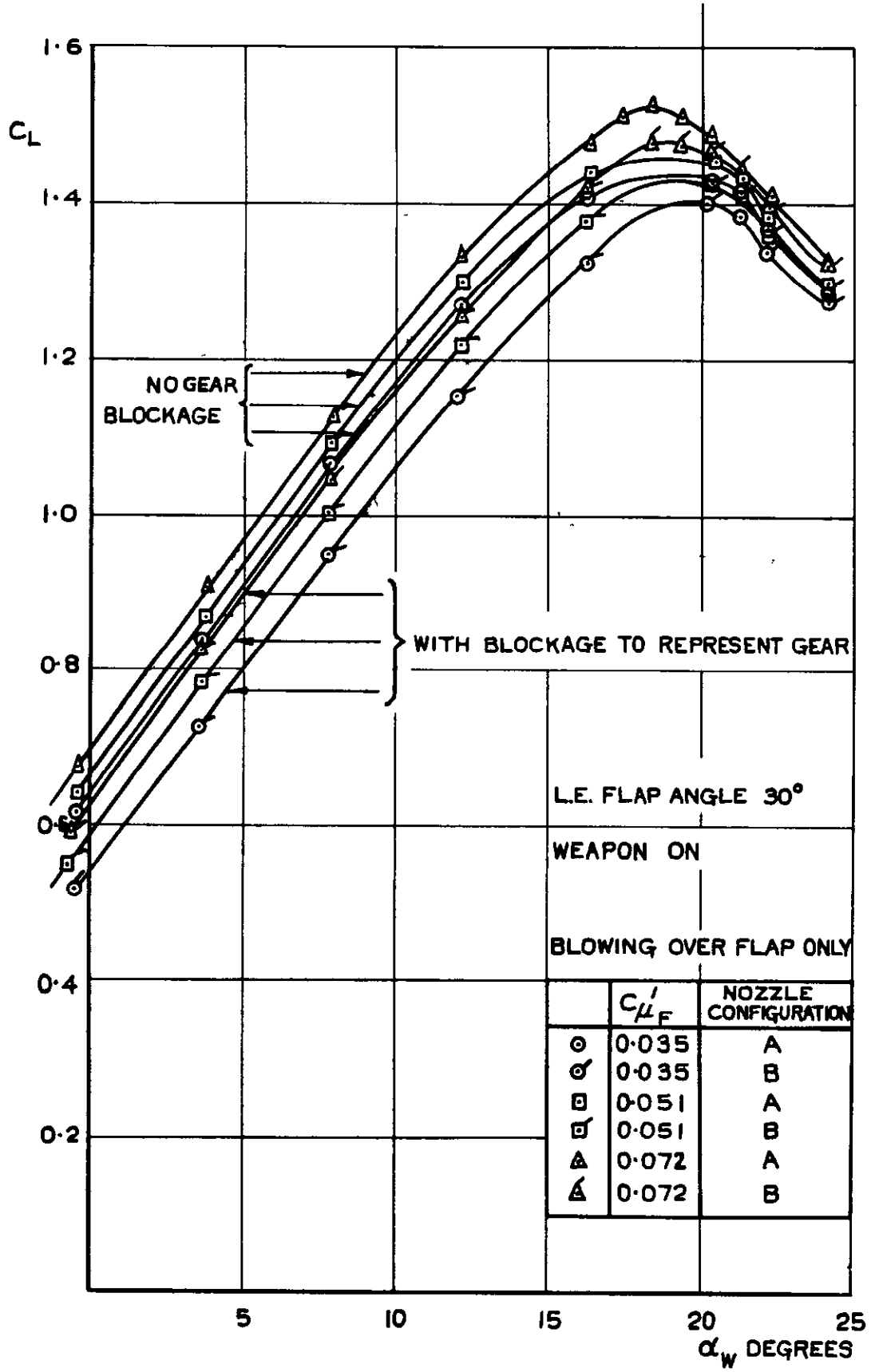

(b). FLAP ANGLE = 60°; AILERON UNDEFLECTED.

FIG. 21 (CONT'D).

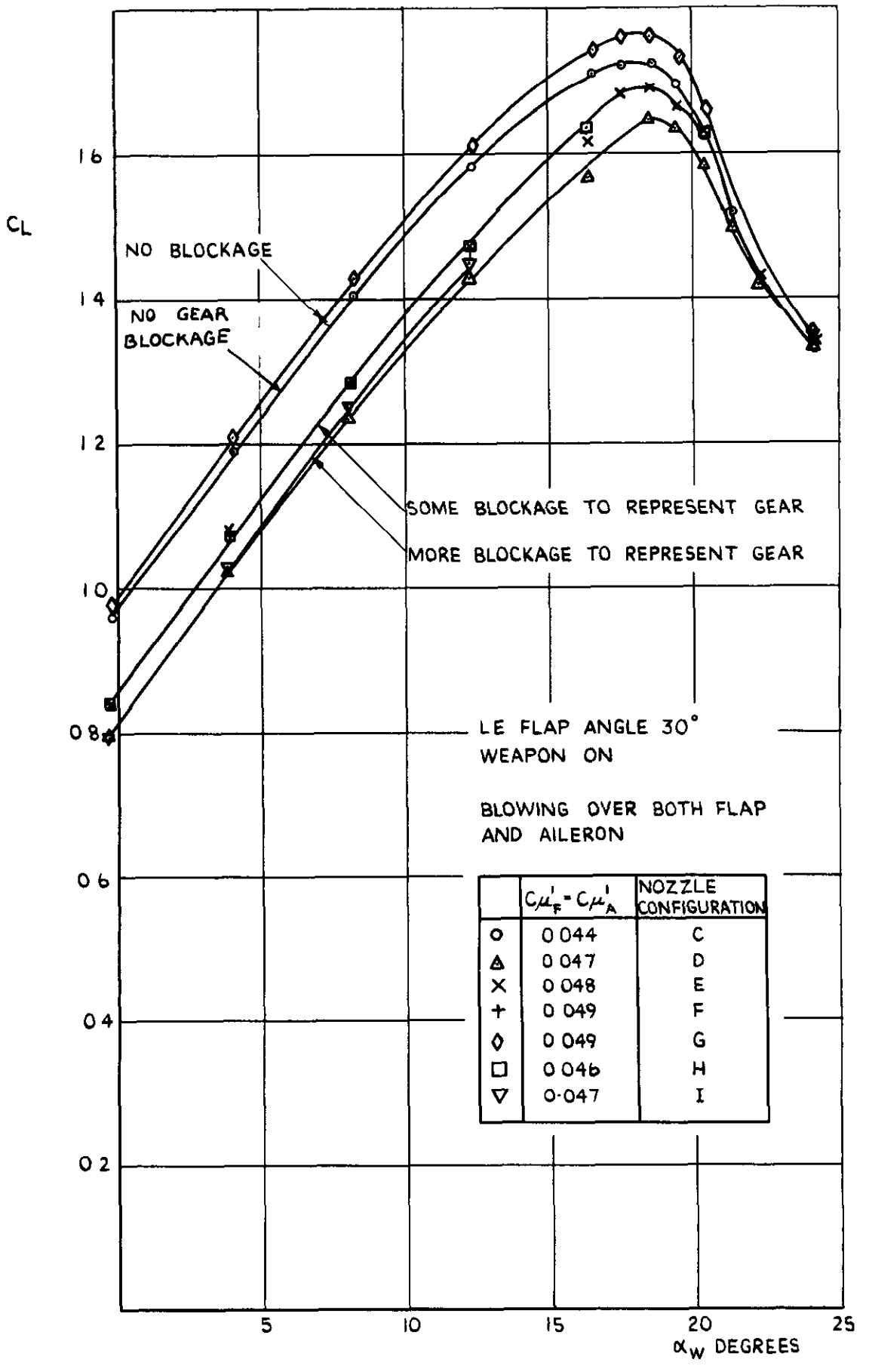

(C). FLAP ANGLE = 60°; AILERON ANGLE = 30°.

FIG. 21 (CONCL'D.).

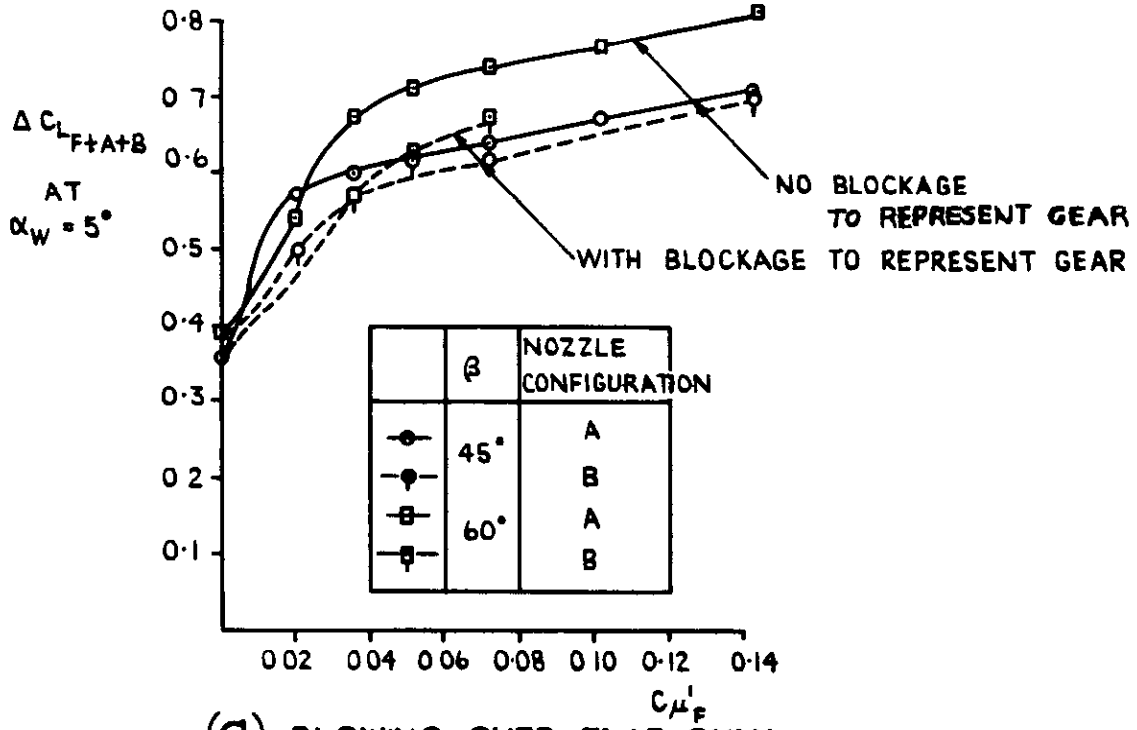

(a). BLOWING OVER FLAP ONLY.

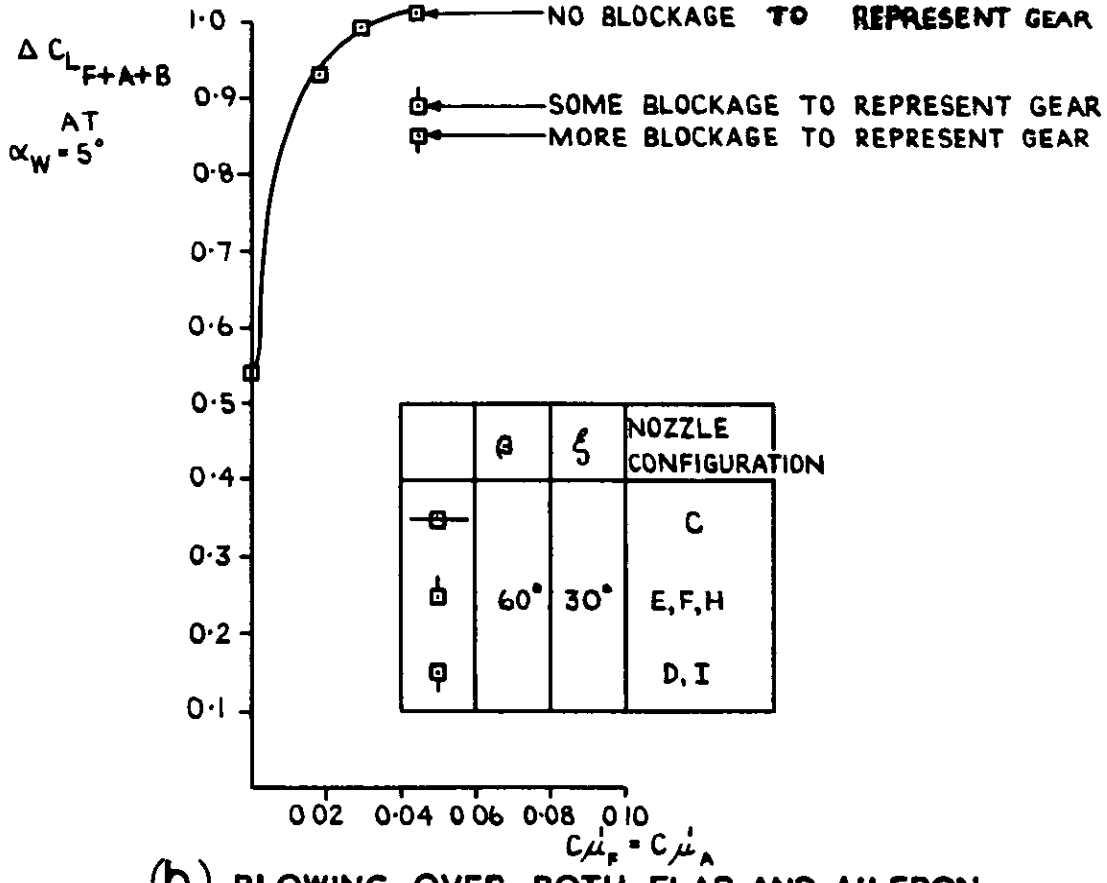

(b). BLOWING OVER BOTH FLAP AND AILERON.

FIG. 22. THE EFFECT OF LOCAL NOZZLE BLOCKAGE TO REPRESENT FLAP AND AILERON SUPPORT GEAR ON $\Delta C_{L_{F+A+B}}$ AT $\alpha_W = 5°$.

L.E. FLAP ANGLE 30°
WEAPON ON
NO TAILPLANE

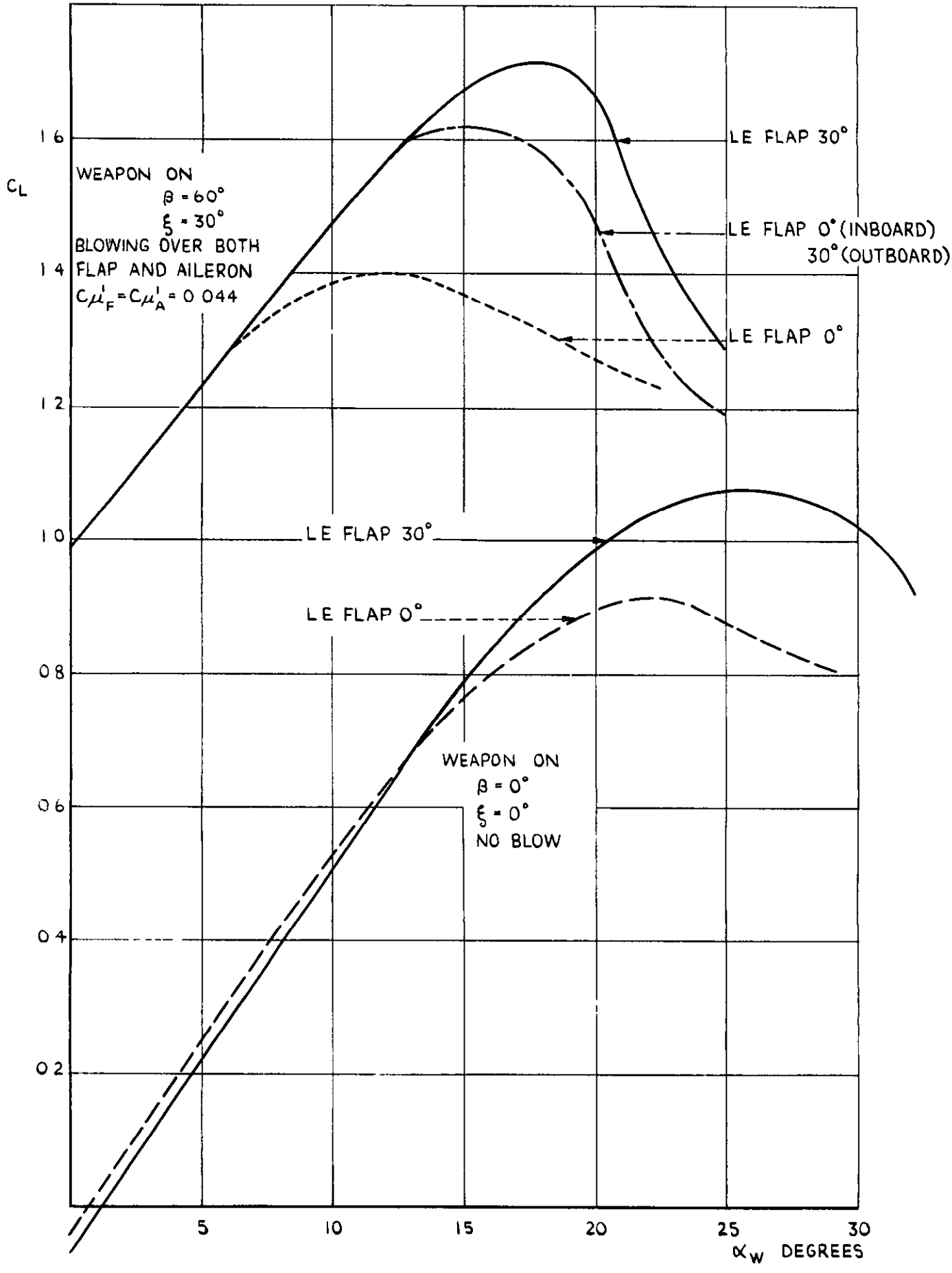

(a). C_L (NO TAILPLANE) ν α_W

FIG. 23. THE EFFECT OF THE LEADING - EDGE FLAP.

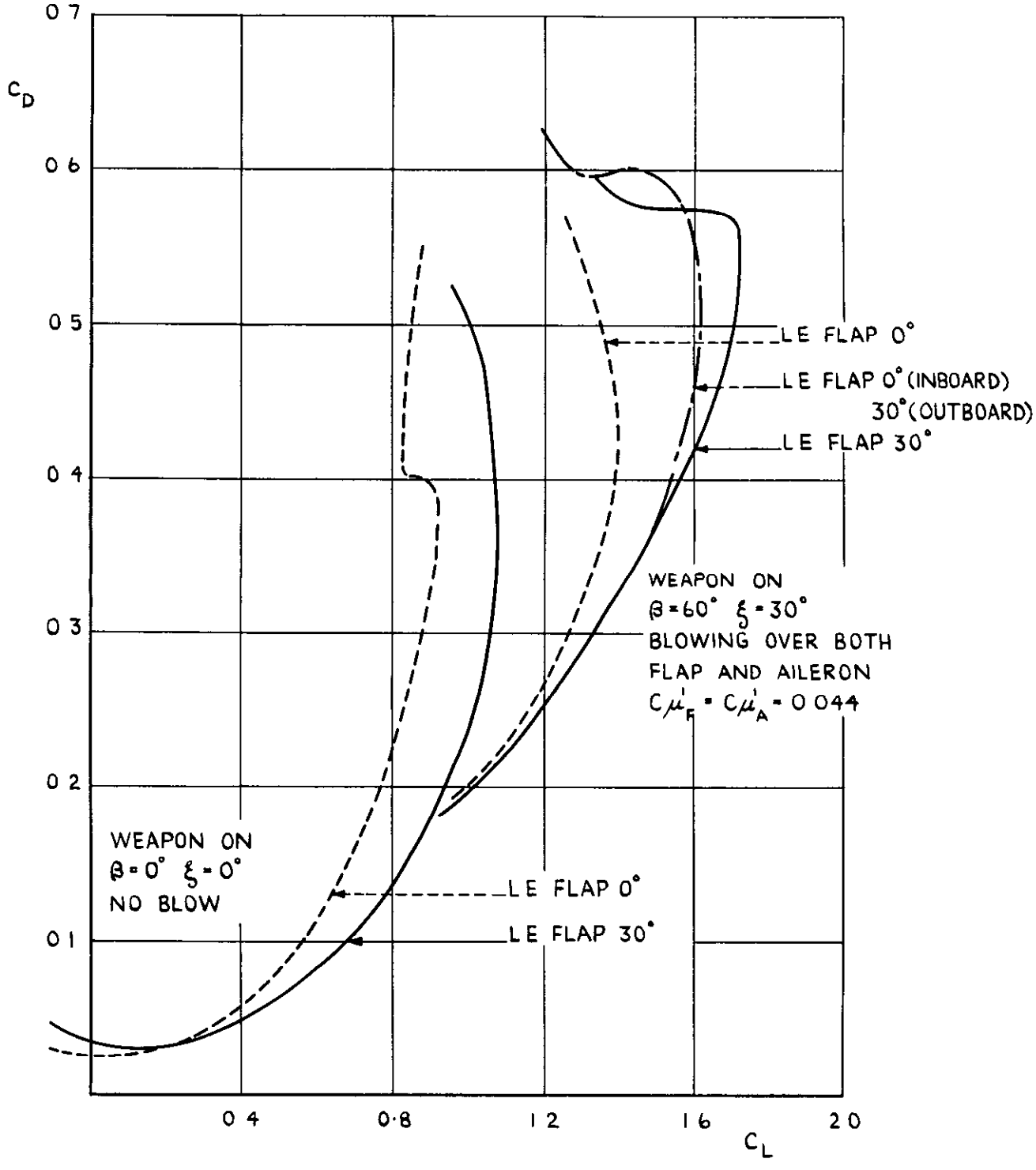

(b). C_D V C_L (NO TAILPLANE).

FIG. 23 (CONT'D).

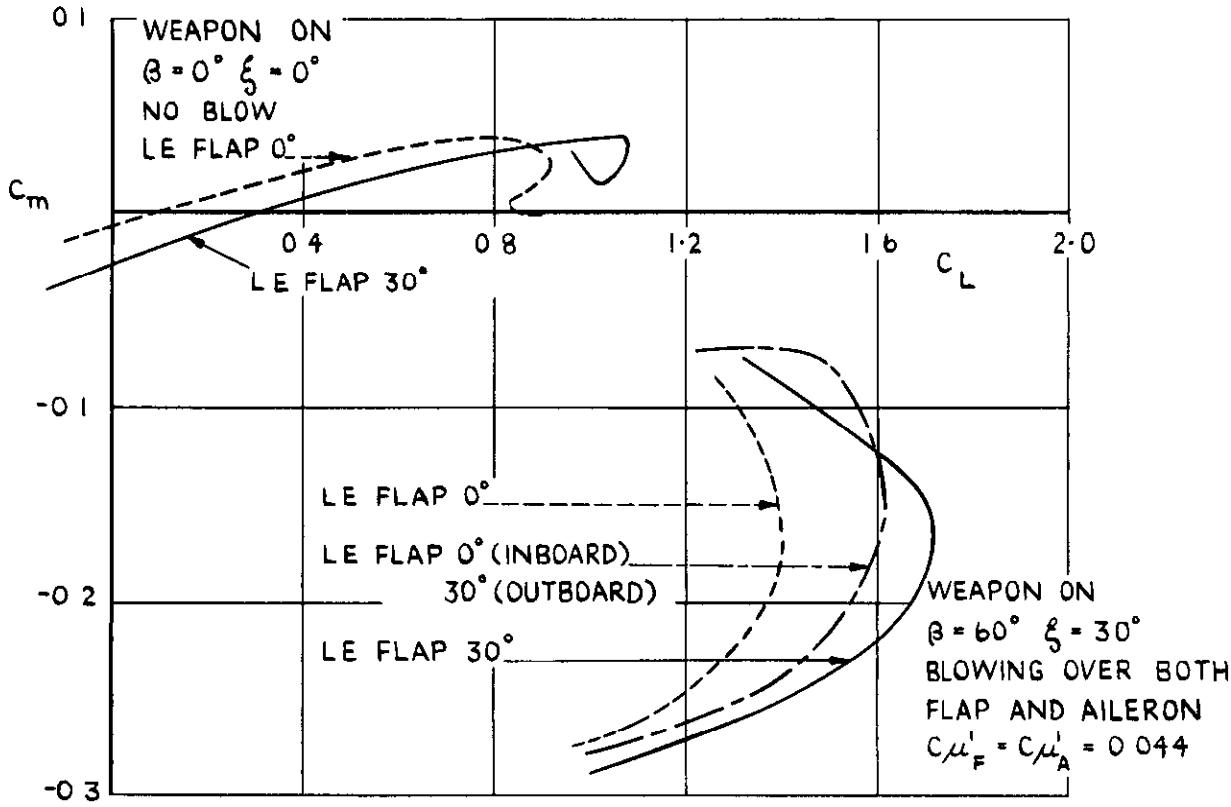

NO TAILPLANE

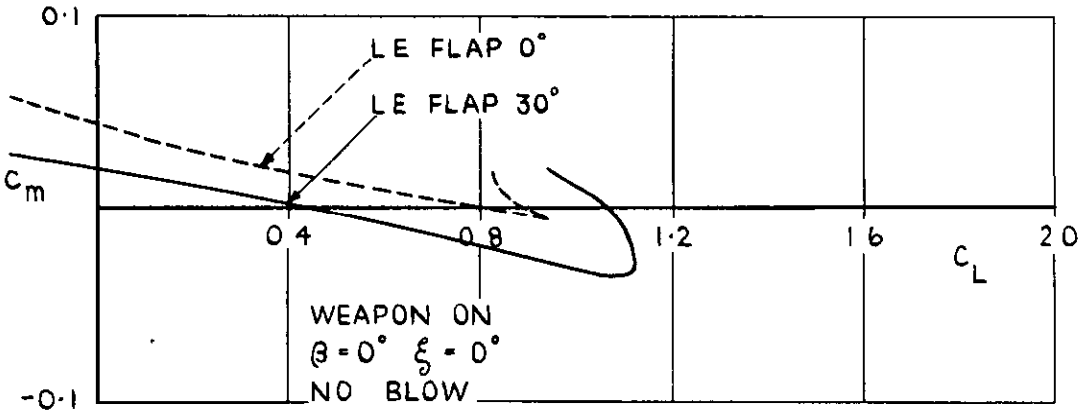

$\eta_T = -3°$

(C). C_m v C_L.

FIG. 23 (CONCL'D.).

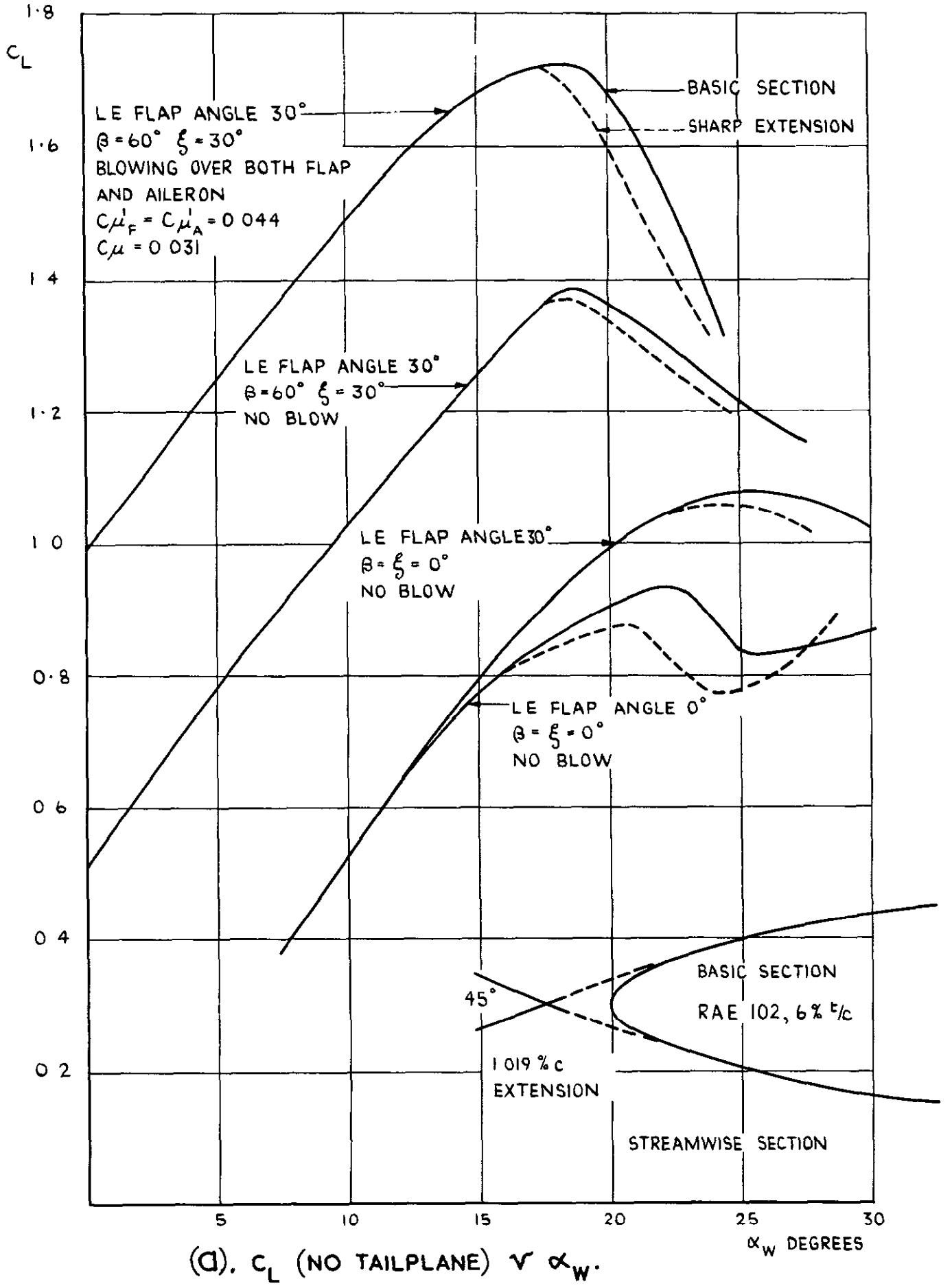

(a). C_L (NO TAILPLANE) v α_W.

FIG. 24. THE EFFECT OF THE SHARP WING LEADING-EDGE EXTENSION.

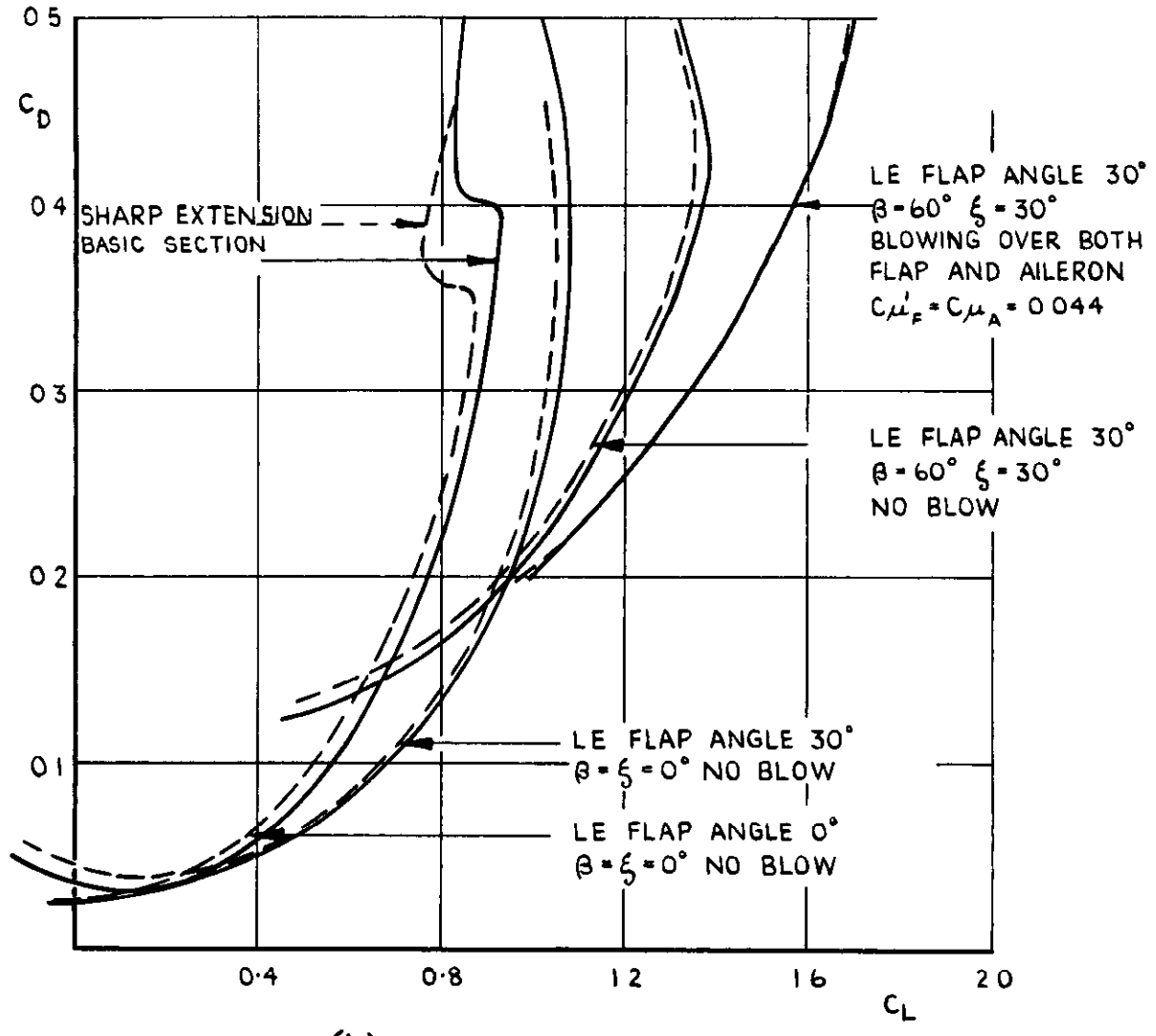

(b). C_D v C_L (NO TAILPLANE).

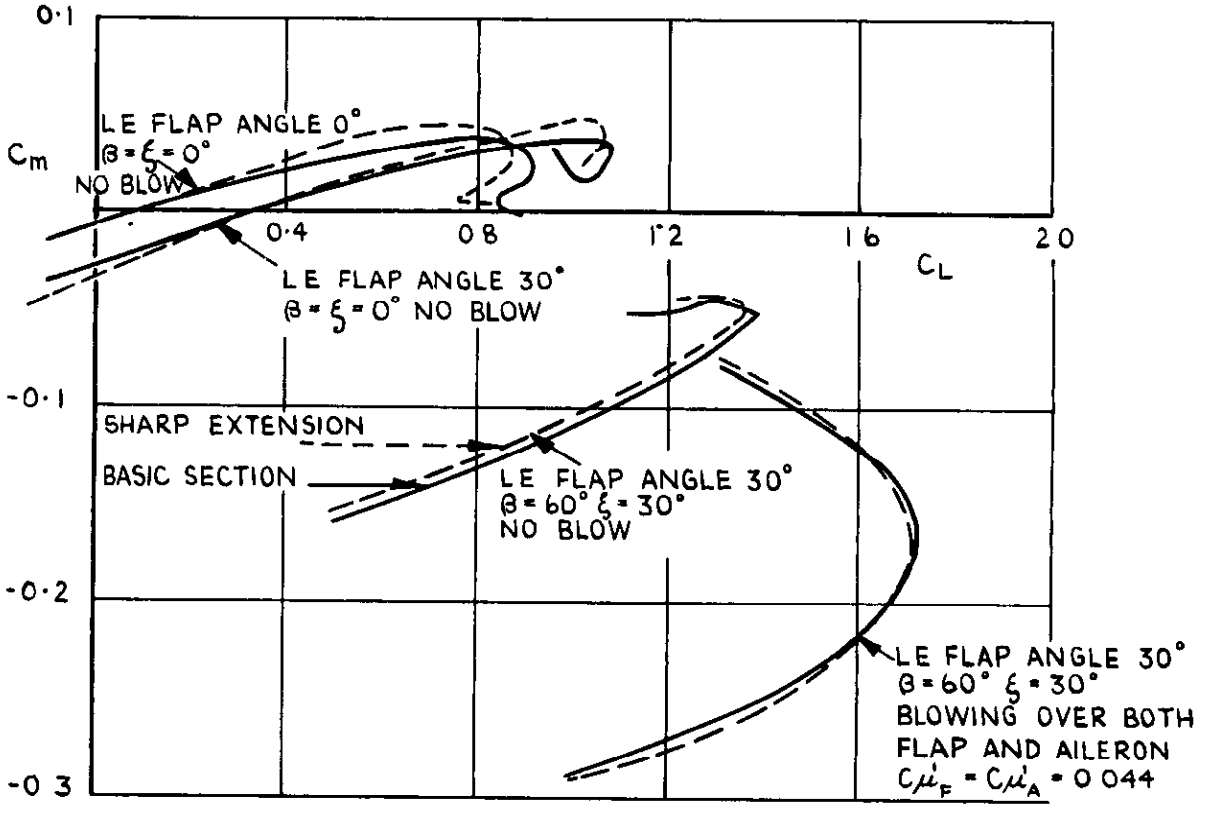

(C). C_m v C_L (NO TAILPLANE).

FIG. 24 (CONCL'D.).

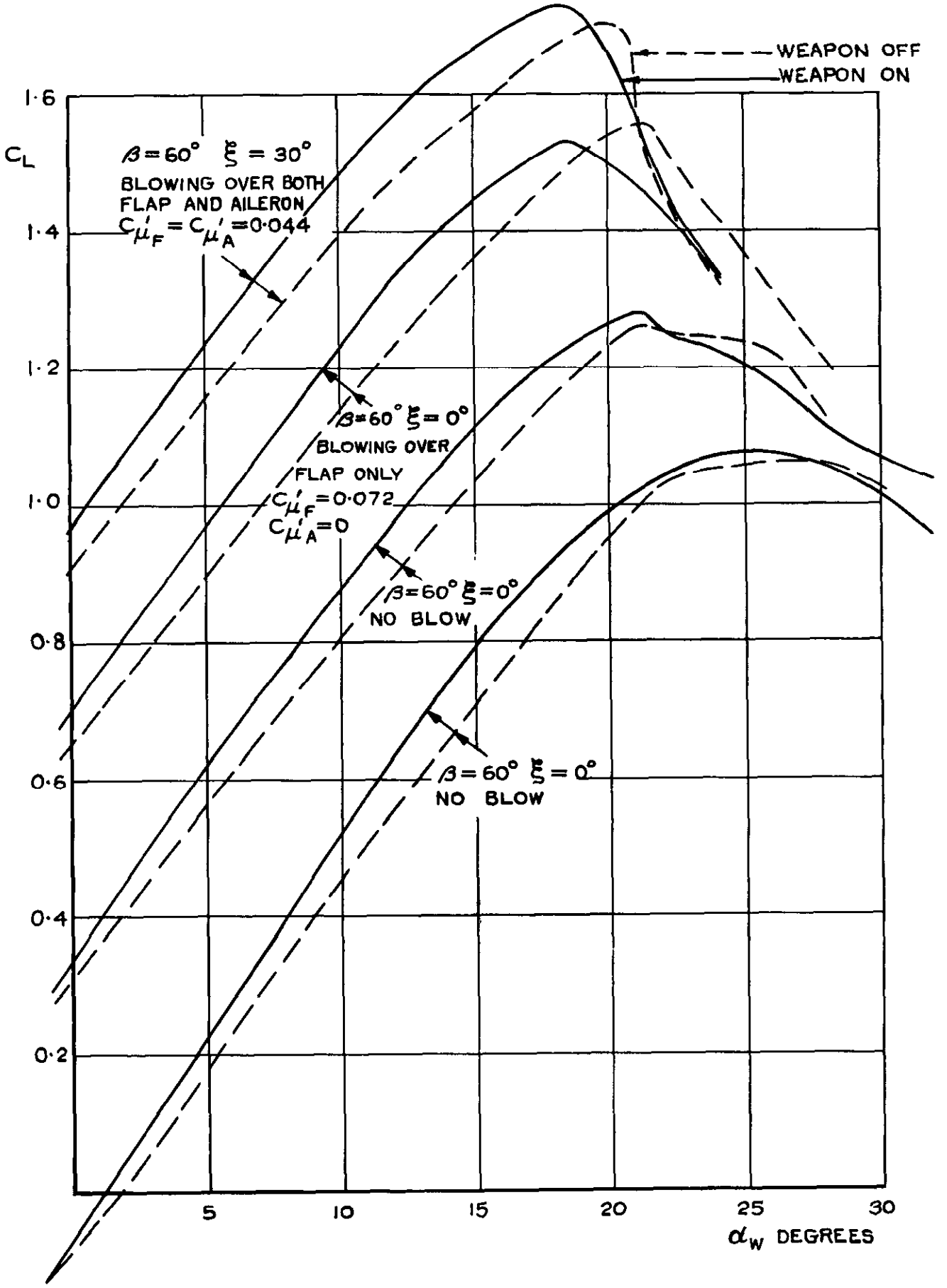

(a). C_L (NO TAILPLANE).

FIG. 25. THE EFFECT OF THE TIP WEAPON.

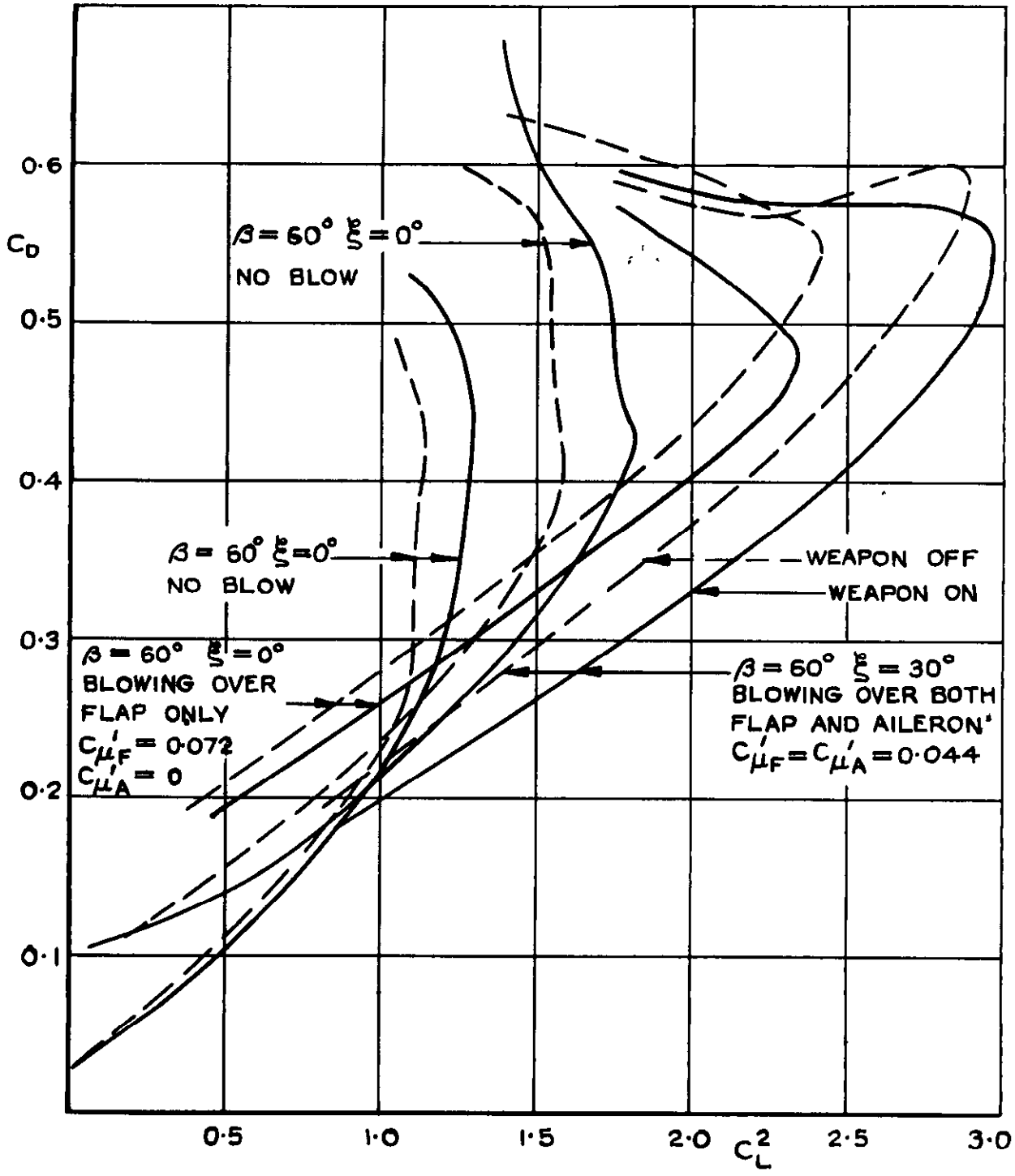

(b). C_D v C_L^2 (NO TAILPLANE).

FIG. 25 (CONT'D).

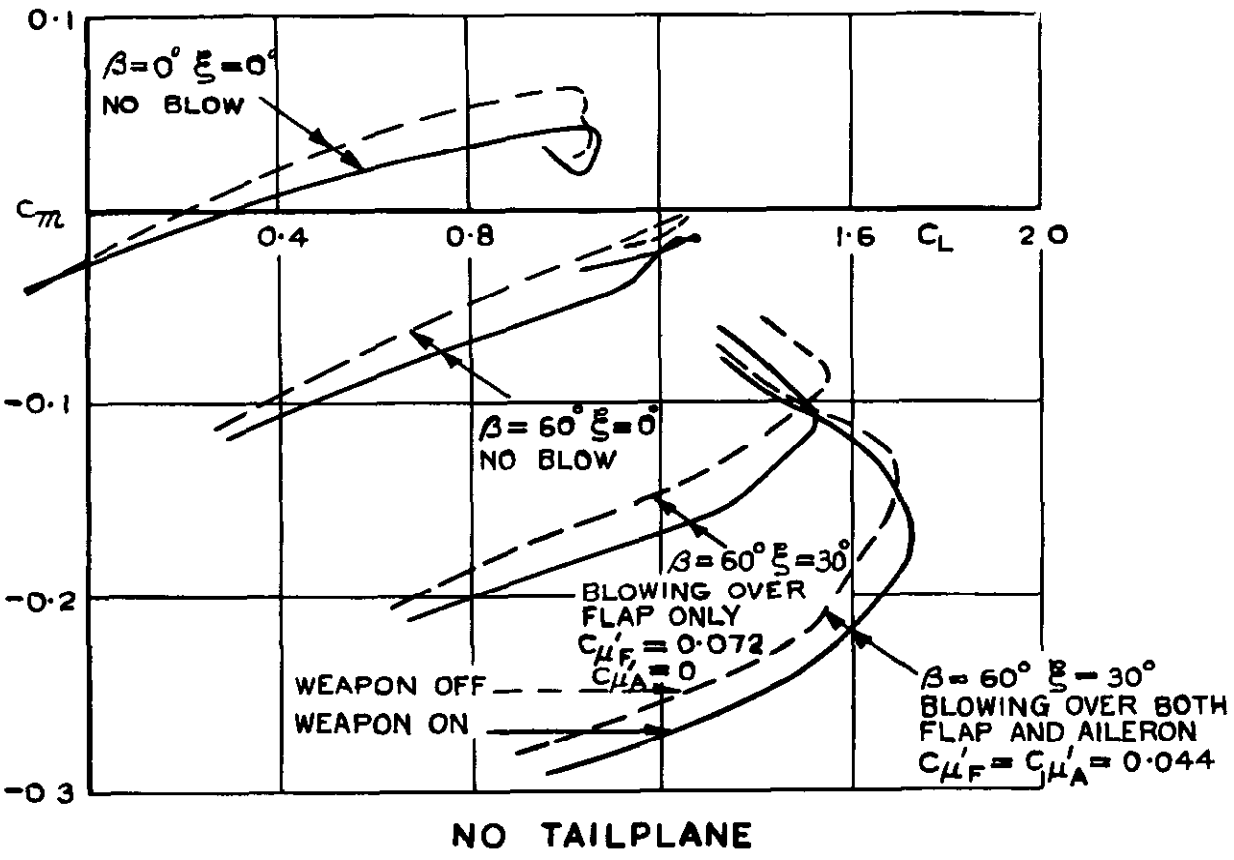

NO TAILPLANE

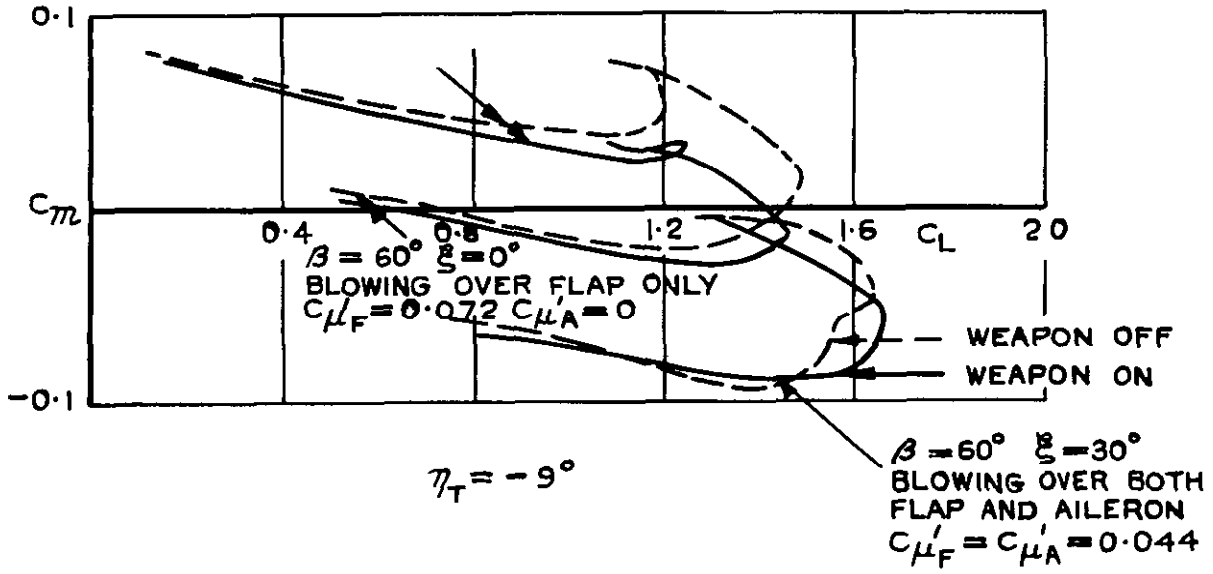

$\eta_T=-9^\circ$

(c). C_m v C_L

FIG. 25 (CONCL'D.).

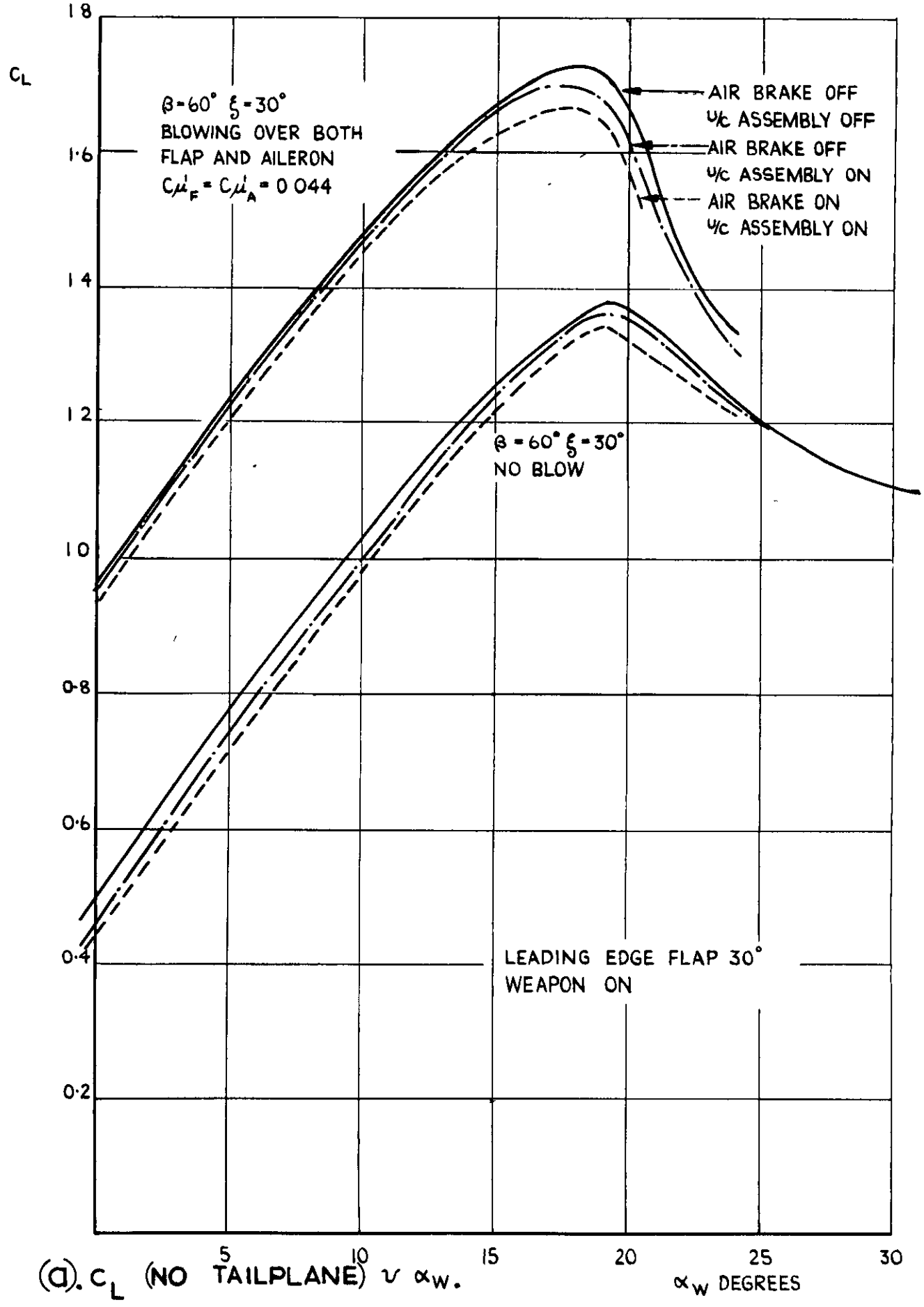

(a). C_L (NO TAILPLANE) v α_W.

FIG .26. THE EFFECTS OF THE MAIN UNDERCARRIAGE ASSEMBLY AND THE AIRBRAKE

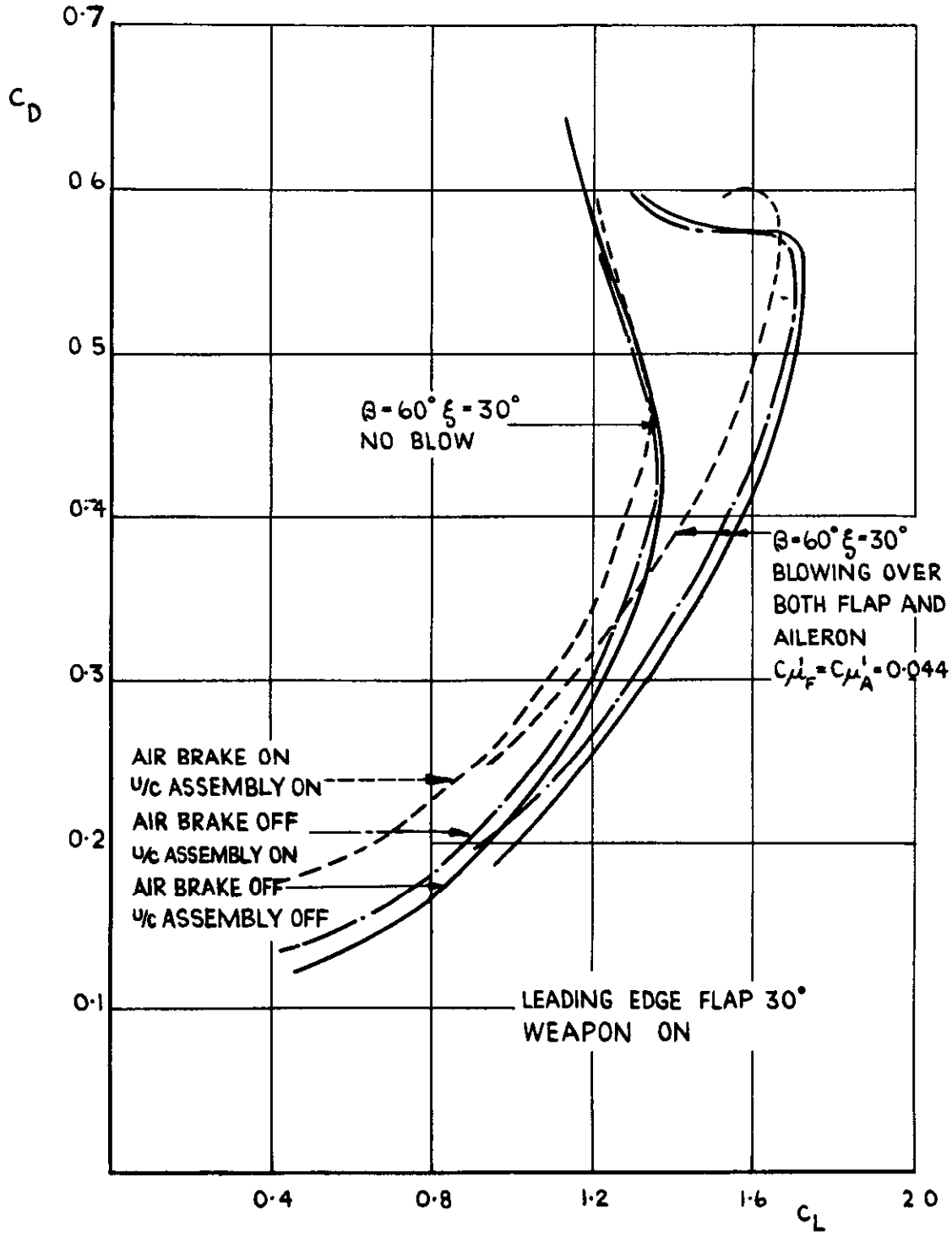

(b). C_D v C_L (NO TAILPLANE).

FIG. 26 (CONT'D.).

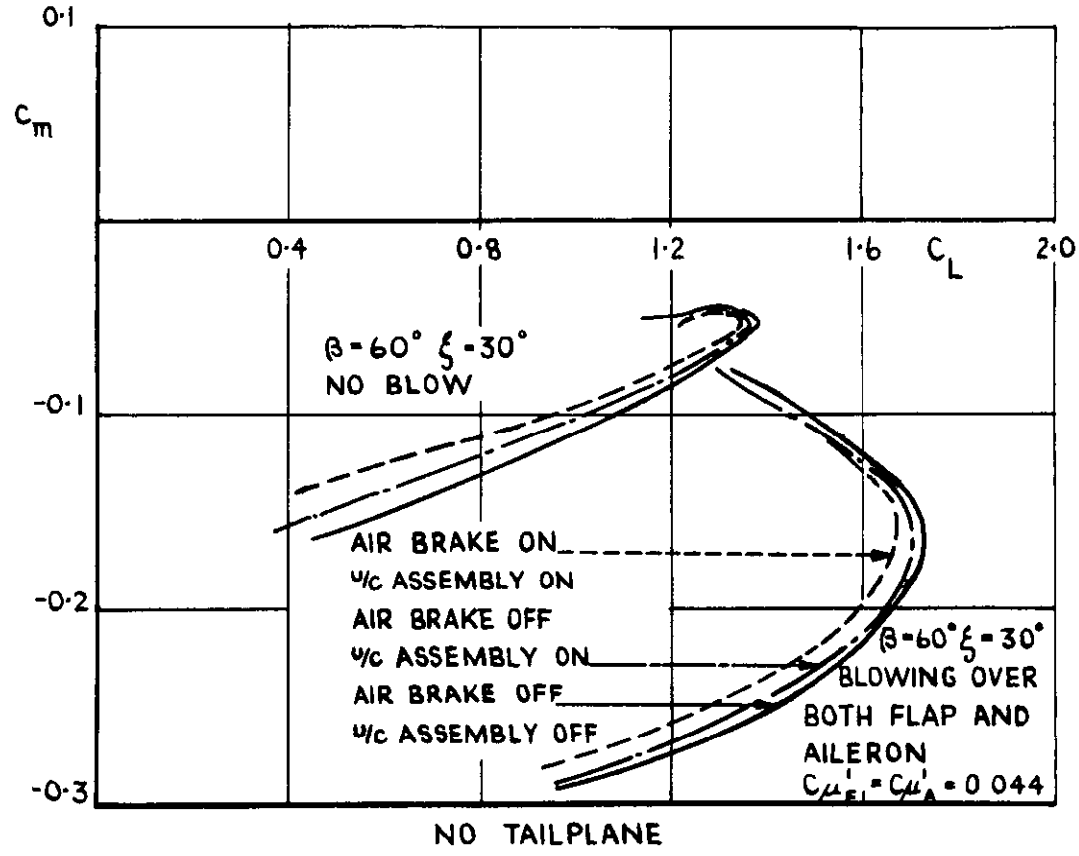

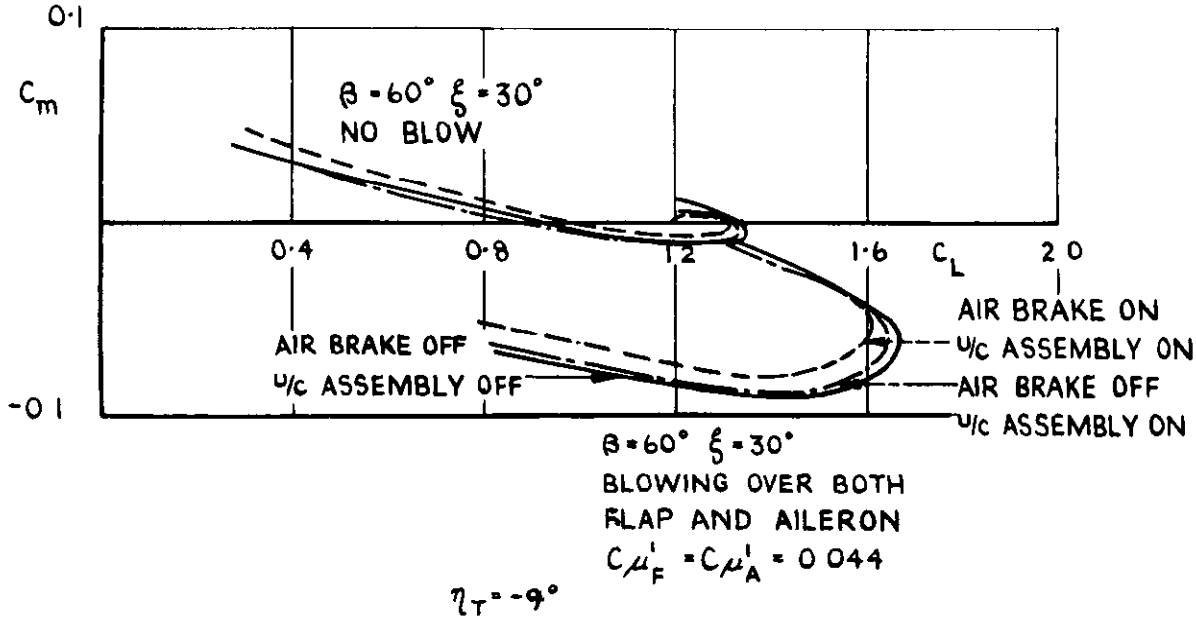

(C). C_m v C_L.

FIG. 26 (CONCL'D).

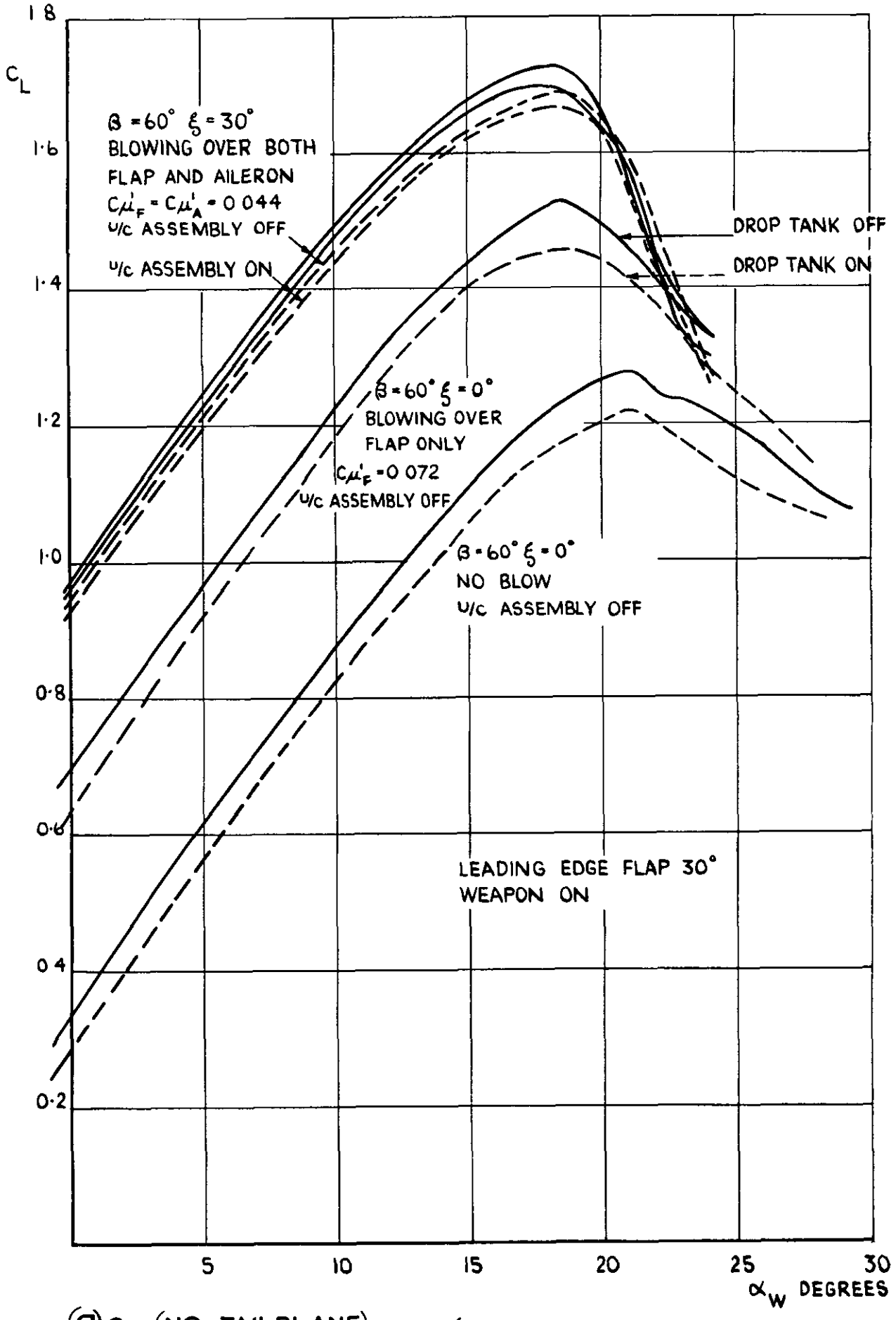

(a), C_L (NO TAILPLANE) ν α_W.

FIG. 27. THE EFFECT OF THE DROP TANK.

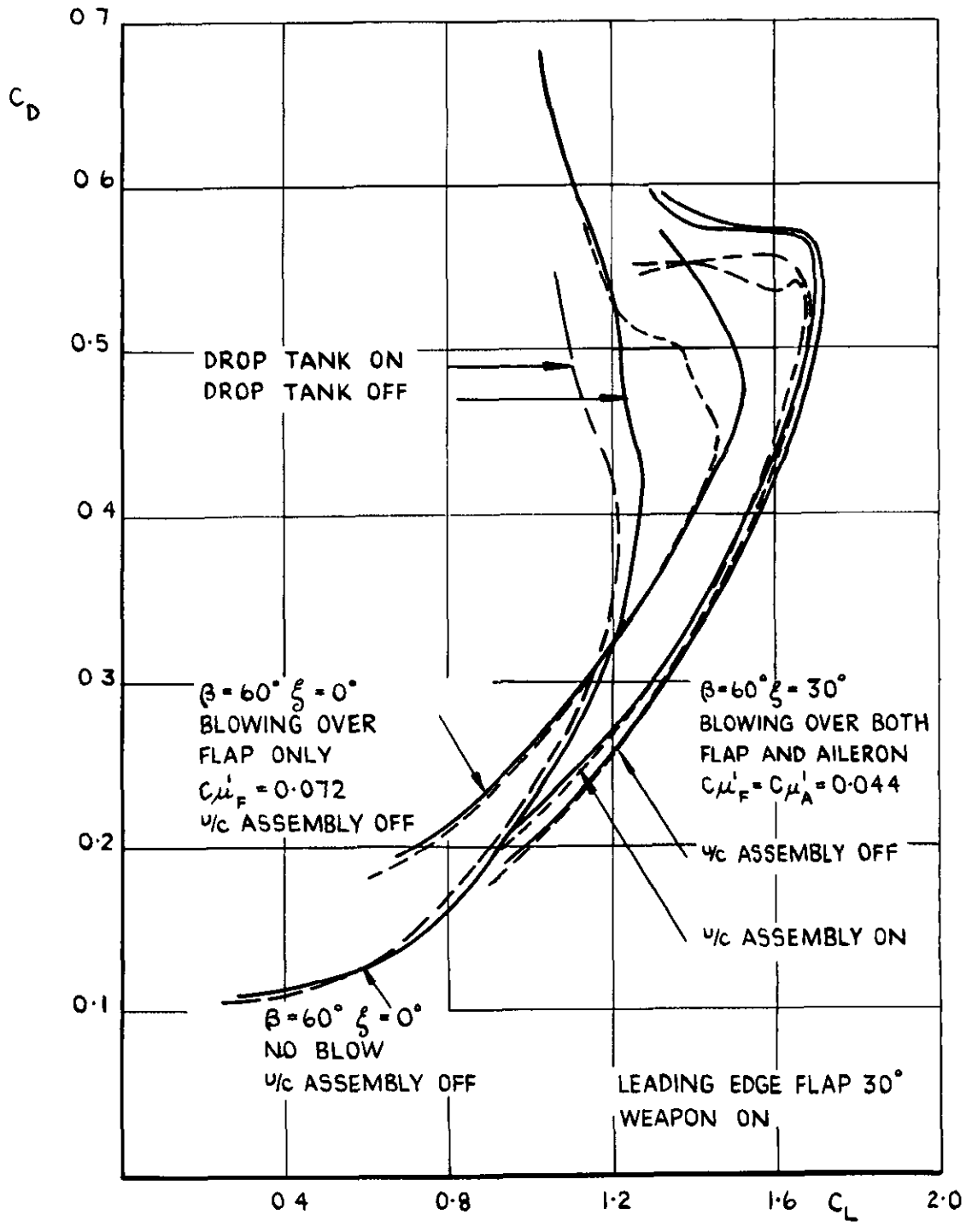

(b). C_D v C_L (NO TAILPLANE).

FIG. 27 (CONT'D).

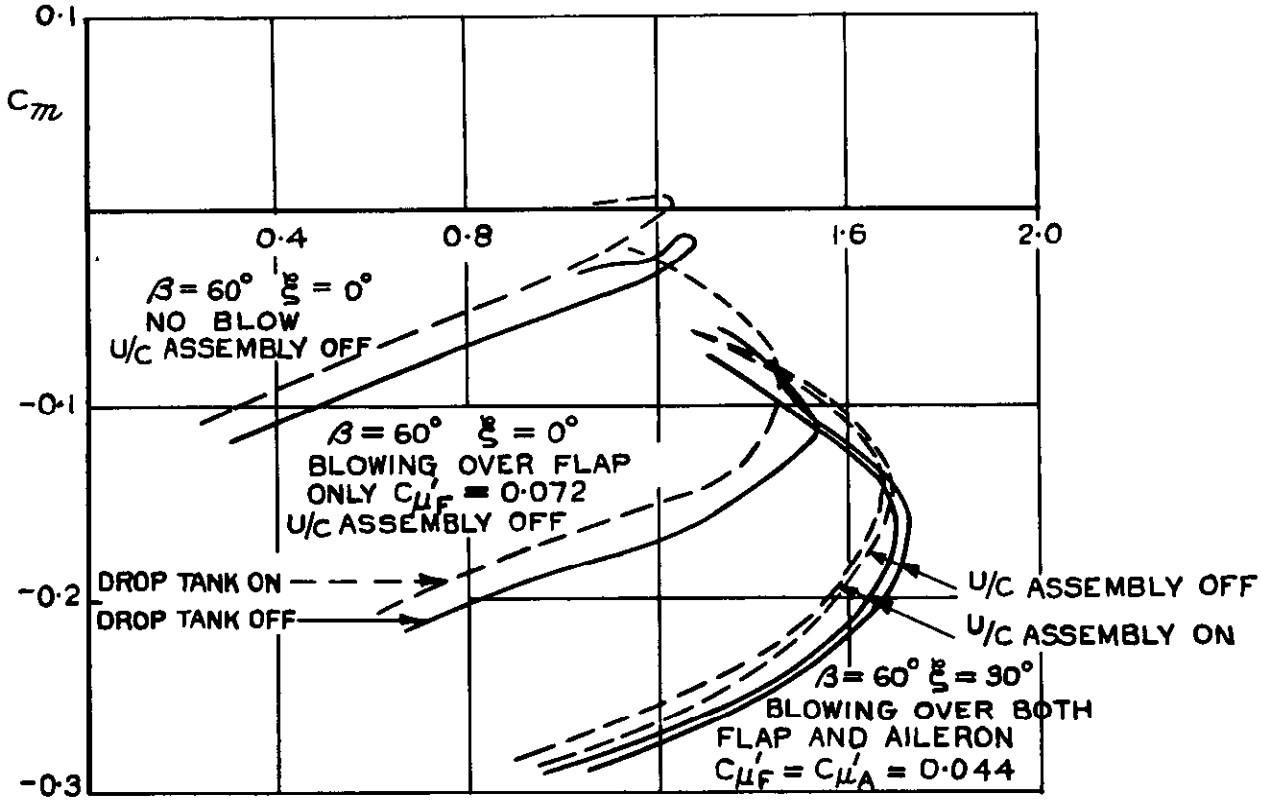

NO TAILPLANE

LEADING EDGE FLAP 30° WEAPON ON

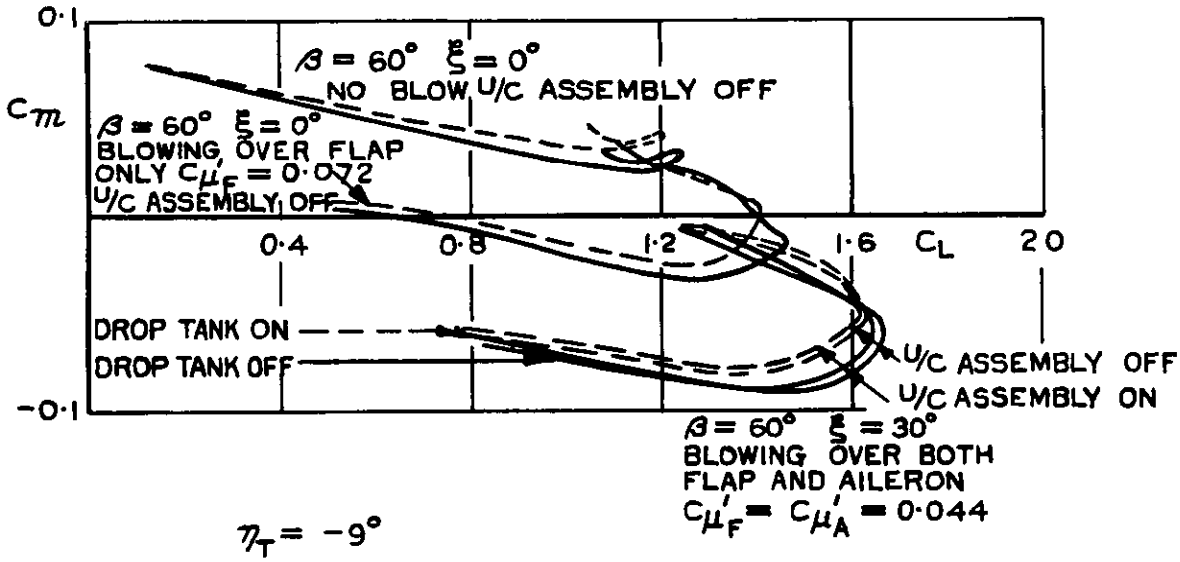

$\eta_T = -9°$

(C). C_m v C_L.

FIG. 27 (CONCL'D.).

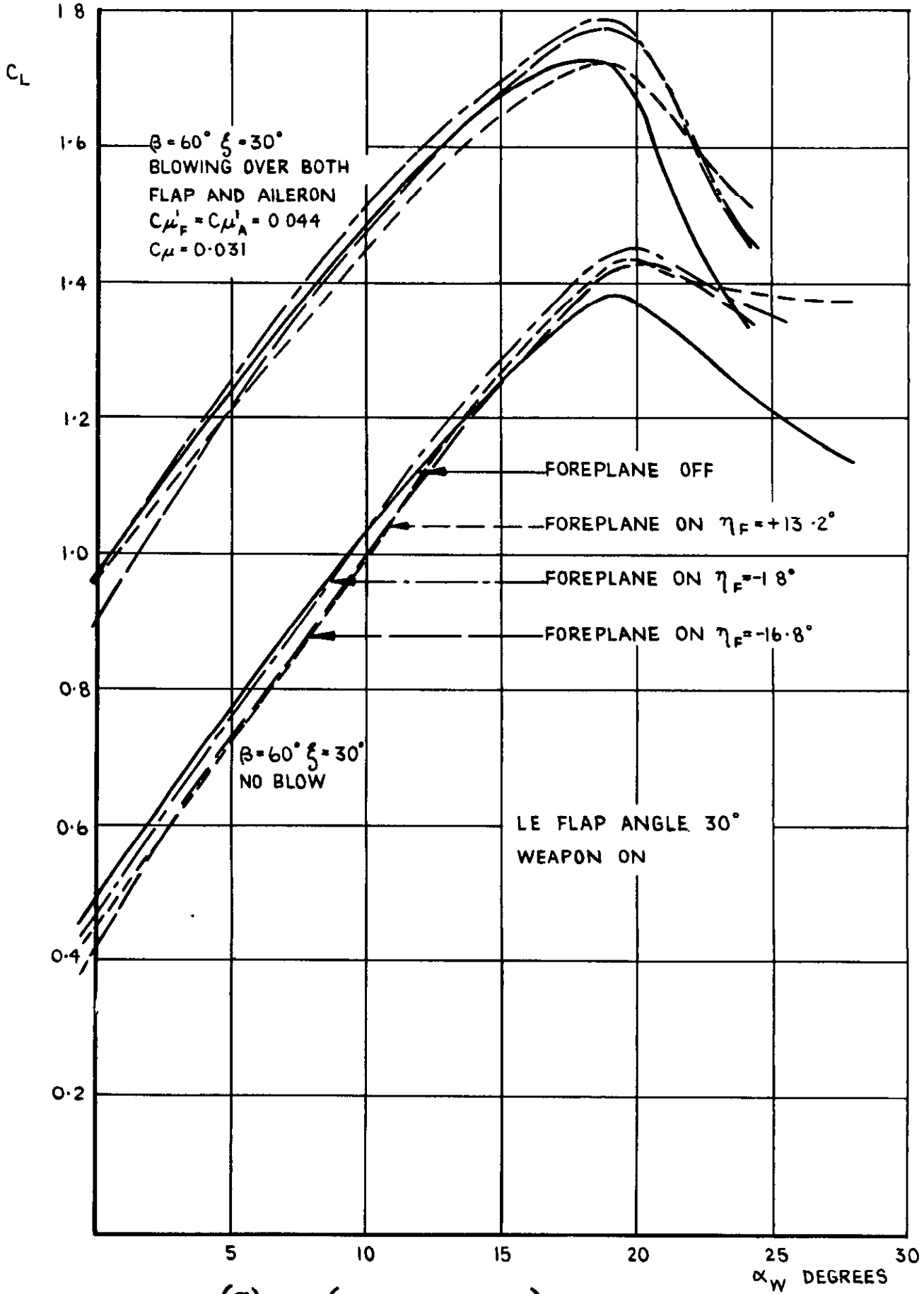

(a). C_L (NO TAILPLANE) ~ α_W.

FIG.28. THE EFFECT OF THE FOREPLANE (L.E. FLAP ANGLE 30°).

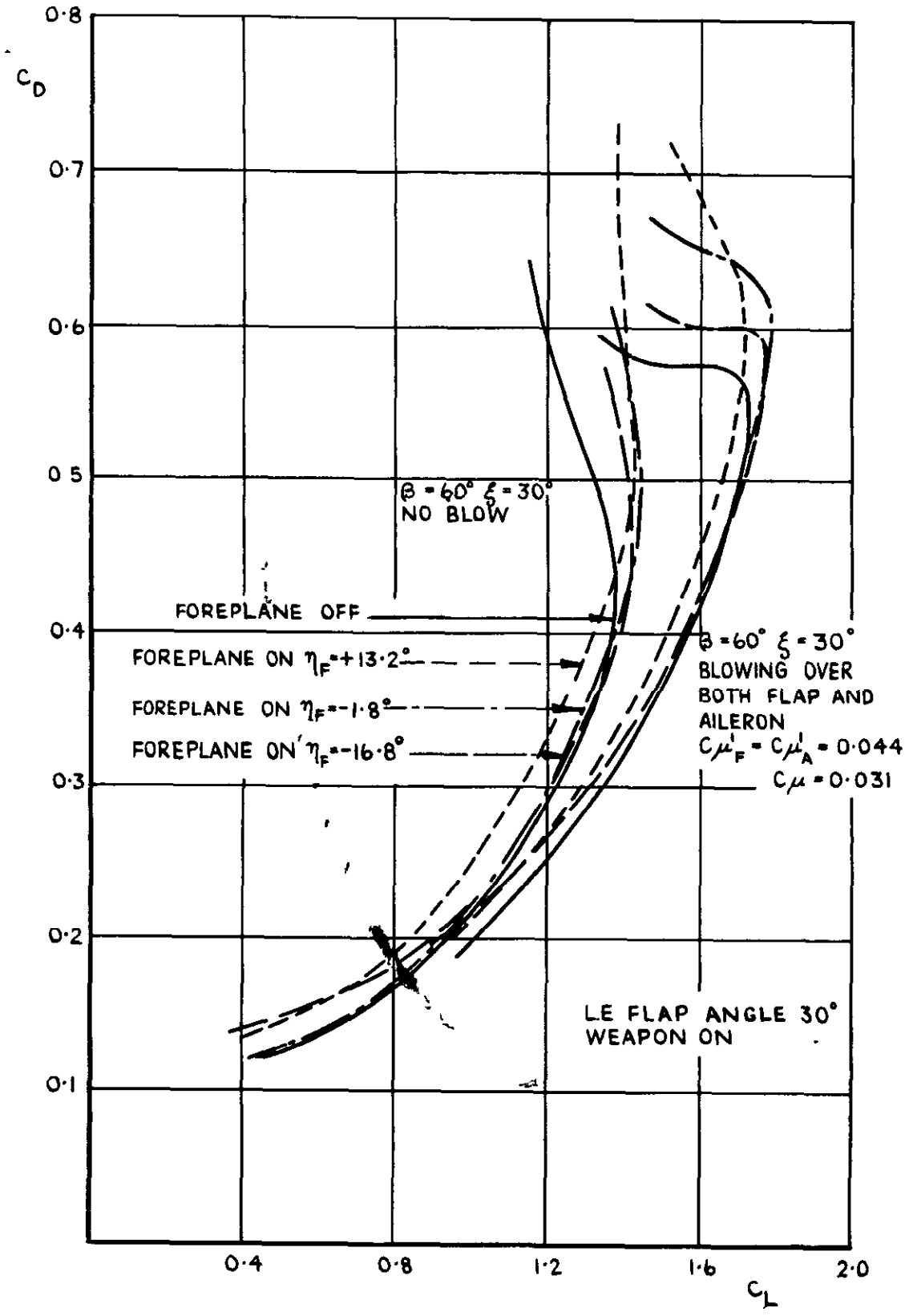

(b). C_D v C_L (NO TAILPLANE).

FIG. 28 (CONT'D).

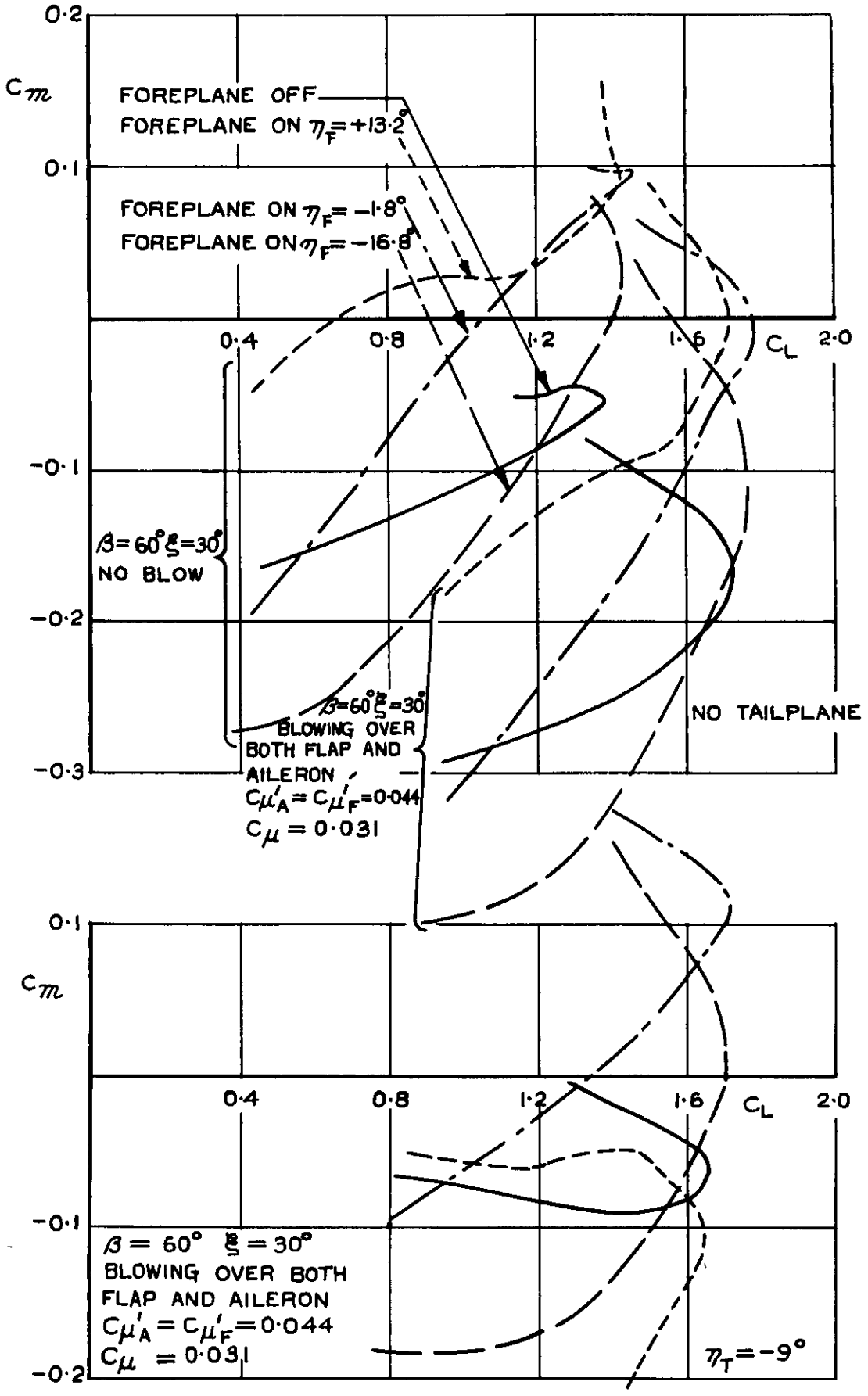

(C). C_m v C_L.

FIG. 28 (CONCL'D).

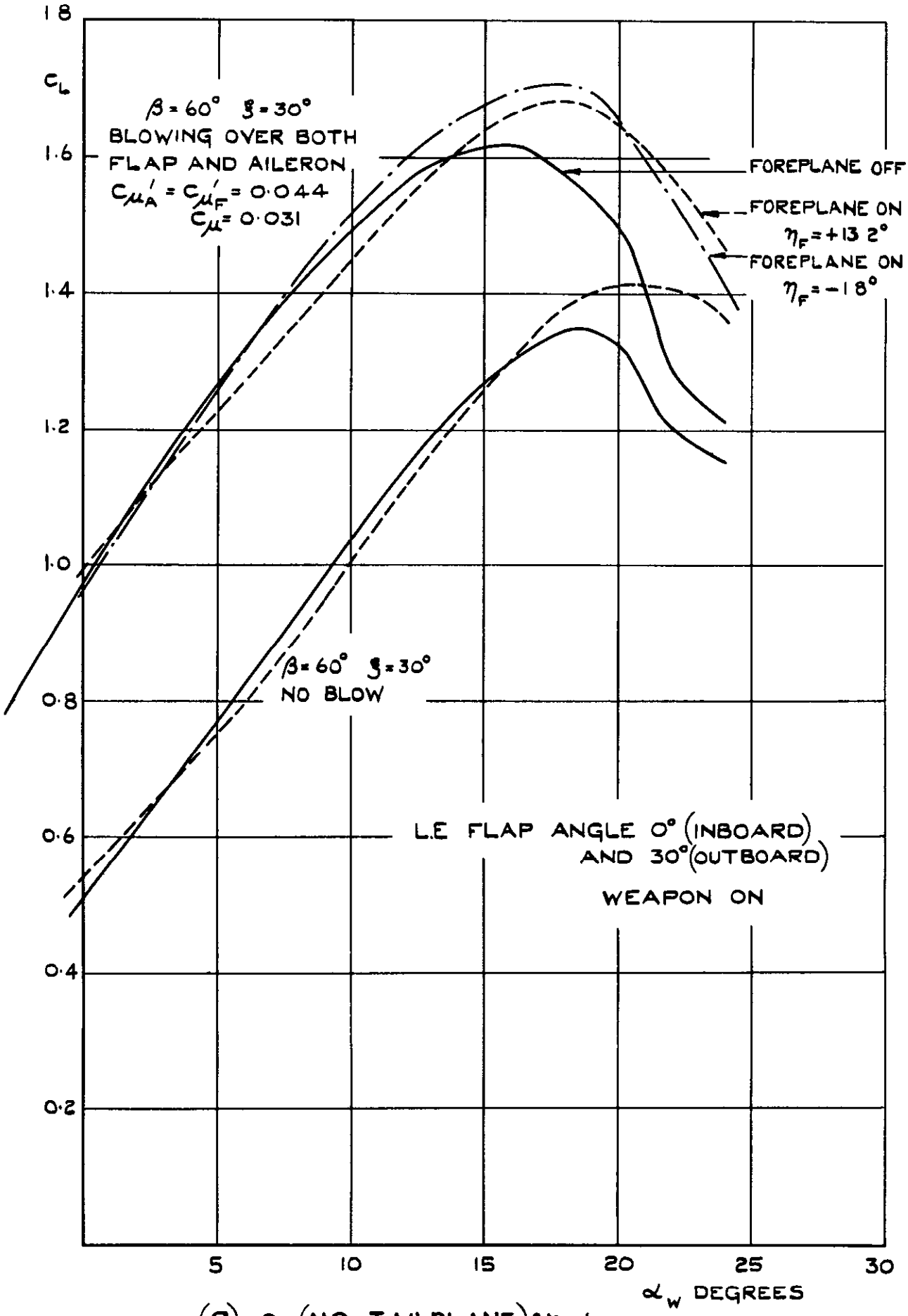

(a). C_L (NO TAILPLANE) υ α_w.

FIG. 29. THE EFFECT OF THE FOREPLANE (L.E. FLAP ANGLE 0° INBOARD AND 30° OUTBOARD).

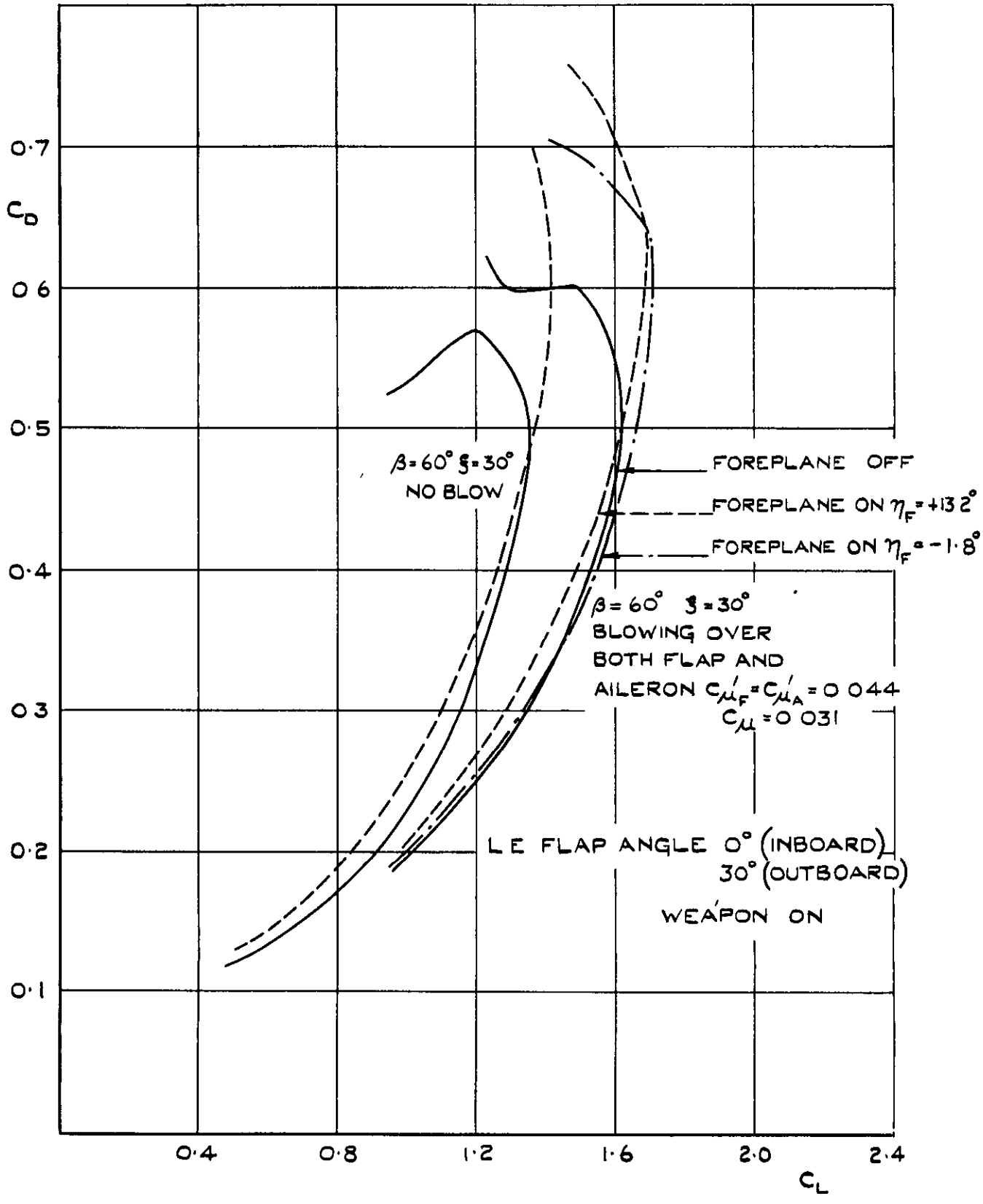

(b). C_D v C_L (NO TAILPLANE).

FIG. 29 (CONT'D).

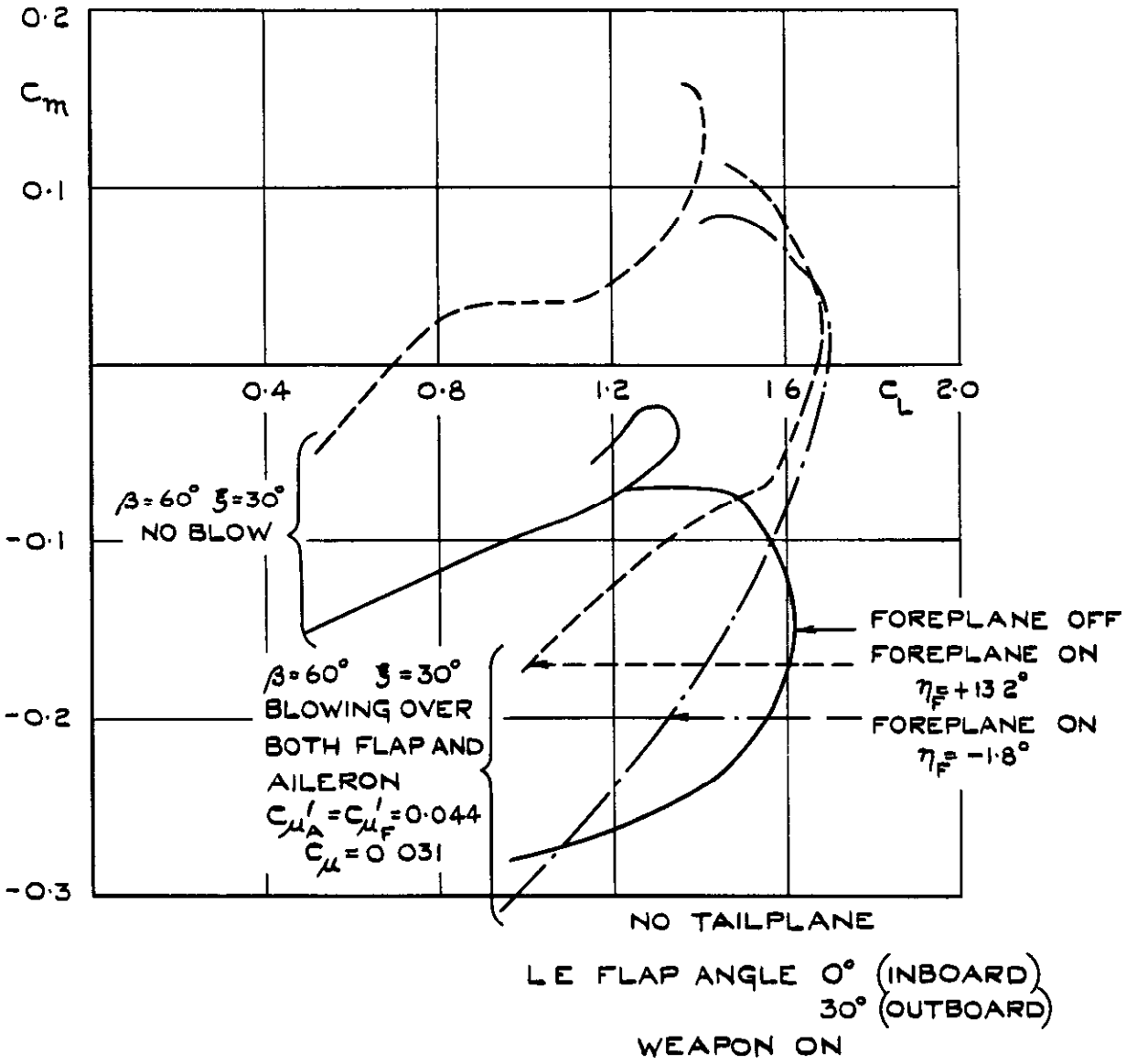

(c) C_m v C_L

FIG. 29. (CONCL'D.).

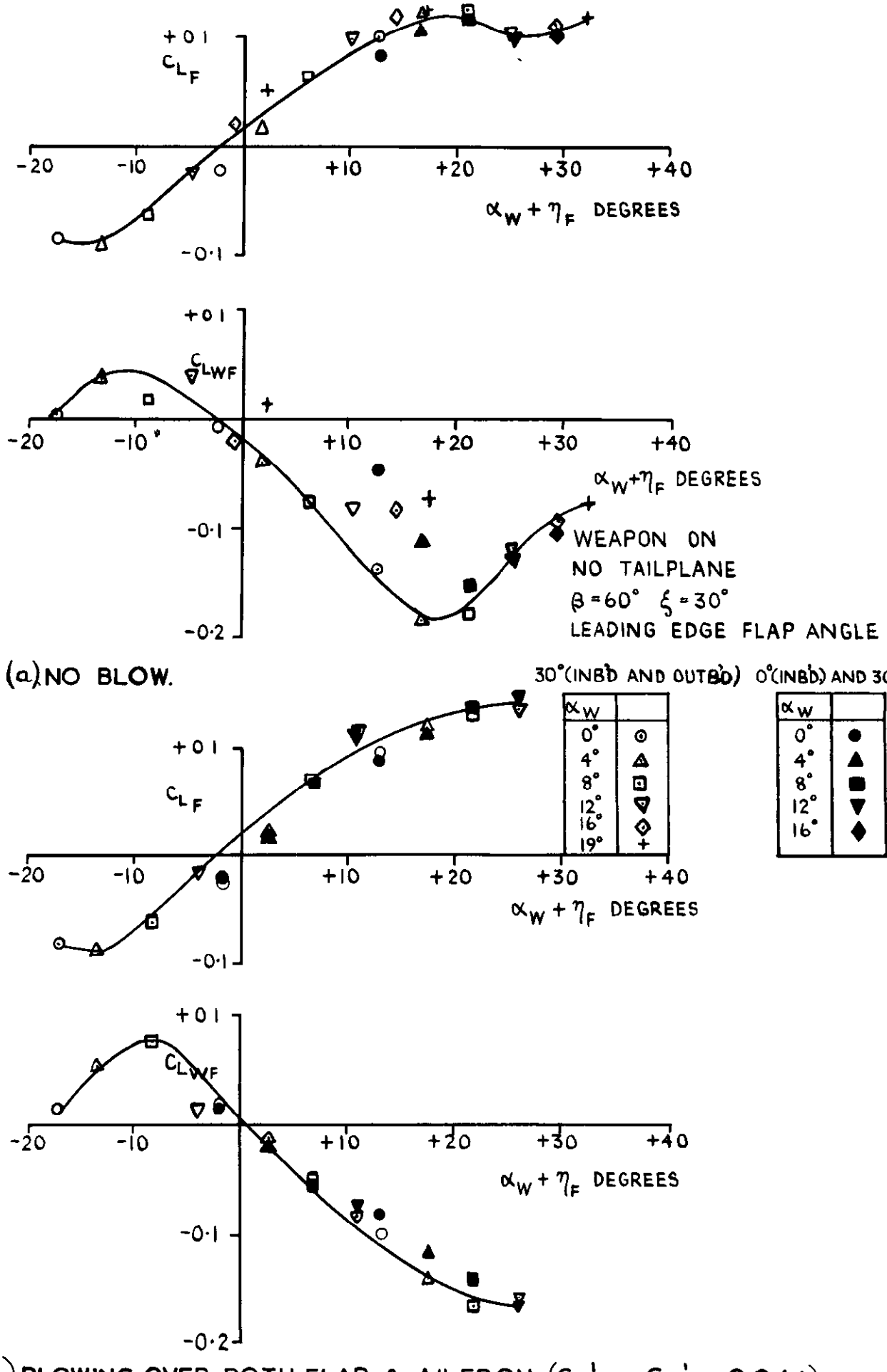

(a) NO BLOW.

(b). BLOWING OVER BOTH FLAP & AILERON ($C\mu'_F = C\mu'_A = 0.044$).

FIG. 30. THE EFFECT OF THE FOREPLANE. VARIATION OF C_{L_F} & $C_{L_{WF}}$ WITH $\alpha_W + \eta_F$.

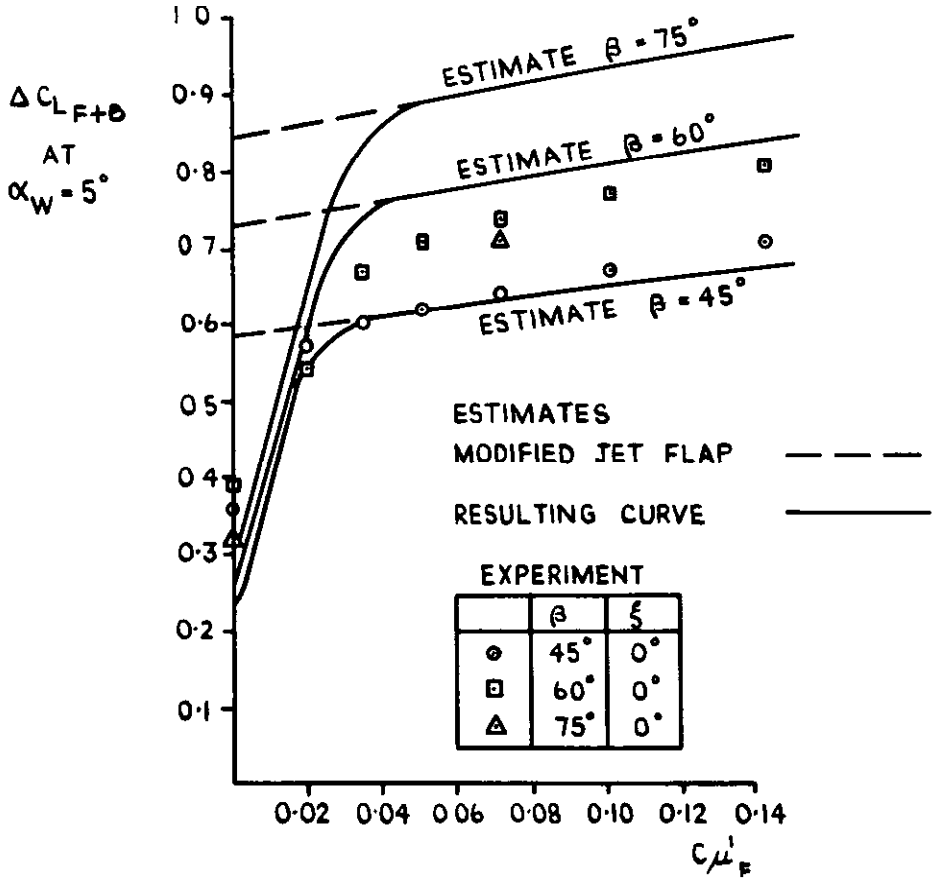

FIG. 31. A COMPARISON BETWEEN THE ESTIMATED AND THE MEASURED VALUES OF $\Delta C_{L_{F+B}}$ AT $\alpha_W = 5^\circ$ (BLOWING OVER FLAP ONLY WITH AILERON UNDEFLECTED).

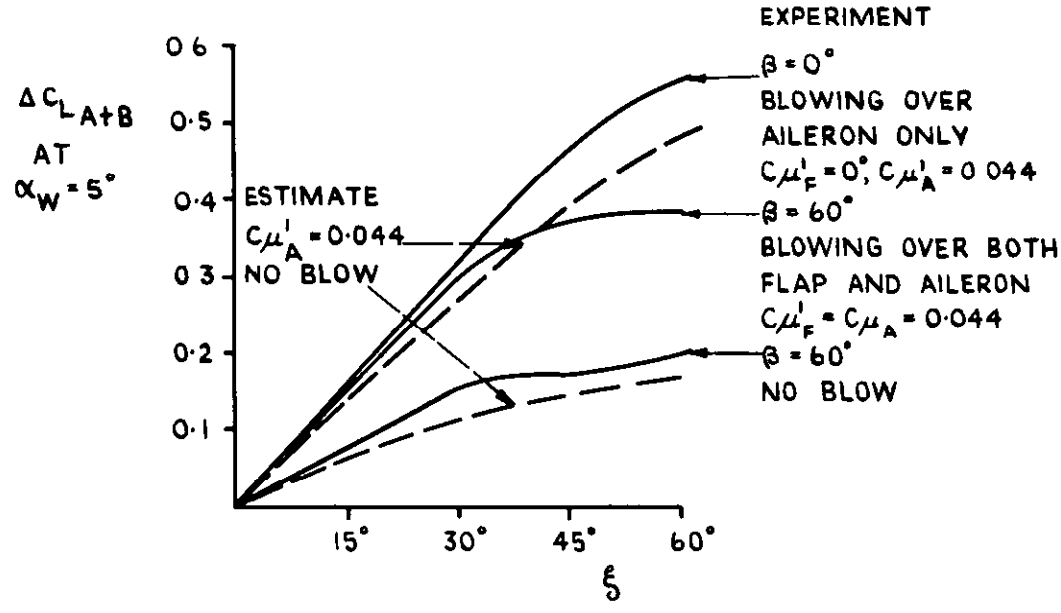

FIG. 32. A COMPARISON BETWEEN THE ESTIMATED AND THE MEASURED VALUES OF $\Delta C_{L_{A+B}}$ AT $\alpha_W = 5^\circ$.

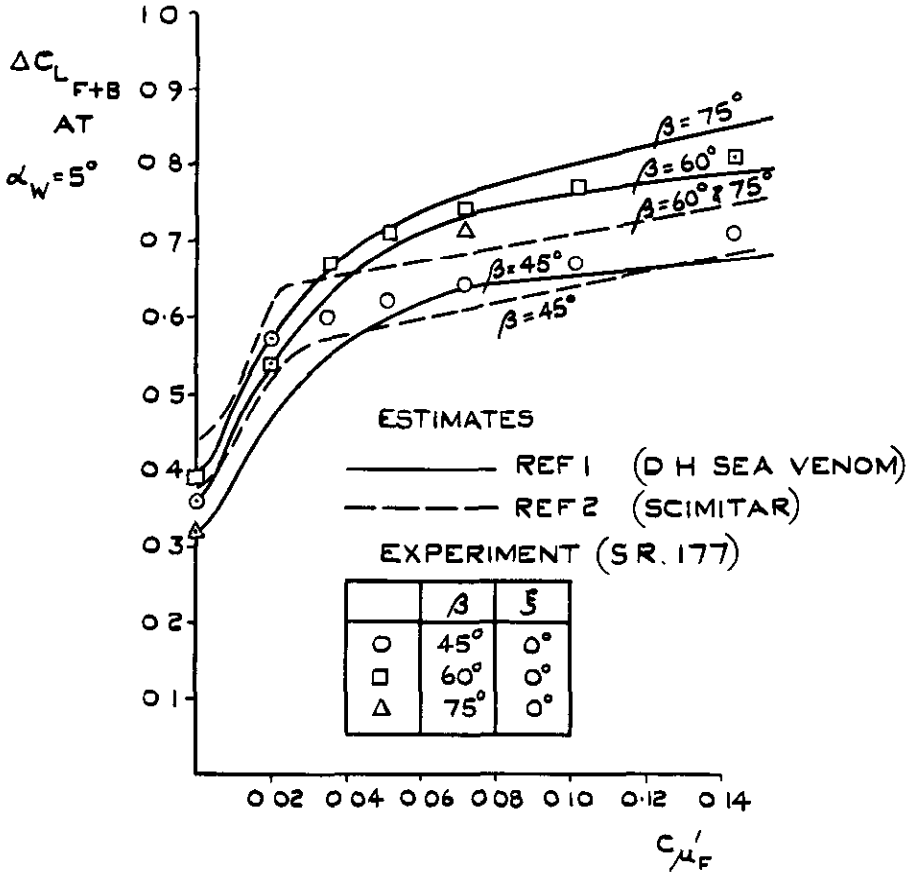

(a). BLOWING OVER FLAP ONLY WITH AILERON UNDEFLECTED.

FIG. 33. A COMPARISON BETWEEN LIFT INCREMENTS MEASURED IN PRESENT TESTS AND ESTIMATES BASED ON TESTS OF OTHER AIRCRAFT MODELS.

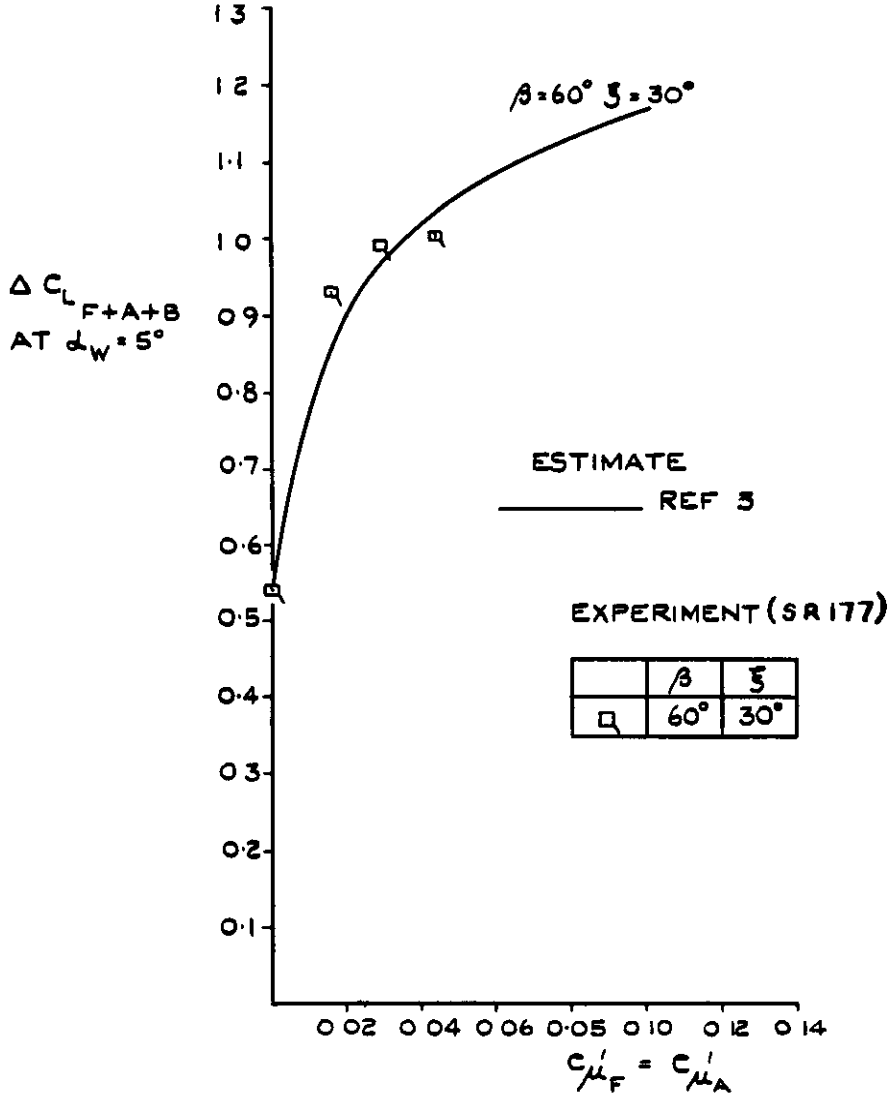

(b) BLOWING OVER BOTH FLAP AND AILERON.

FIG. 33 (CONCLD.)

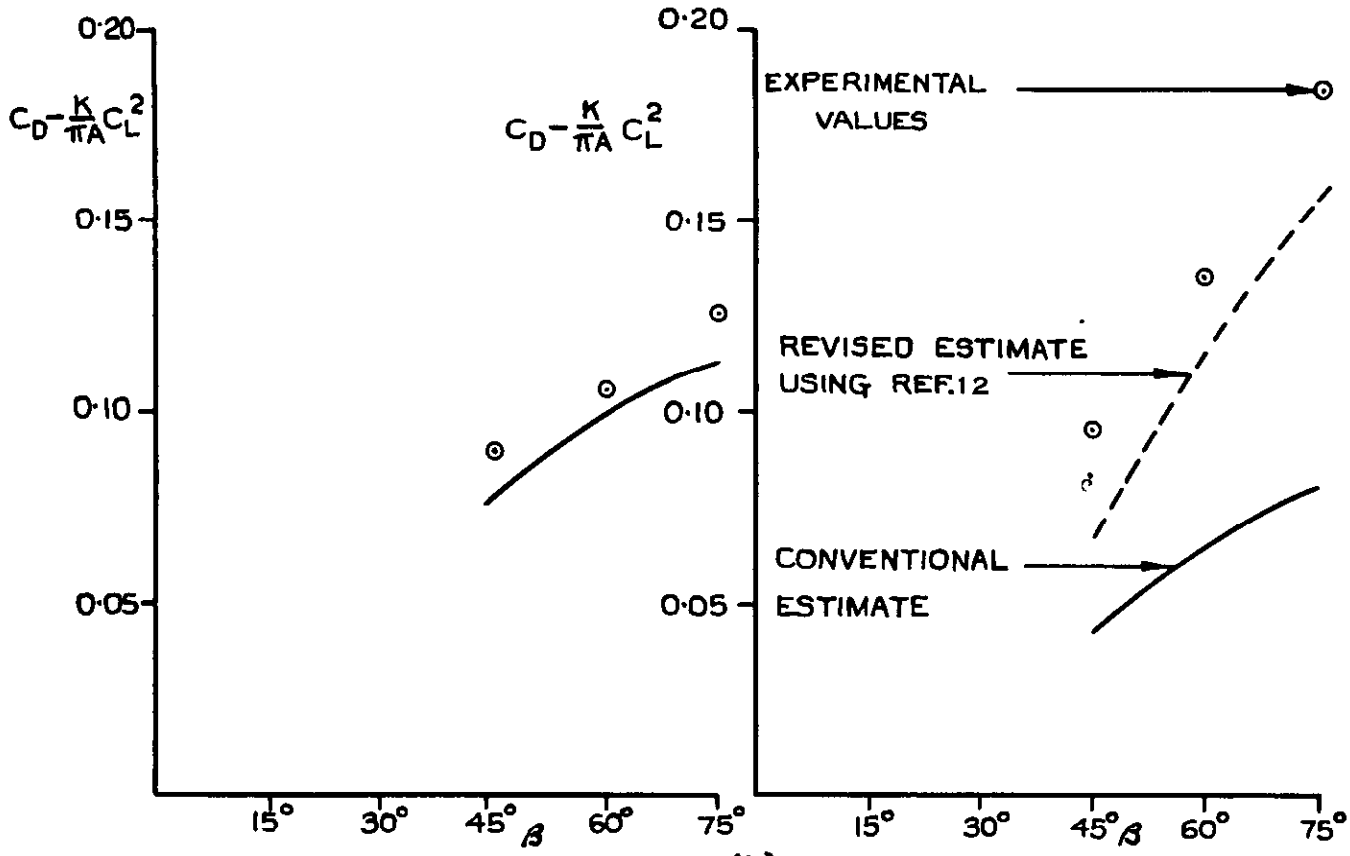

(a). NO BLOW. (b). BLOWING OVER FLAP ONLY $C_{\mu'_F} = 0 \cdot 072$.

FIG. 34. A COMPARISON BETWEEN THE ESTIMATED AND THE MEASURED VALUES OF C_D AT ZERO C_L (BLOWING OVER FLAP ONLY WITH AILERON UNDEFLECTED).

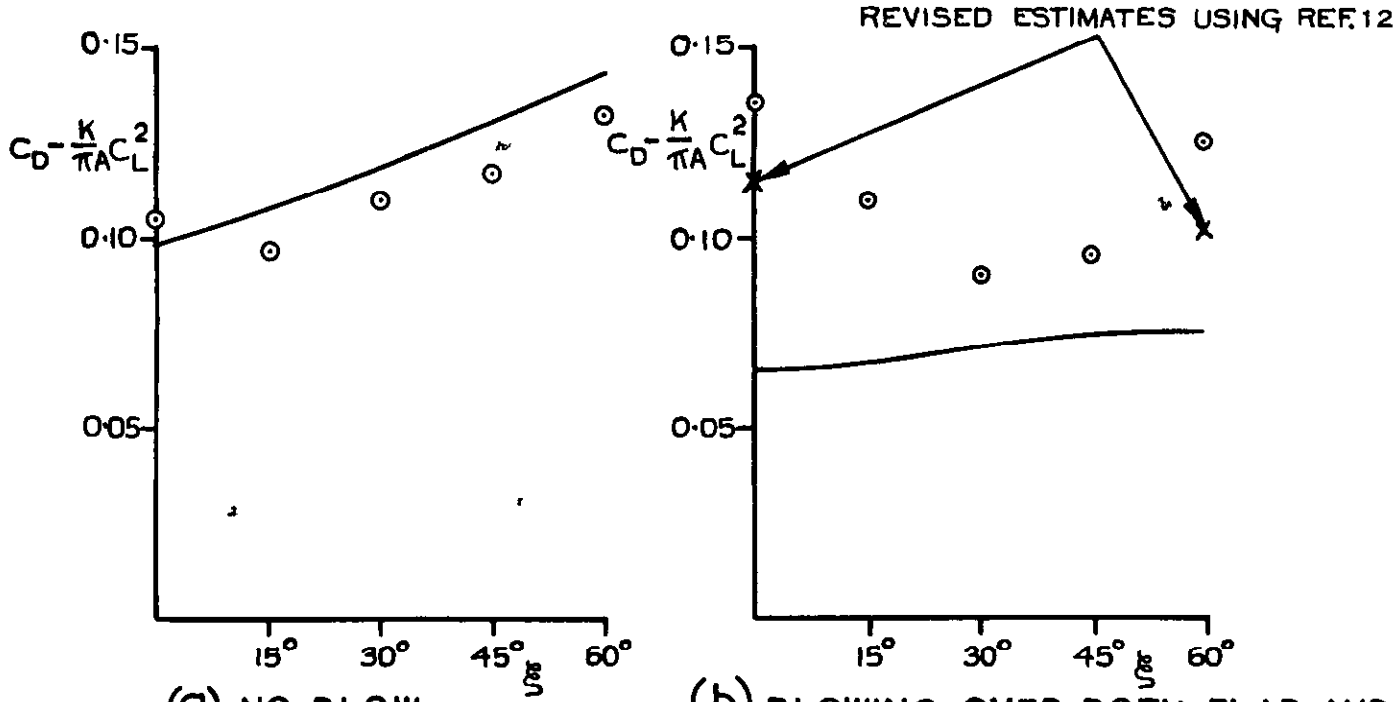

(a). NO BLOW. (b). BLOWING OVER BOTH FLAP AND AILERON. $C_{\mu'_F} = C_{\mu'_A} = 0 \cdot 044$.

FIG. 35. A COMPARISON BETWEEN THE ESTIMATED AND THE MEASURED VALUES OF C_D AT ZERO C_L FOR DIFFERENT AILERON ANGLES (BLOWING OVER BOTH FLAP AND AILERON WITH FLAP ANGLE = 60°).

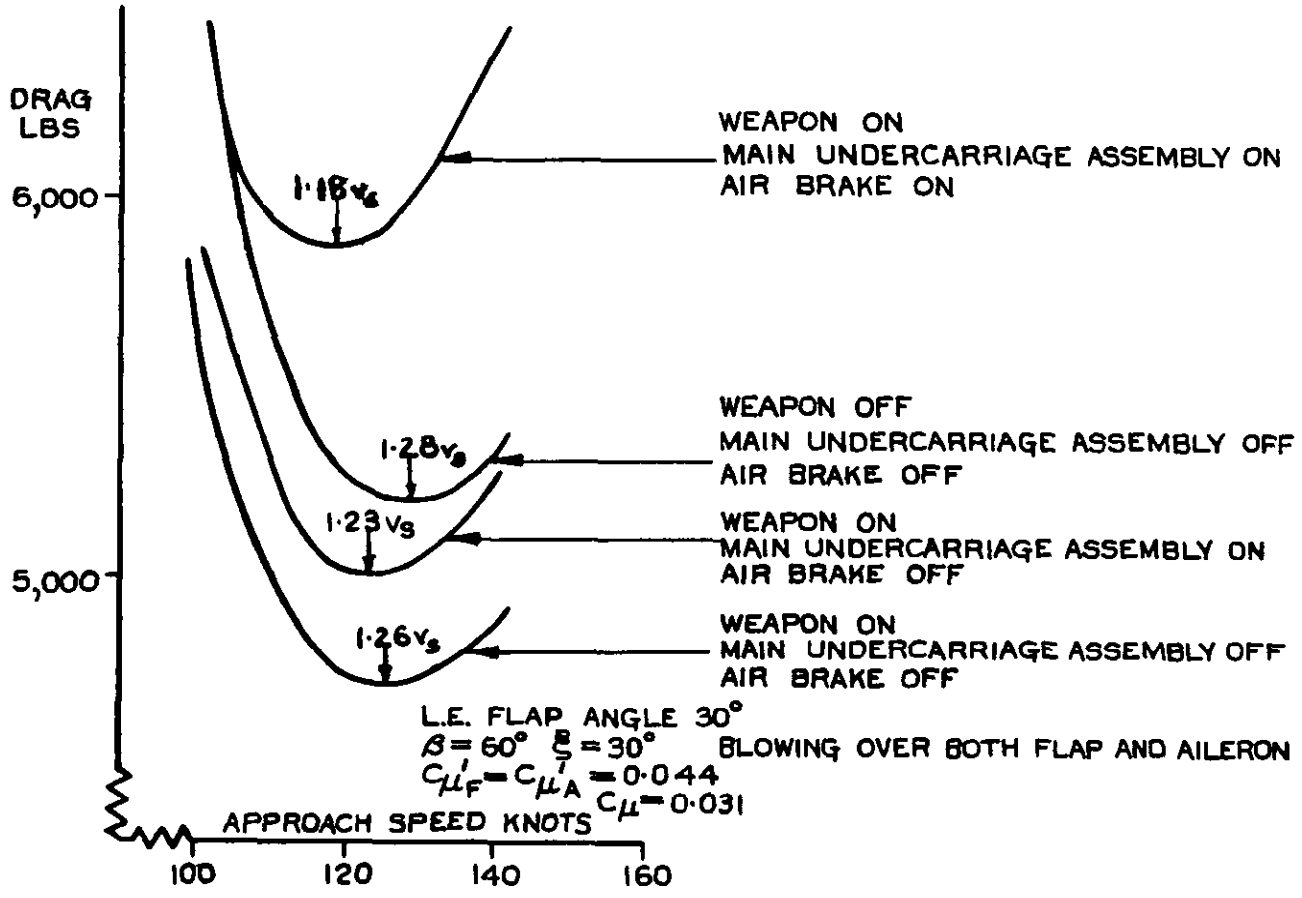

FIG.36. THE EFFECTS OF THE MAIN UNDERCARRIAGE ASSEMBLY, THE AIRBRAKE, AND THE WEAPON ON DRAG ∿ APPROACH SPEED.

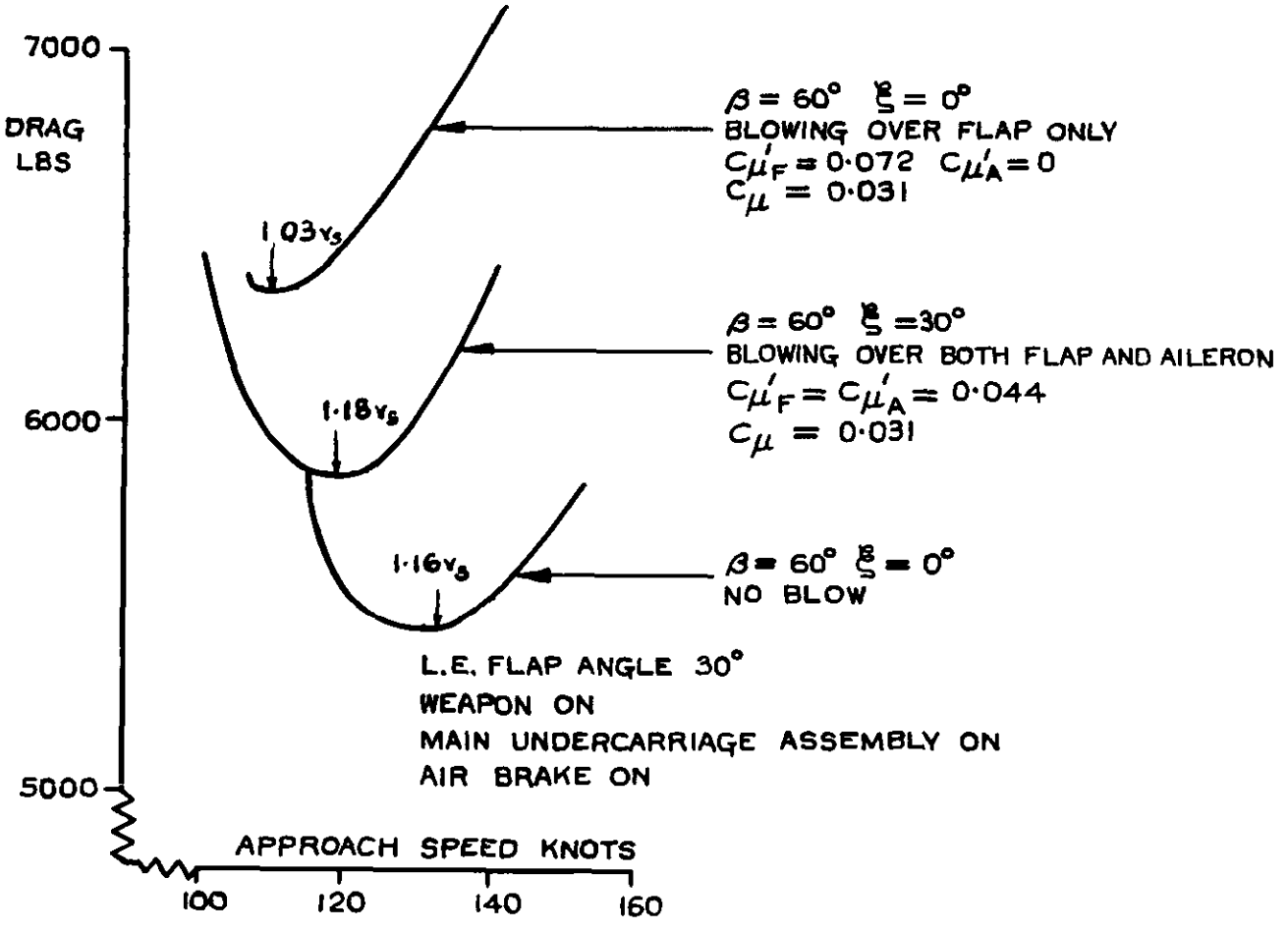

FIG.37. THE EFFECTS OF FLAP ANGLE, AILERON ANGLE, AND BLOWING ON DRAG ∿ APPROACH SPEED.

A.I.(42) Saunders-Roe P177 :
533.693.3 :
533.6.013.412 :
LOW-SPEED WIND-TUNNEL TESTS ON A DELTA-WING 533.694.72 :
AIRCRAFT MODEL (S.R.177), WITH BLOWING OVER 533.6.011.34
THE TRAILING-EDGE FLAPS AND AILERONS.
Butler, S.F.J. and Guyett, M.B. August, 1962.

Low speed longitudinal stability measurements are described on a delta-wing aircraft model of aspect-ratio 2.9 and 40° leading-edge sweepback, with shroud blowing over trailing-edge flaps and ailerons.

With blowing over the flap alone at a flap angle of 60° (aileron undeflected), increases were obtained of 0.27 in trimmed C_L at constant

A.I.(42) Saunders-Roe P177 :
533.693.3 :
533.6.013.412 :
LOW-SPEED WIND-TUNNEL TESTS ON A DELTA-WING 533.694.72 :
AIRCRAFT MODEL (S.R.177), WITH BLOWING OVER 533.6.011.34
THE TRAILING-EDGE FLAPS AND AILERONS.
Butler, S.F.J. and Guyett, M.B. August, 1962.

Low speed longitudinal stability measurements are described on a delta-wing aircraft model of aspect-ratio 2.9 and 40° leading-edge sweepback, with shroud blowing over trailing-edge flaps and ailerons.

With blowing over the flap alone at a flap angle of 60° (aileron undeflected), increases were obtained of 0.27 in trimmed C_L at constant

A.I.(42) Saunders-Roe P177 :
533.693.3 :
533.6.013.412 :
LOW-SPEED WIND-TUNNEL TESTS ON A DELTA-WING 533.694.72 :
AIRCRAFT MODEL (S.R.177), WITH BLOWING OVER 533.6.011.34
THE TRAILING-EDGE FLAPS AND AILERONS.
Butler, S.F.J. and Guyett, M.B. August, 1962.

Low speed longitudinal stability measurements are described on a delta-wing aircraft model of aspect-ratio 2.9 and 40° leading-edge sweepback, with shroud blowing over trailing-edge flaps and ailerons.

With blowing over the flap alone at a flap angle of 60° (aileron undeflected), increases were obtained of 0.27 in trimmed C_L at constant

incidence and of 0.18 in trimmed $C_{L_{max}}$, at the value of C_μ (0.031) envisaged for the projected aircraft. Corresponding reductions in landing and take-off speeds of about 10 knots could have been expected in practice. By distributing the same total jet momentum to flap and aileron, with 30° aileron mean droop, further lift increases were obtained corresponding to additional reductions of about 8 knots in aircraft speeds.

The beneficial effect of the L.E. flap was large, amounting to 5° increase of stalling angle and 0.3 increase in $C_{L_{max}}$ with blowing over trailing-edge flaps and ailerons.

The measured effects of blowing correlated well with results of other model tests involving similar wing-flap arrangements. In particular, part-span blown flaps were again found to produce large drag increments significantly affecting the aircraft minimum drag speed.

incidence and of 0.18 in trimmed $C_{L_{max}}$, at the value of C_μ (0.031) envisaged for the projected aircraft. Corresponding reductions in landing and take-off speeds of about 10 knots could have been expected in practice. By distributing the same total jet momentum to flap and aileron, with 30° aileron mean droop, further lift increases were obtained corresponding to additional reductions of about 8 knots in aircraft speeds.

The beneficial effect of the L.E. flap was large, amounting to 5° increase of stalling angle and 0.3 increase in $C_{L_{max}}$ with blowing over trailing-edge flaps and ailerons.

The measured effects of blowing correlated well with results of other model tests involving similar wing-flap arrangements. In particular, part-span blown flaps were again found to produce large drag increments significantly affecting the aircraft minimum drag speed.

incidence and of 0.18 in trimmed $C_{L_{max}}$, at the value of C_μ (0.031) envisaged for the projected aircraft. Corresponding reductions in landing and take-off speeds of about 10 knots could have been expected in practice. By distributing the same total jet momentum to flap and aileron, with 30° aileron mean droop, further lift increases were obtained corresponding to additional reductions of about 8 knots in aircraft speeds.

The beneficial effect of the L.E. flap was large, amounting to 5° increase of stalling angle and 0.3 increase in $C_{L_{max}}$ with blowing over trailing-edge flaps and ailerons.

The measured effects of blowing correlated well with results of other model tests involving similar wing-flap arrangements. In particular, part-span blown flaps were again found to produce large drag increments significantly affecting the aircraft minimum drag speed.

Published by
HER MAJESTY'S STATIONERY OFFICE
To be purchased from
49 High Holborn, London, W C 1
423 Oxford Street, London, W 1
13A Castle Street, Edinburgh 2
109 St. Mary Street, Cardiff
Brazennose Street, Manchester 2
50 Fairfax Street, Bristol 1
35 Smallbrook, Ringway, Birmingham 5
80 Chichester Street, Belfast 1
or through any bookseller

Printed in England for H M Stationery Office by Keyswift Ltd , Edgware, Middx
Wt No [redacted] K 4 3 66
59

S O Code No 23-9015-10